



Quantum Dots: Synthesis, characterization and electrochemical sensing for life sciences

Dissertation

zur Erlangung des Doktorgrades
der Naturwissenschaften
(Dr. rer. nat.)

Dem
Fachbereich Physik
der Philipps-Universität Marburg
vorgelegt von

Nadeem Sabir

aus

Faisalabad, Pakistan

Marburg, 2015

Vom Fachbereich Physik der Philipps-Universität (Hochschulkenziffer: 1180) als
Dissertation angenommen am

Erstgutachter: Prof. Dr. Wolfgang J. Parak

Zweitgutachter: Prof. Dr. Gregor Witte

Prüfer: Prof. Dr. Manfred Konrad

Tag der mündlichen Prüfung:

Die Vorliegende Arbeit wurde am Fachbereich Physik
Der Philipps-Universität Marburg unter Anleitung von

Herrn Prof. Dr. Wolfgang. J. Parak

In der Zeit von September 2011 bis November 2015 angefertigt.

Abstract

Subjects of the present dissertation are the synthesis, and the characterization of colloidal Quantum dots and their application in electrochemical biosensors for biological and life sciences. This study splits into two parts. The first part consists on the synthesis and the characterization of various types of quantum dots (QDs), i.e., doped (CdS:Mn and CdS/Mn:ZnS/ZnS core/shell) and undoped (CdS, CdS/ZnS core/shell, CdSe and CdSe/ZnS core/shell QDs) QDs. The second part concerns the fabrication of a bioelectrochemical sensor based on CdS/ZnS QDs.

Mn-doped CdS and CdS/ZnS QDs were synthesized in organic solvent; Mn ions were incorporated into CdS QDs (CdS:Mn) and in the case of the CdS/ZnS QDs, Mn ions were incorporated into a thin (2 atomic monolayers) ZnS shell, which after Mn doping was further grown (2 atomic monolayers). In order to study the optical properties of Mn doped CdS/ZnS core shell QDs, a fluorescence resonance energy transfer (FRET) system was performed, in which the Mn^{2+} ions and organic dyes(ATTO633) as acceptors were incorporated into the ZnS shell and polymer shell, respectively. The polymer shell was used to provide colloidal stability for the CdS/ZnS QDs. In this study, we propose that the double energy transfer process take place among the three fluorescence sources, first within the Mn-doped CdS/ZnS QDs, i.e., from the CdS/ZnS QDs to the Mn ions and then, from the excited Mn ions to the organic dye, the organic fluorophore ATTO633 incorporated within the polymer coating of Mn-doped CdS/ZnS QDs.

A bioelectrochemical sensor for specific detection of guanosine monophosphate (GMP) is demonstrated based on the combination of three enzymatic reactions. We have combined all three enzymatic reactions with the detection at the QD electrode. In both cases, all three enzymes (i.e., Guanylate monophosphate kinase (GMPK), pyruvate kinase (PK) and lactate dehydrogenase (LDH)) were immobilized together, on top of the QD electrodes, or added directly to the electrolyte solution. Photocurrent measurements were performed with varying concentrations of GMP, but with fixed concentration of the three enzymes and other enzymes /coenzymes like adenosine triphosphate (ATP), phosphoenolpyruvat (PEP), and nicotinamide adenine dinucleotide hydrogen NADH. Clearly the photocurrent response

was found to be dependent on the GMP concentration added to the solution. This verifies that a signal cascade from the first GMPK reaction through the PK and LDH reaction, and finally to the NADH to NAD⁺ oxidation at the QD electrode could be measured. In the first reaction, the enzymatic conversion of GMP by GMPK produces adenosine diphosphate (ADP). In the second reaction, ADP and phosphoenolpyruvate (PEP) are converted into Adenosine triphosphate (ATP) and pyruvate. In the third reaction pyruvate (Py) and nicotinamide adenine dinucleotide hydrogen (NADH) are converted to lactate and nicotinamide adenine dinucleotide (NAD⁺). Finally Py was converted by LDH under consumption of NADH, which was electrochemically determined. The photocurrent response to GMP for the combined reaction demonstrates that GMP could be detected electrochemically.

Zusammenfassung

Gegenstand der vorliegenden Dissertation ist die Synthese und Charakterisierung kolloidaler Quantenpunkte und ihre Anwendung in elektrochemischen Biosensoren für Biologie- und Lebenswissenschaften. Diese Studie teilt sich in zwei Teile. Der erste Teil setzt sich aus der Synthese und Charakterisierung verschiedener Arten von Quantenpunkten (QPs) zusammen wie dotierte (CdS:Mn und CdS/Mn:ZnS/ZnS Kern/Hülle) sowie undotierte (CdS, CdS/ZnS Kern/Hülle, CdSe und CdSe/ZnS Kern/Hülle) QPs. Der zweite Teil bezieht sich auf die Herstellung eines bio-elektrochemischen Sensors auf Basis von CdS/ZnS QPs.

Mn-dotierte CdS und CdS/ZnS-QPs wurden in organischen Lösungsmittel synthetisiert wobei Mn-Ionen zunächst in CdS-QPs (CdS:Mn) eingebracht wurden. Im Falle der CdS/ZnS-QPs wurden Mn-Ionen in eine dünne Schicht aus ZnS (bestehend aus 2 molekularen Einzelschichten) eingebracht, welche nach Mn-dotierung mit zwei weiteren ZnS-Einzelschichten versiegelt wurde. Um die optischen Eigenschaften Mn-dotierter CdS/ZnS-QPs zu untersuchen, wurde ein System basierend auf strahlungsfreiem Fluoreszenz-Resonanzenergietransfer erarbeitet, wobei zusätzlich Farbstoffmoleküle (ATTO633) als Akzeptor in die Polymerhülle eingebracht wurden. Die Polymerhülle wurde verwendet, um die kolloidale Stabilität der CdS/ZnS-QPs zu gewährleisten. Es ist anzunehmen dass der Energieübertragungsprozess zwischen den drei Fluoreszenzquellen in bestimmter Reihenfolge stattfindet. Zunächst innerhalb der QPs, d.h. zwischen CdS/ZnS-QPs und Mn^{2+} -Ionen und dann von den angeregten Mn^{2+} -Ionen zu den Farbstoffmolekülen innerhalb Polymerhülle.

Ein bio-elektrochemischer Sensor für den spezifischen Nachweis von Guanosinmonophosphat (GMP) wird vorgestellt, basierend auf der Kombination dreier enzymatischer Reaktionen. Alle drei enzymatische Reaktionen wurden mit der Detektion an der QP-Elektrode kombiniert. In beiden Fällen wurden alle drei Enzyme (Guanylat-Monophosphatkinase (GMPK), Pyruvatkinase (PK) und Lactatdehydrogenase (LDH)) auf der Oberseite der QP-Elektrode immobilisiert oder direkt zu der Elektrolytlösung gegeben. Photostrommessungen wurden mit variierenden Konzentrationen von GMP durchgeführt aber mit festen Konzentration der drei Enzyme sowie weiterer Enzyme bzw. Coenzyme wie

Adenosintriphosphat (ATP), Phosphoenolpyruvat (PEP) und Nicotinamidadenindinukleotid Wasserstoff (NADH). Die Resonanz des Photoelektronenstroms war proportional zur GMP-Konzentration in Lösung. Dies lässt auf eine Signalkaskade schließen, anfangend mit der ersten GMPK-Reaktion, weiter zur PK- und LDH-Reaktion und schließlich auf die Oxidationsreaktion von NADH zu NAD⁺, welche an der QP-Elektrode gemessen werden konnte. In der ersten Reaktion erzeugt die enzymatische Umwandlung von GMP durch GMPK, Adenosindiphosphat (ADP). In der zweiten Reaktion werden ADP und Phosphoenolpyruvat (PEP) in Adenosintriphosphat (ATP) und Pyruvat umgewandelt. In der dritten Reaktion werden Pyruvat (Py) und Nicotinamidadenindinukleotid Wasserstoff (NADH) zu Lactat und Nicotinamidadenindinukleotid (NAD⁺) umgewandelt. Schließlich wurde Py von LDH unter Verbrauch von NADH umgewandelt was elektrochemisch bestimmt wurde. Die Resonanz des Photoelektronenstroms zu GMP der kombinierten Reaktion beweist den elektrochemischen Nachweis von GMP.

Dedicated to
My beloved Wife Shahzadi,
My Children's Raveeha, Sabeeha, Ali
&
My parents (Late)

Acknowledgements

First of all, I would like to convey my sincere gratitude to my supervisor Prof. Dr. Wolfgang J. Parak, who gave me the opportunity to conduct my research work in his group Biophotonik. I appreciate all his contributions of time, ideas and encouragement from the start until the end to make my Ph.D. experience productive and stimulating. The pleasure and enthusiasm he has for his research was communicable and motivational for me, even during hard times in the Ph.D. quest. I am also thankful for the excellent example he has provided as a successful physicist and professor.

Many thanks to my co-supervisor Dr. Pablo del Pino for his guidance, valuable comments, scholarly inputs and for his unconditional confidence in me. Also great thanks for the proof reading of my thesis.

I want to express my sincere gratitude to Prof. Dr. Fred Lisdat (Biosystems Technology, Institute of Applied Life Sciences, Technical University Wildau, Wildau), Prof. Dr. Gregor Witte, Prof. Dr. Manfred Konrad (Max Planck Institute for Biophysical Chemistry, Göttingen) and Prof. Dr. Wolfram Heimbrodt for their time, valuable suggestions and concise comments on the research papers of the thesis. I thank the colleagues with whom I was working within collaborative projects. Special thanks go to Nazimuddin Khan (Max Planck Institute for Biophysical Chemistry, Göttingen) for GMPK detection study, and Uwe Kaiser for the Mn doped QDs experiments.

I am very indebted for all the support I got from the current and past members of the Biophotonik group. Special thanks go to Dr. Nadja C. Bigall, Dr. Beatriz Pelaz and Dr. Faheem Amin for their encouragement and help during the Ph.D. research work. Thanks to Jonas Hühn for translating the abstract of my thesis in German.

I am also very thankful to Stefanie Kramer for the administrative and Andreas Rentzos for the technical support during my PhD in Marburg.

I would like to thank GC University Faisalabad (GCUF) Pakistan and Higher Education Commission (HEC) Pakistan for financial support of PhD and stay in Germany. Research

Training Group "Functionalization of Semiconductors" (GRK 1782; funded by the DFG) and DAAD Germany are gratefully acknowledged.

I am very much indebted to my family members, my wife Shahzadi, Children's Raveeha, Sabeeha, Ali and also my brother Asif, who supported me in every possible way to see the completion of this work.

Table of Contents

1. Introduction	1
1.1 Nanofabrication	2
1.2 Doped CdS/ZnS core/shell QDs	3
1.2.1 Photoluminescence of Mn doped CdS/ZnS NP	5
1.2.2 Förster resonance energy transfer (FRET) in Mn doped NPs	6
1.3 Biosensors	8
1.3.1 Enzymes	9
1.3.1.1 Guanylate kinase (GMPK)	10
1.3.1.2 Guanylate monophosphate (GMP)	11
1.3.1.3 Pyruvate kinase (PK)	11
1.3.1.4 Lactate dehydrogenase (LDH)	12
1.3.1.5 Nicotinamide adenine dinucleotide hydrogen (NADH)	12
1.3.2 QD-Based Electrochemical biosensors	12
1.3.2.1 Guanosine Monophosphate detection	15
2. Synthesis and characterization of the QDs	16
2.1 Synthesis of CdS QDs	16
2.2 Synthesis of ZnS shell around CdS core (CdS/ZnS QDs)	17
2.3 Doping of Mn in ZnS shell of the CdS/ZnS QDs (CdS/Mn:ZnS QDs)	18
2.4 Passivation of CdS/Mn:ZnS NPs with ZnS shell	19
2.5 Synthesis of Mn doped CdS quantum dots (CdS:Mn QDs)	20
2.6 Synthesis of the CdSe/ZnS core/shell QDs	21
3. Conclusions and outlook.....	24
4. Publications	26
5. Bibliography	28
6. Appendix	41

Quantum Dots: Synthesis, characterization and electrochemical sensing for life sciences

1. Introduction

Nanotechnology deals with nano-meter sized objects. Nanosized structures are formed of clusters of few numbers of atoms or molecules. Nanostructure size is in-between atoms or molecules and bulk materials. The term 'Nanotechnology' is realized by three levels: materials, devices and systems.¹ The nanomaterial level, both in scientific understanding and in commercial usage, is the more advanced one during the last decade. Advancement in nanoscience has permitted scientists to develop materials that have highly controlled and unique properties. Later on, nanomaterials have started to be used in different applications of the biological sciences, such as therapy, diagnostic tools, labeling, and drug delivery to enumerate.² Importantly, nanomaterial's properties can be regulated by manipulating their physical dimensions and composition. A number of eminent physical properties of the nanomaterials are related to different origins: for example large fraction of surface atoms per unit volume, large surface energy, special confinement effect etc.²⁻⁷

The term colloid was initially used to explain a wide range of solid-liquid solution, all of which contain different solid particles dispersed to various degrees in a solution. Remarkable advancement has been made in fabrication of colloidal nanoparticles (NPs) with well-defined sizes and shapes.³ Many efforts have been devoted for the investigation of the synthesis, characterization and application of NPs.⁴⁻⁷

Some metals, namely gold and silver, exhibit poor reactivity on the bulk scale. Gold (Au), a noble material for example, is exceptionally non reactive in bulk state. On the other hand, Au clusters are found to be catalytically very active in reactions; numerous potential reasons have been suggested.^{8, 9} Concerning biomedical applications, silver (Ag), being another noble metal, at nanoscale plays an important role in daily life goods, mainly due to their antimicrobial properties.^{10, 11} The applications of Ag NPs are very much similar to those of Au NPs. Furthermore silver NPs catalytic activity is strongly dependent on particle size.^{12, 13} Semiconductor nanocrystals, i.e., colloidal QDs, are in the range of few nanometers in diameter, with unique photophysical and chemical properties which depend on their size.¹⁴⁻

¹⁷ The fluorescent QDs are metal chalcogenide alloys mainly consisting of cadmium selenide

Quantum Dots: Synthesis, characterization and electrochemical sensing for life sciences

(CdSe)¹⁷ and cadmium sulfide (CdS)¹⁷. However, cadmium substitutes like Zinc and Lead have been reported.¹⁸⁻²⁰ QDs have been suggested as surrogates for conventional organic fluorophore and fluorescent proteins in bioimaging.²¹⁻²³ These are also used in lasers²⁴, light emitting diodes²⁵, solar cells^{26, 27} and different electronic and optical devices.

1.1. Nanofabrication

The two major approaches involved in the nanofabrication are typically categorized into top-down and bottom-up techniques. Top-down techniques begin with a pattern made on a larger scale and reducing its dimensions into nanoscale. Top-down means getting a bulk material and breaking into small pieces; the main advantages are universality and cost effective.^{28, 29} Top-down techniques for nanostructure fabrication are based on a number of tools and techniques, which relies on the thin film deposition/coating technique on a substrate, lithography and etching technique etc. In recent years, electron beam lithography is used for fabricating semiconductor components, and nanoscale devices.^{30, 31}

The second approach is the so-called bottom-up, in which nanosized objects like nanoparticles, nanowires and nanotubes are produced by self-assembly of nano-objects or thin layers to form arrays or phase parting molds.²⁸⁻³⁴ Inorganic NPs are synthesized through wet chemical methods by swiftly mixing suitable reagents, leading to a solid phase formation, *i.e.*, nucleation (the formation of the first small solid particles range of 1-2 nm or less, mentioned in Figure 1). The growth of small crystals into larger crystals is thermodynamically favored to decrease in the specific surface energy during crystal growth. The growth of crystals must be prevented by suitable capping agents (charged molecules, surfactants, or polymers), which also prevent agglomeration. The colloidal stability can be obtained due to electrostatic repulsion (as measurable by zeta potential), due to steric stabilization (by polymer shell), or due to combination of both (electrostatic stabilization by a polyelectrolyte).

Growth and stabilization of nanoparticles

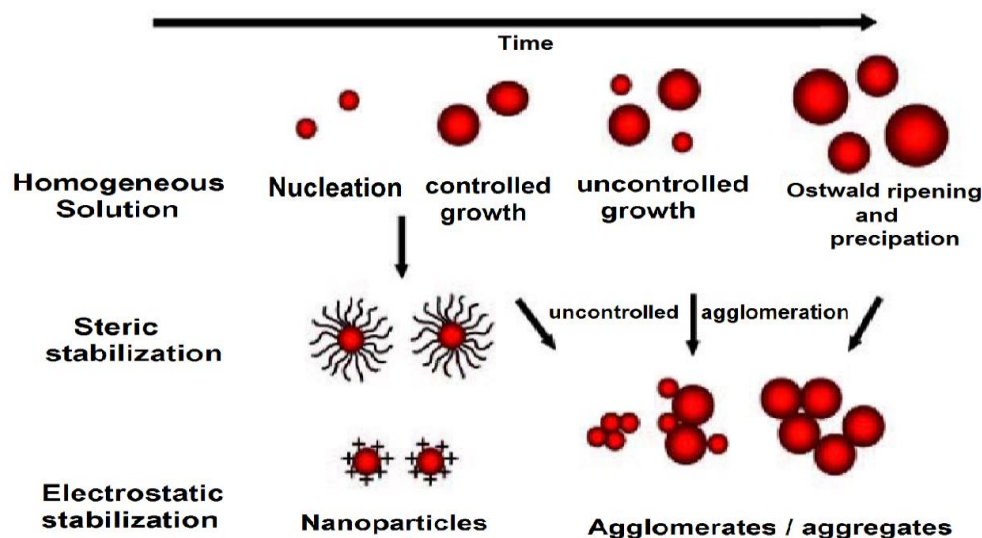


Figure 1: Simple demonstration of the nucleation, growth and ripening process. In particular here is possible to see that stopping the synthesis after a certain interval of time from the nucleation is possible to synthesize nanoparticles with approximately the same size. Figure adapted from Goesmann et al.³⁵

1.2. Doped CdS / ZnS core/shell QDs

Semiconductor nanocrystals CdS has a Bohr radius of 2.4 nm³⁶ and direct band with band gap of 2.4 eV.³⁷ Various methods to synthesize the CdS quantum dots of particular size and shape have been studied. Emission spectrum of CdS quantum dots lies in the visible spectrum range between 350 nm(violet) and 500 nm (green). CdS QDs are used in many research areas including single-electron transistors, light emitting diodes, solar cells, lasers and biological labels.^{14, 22, 38-44} The key advantage offered by these systems over traditional CdSe quantum dots is their relatively small red shift with increasing size. This allows more comfort during the synthesis for tailor made sizes of such QDs.

Transition metals such as Cr⁵², Mn^{45, 46}, Co⁴⁷⁻⁴⁹, Ni⁵⁰, Cu⁵¹, , Hg⁵³ have been introduced in semiconductor QDs as dopant.^{51, 52, 54-57} These doped semiconductors have recently gained fabulous attraction due to their unique optical and magnetic properties. The presence of dopant atoms in QDs establishes new energy levels, which are responsible for the optical

Quantum Dots: Synthesis, characterization and electrochemical sensing for life sciences

absorption at longer wavelengths. The additions of dopants are also widening the range of fluorescence properties.⁵⁸

Fluorescent Manganese (Mn) doped II-VI semiconductor nanocrystals have been thoroughly studied in the last decade. CdS, ZnS and ZnSe semiconductor materials have been utilized as host for Mn-dopant prepared via different synthetic paths.^{57, 59-62} Additionally, doping with magnetic material (in this case Mn) has paved the way for dilute magnetic semiconductors (DMS).⁶³ Mn^{2+} ions in the semiconductor nanocrystal can act as paramagnetic hubs. Mn^{2+} ion has $d5$ electronic configuration. The bulk dilute magnetic semiconductors (DMS) show interesting magnetic properties, due to exchange interaction of the $sp-d$ orbitals between magnetic impurities and semiconductor host nanoparticles.^{56, 64} Mn^{2+} ion shows a broad emission peak when incorporated into the CdS host structure.⁴⁵ Due to changes in crystal field strength with respect to host crystal, Mn^{2+} ion position depends on the host QDs lattice⁴⁵. The emission color can vary from green to deep red, depending on the transition. The typical fluorescent relaxation time of this emission is of the order of milliseconds.^{55, 65, 66} The Mn doping growth scheme is used to control the radial position of dopants within the core/shell NPs.^{45, 54, 67, 68} The ZnS shell helps not only for holding the dopants in the core or shell, but additionally increases the range of optical properties that can be derived from the dopant inclusion with QDs. Yang et al. reported the synthesis of Mn^{2+} doped CdS/ZnS core/shell NPs.⁴⁵ The diameter of the starting host core and the thickness of the host shell determined the radial position of Mn^{2+} inside the CdS/ZnS core/shell NPs. The authors discovered the effects of position controlled Mn-doping on the optical properties by synthesizing three different types of CdS/ZnS core/shell NPs with Mn^{2+} ions in three different locations: within the CdS core, at the core/shell interface, and within the ZnS shell. The electron paramagnetic resonance (EPR) spectra in these three types of core/shell structures indicated that the Mn-dopants were indeed located inside the QDs. The measured quantum yield of the Mn emission was much higher when the dopants resided within the ZnS shell. This was interpreted as an effect partially caused by the inhomogeneity of local crystal-field strain inside the shell. The narrowing of the EPR-peak line-width was also consistent with weaker Mn-Mn interactions and less local strain on the Mn-dopants

Quantum Dots: Synthesis, characterization and electrochemical sensing for life sciences

when they were located in the ZnS shell. For the same system, an interesting strong dependence of the rate of exciton-Mn energy transfer on the doping radial location within the ZnS shell for a given dopant concentration was found by Chen et al.⁵⁸

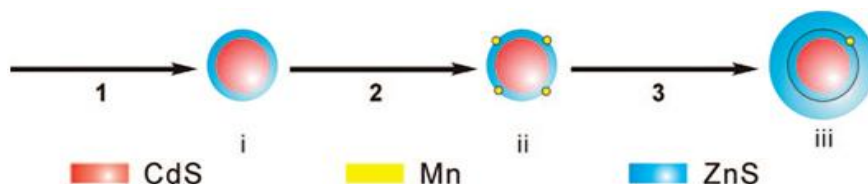


Figure 2: (1) Synthesis of CdS/ZnS Quantum dots, (2) Mn-dopant growth, and (3) hostshell growth; (i) CdS/ZnS host particles, (ii) CdS/ZnS nanoparticle with surface-bound Mn, and (iii) Mn doped CdS/ZnS nanoparticles. (taken from Yang et al.)⁴⁶

1.2.1. Photoluminescence of Mn doped CdS/ZnS QDs

The photoluminescence properties of Mn-doped nanoparticles have been extensively investigated in the last two decades. Generally, while a photon is absorbed by a Mn-doped QDs, an exciton (an electron-hole) is created and confined within this QDs.⁶⁹ This exciton can recombine via three ways, explained by Chen et al: radiative recombination at the nanoparticles band edge, non-radiative recombination at the nanoparticles band edge, and energy transfer to a Mn ion within the QD (as shown in the Figure 3). Later the energy is transferred to Mn; the excited Mn (at 4T_1) relaxes to its ground state (6A_1) with the constant rate.⁵⁸

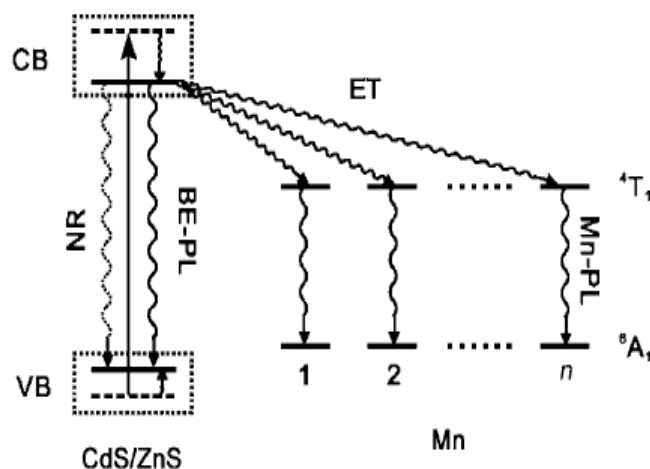


Figure 3: Energy states and carrier relaxation pathways in aMn doped CdS/ZnS NPs. CB conduction band, VB valence band, ET energy transfer, BE band edge, PL photoluminescence (taken from Chen et al.).⁵⁸

Quantum Dots: Synthesis, characterization and electrochemical sensing for life sciences

1.2.2. Förster resonance energy transfer (FRET) in Mn doped NPs.

The Förster resonance energy transfer (FRET) associates a donor fluorophore living in an excited electronic state, which may transfer its energy due to excitation to a neighboring acceptor chromophore in a non-radiative way. The Förster resonance energy transfer (FRET) between two molecules is an important physical phenomenon with considerable interest for the understanding of some biological systems and with potential applications in optoelectronic and thin film device development.^{70,71}

FRET phenomenon can take place in the QDs based system, in which QDs incorporated with organic fluorophores, or with doped material or with combination of both may exchange energy in a non-radiative manner. QDs may be used as acceptors as in case of lanthanides and multiplexed read-out of fluorescence with long lifetimes is possible.^{72,73} QDs can also be used as donors for organic fluorophores and as acceptors.^{74, 75 76} Due to their optical properties, the QDs can be continuously tuned and it is possible to create a FRET donor for any number of organic fluorophores that emit between 510 to 640 nm.^{72, 77-82} Recently, we have demonstrated that lifetime multiplexing is an interesting alternative to spectral multiplexing.⁸³ In this previous study ATTO590 dye molecules incorporated with gold nanoparticles (NPs) exhibited an exponential decay with a lifetime of a few ns (corresponding to the lifetime of free dye molecules), while dye molecules incorporated to CdSe/ZnS QDs confirmed a non-exponential decay with a slow component of more than 100 ns due to the FRET from the QDs to the dye. Kaiser et al. demonstrated the fundamental possibility to find out the mixing ratio for dyes with equal luminescence spectra but very different transients.^{83, 84} Doping of CdS/ZnS QDs with Mn ions leads to long-lived fluorescence lifetimes based on the dipole forbidden internal 3d-transition.^{85, 86} Uwe et al. [A2] reported that the photoluminescence decay time of organic fluorophores can be amplified up to the millisecond time scale by combining them to Mn-doped CdS/ZnS QDs. These Mn doped CdS/ZnS core/shell nanocrystals were reported by Yang et al., based on a four step synthesis (Figure 2).⁴⁶

Quantum Dots: Synthesis, characterization and electrochemical sensing for life sciences

In a recent study, we demonstrated that the double energy transfer process occurred within the three fluorescence sources, first among the Mn-doped CdS/ZnS QDs, *i.e.* from the CdS/ZnSQDs to the Mn ions, and then second from the excited Mn ions to an organic dye, the organic fluorophore ATTO633 incorporated at the surface of Mn-doped CdS/ZnS QDs (Figure 4). The fluorescent spectrum of Mn-doped CdS nanocrystals shows yellow emission at 585 nm as well as blue emission at 400 nm (Figure 4). The comparison of two emission spectra, where emission 1 and emission 2 were collected by monitoring blue and yellow emission, respectively, also suggested that Mn-related yellow emission results from the energy transfer from the photoexcited CdS host core to the Mn activator resided in ZnS shell.

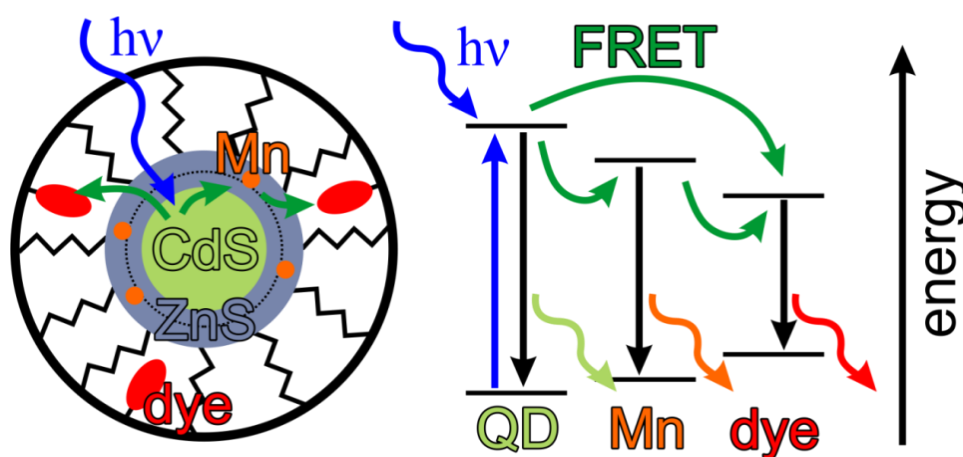


Figure 4: On the left a sketch of CdS/Mn:ZnS/ZnS QDs incorporated dye molecules is shown. The Mn ions are located inside the ZnS shell. A scheme of the different energy states is shown on the right. The excitation of the CdS core is indicated by the blue wavy arrow and the green arrows show the possible energy transfer pathways. The QD, the Mn^{2+} ions, and the dye can all undergo a radiative recombination to the respective ground state under emission of photons. This Figure was adapted from Uwe et al.[A2].

Mn ions are adsorbed onto the surface of CdS or CdS/ZnS core/shell nanocrystals. Mn adsorption on the surface of nanocrystals includes the formation of weakly and strongly attached Mn. The creation of weakly attached Mn is linked with a chemical equilibrium between adsorbed Mn atoms on the nanocrystal surface and the unattached Mn atoms in the reaction solution. An activation-energy barrier $(211 \pm 13 \text{ kJ/mol})^{46}$ is calculated by unimolecular decomposition reaction for the formation of strongly attached Mn atom.

Quantum Dots: Synthesis, characterization and electrochemical sensing for life sciences

Additionally, both weakly and strongly attached Mn atoms can be detached through ZnS shell growth. The substitution of weakly attached Mn can occur at or below 240 °C, although the substitution of strongly attached Mn atom needs a slight higher temperature. The reaction yield of substitution is strongly dependent on ZnS shell growth temperature, explaining that the Mn substitution to overcome activation energy limit. The Mn growth yield is not dependent on the size, shape and nanocrystal structure of nanocrystals.⁴⁶ The diameter of the core and the thickness of the shell determined the radial position of Mn dopants within the host core/shell. The calculated quantum yield of the Mn fluorescence was much higher while the dopants were placed within the ZnS shell. This was explained as a result partially caused by the inhomogeneity of host crystal field strain inside the ZnS shell.⁴⁶

1.3. Biosensors

Biomolecular sensing is a pivotal tool for diagnostics of various diseases. For instance, abnormal protein/gene expression may be triggered during a functional disorder of an organ from a living organism. However sensing can be really onerous owing to very weak signals from the analyte. The signal can be enhanced by the use of catalysts which not only accelerate the reaction but also can amplify the signal if properly handled.

The first biosensor based on glucose was introduced by Clark and Lyons.⁸⁷ After that, hundreds of biosensors have been developed by many researchers around the world. Sensors are instruments that count a physical, chemical, or biological change and convert them into a recordable data.⁸⁸ The sensor contains a detection element that allows the selective response to a specific analyte or a group of analytes, therefore minimizing interferences from other sample components (Fig. 7). One more important part of a sensor is the transducer or the detector device that generates a signal. A signal processor collects, amplifies, and displays the output signal.

Quantum Dots: Synthesis, characterization and electrochemical sensing for life sciences

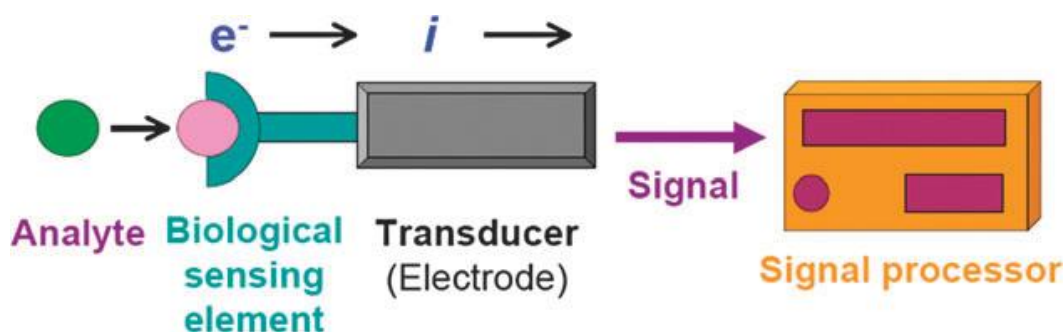


Figure 7: A Biosensor schematic for electrochemical detection (adopted from Ronkainen et al.).⁸⁹

Electrochemical biosensors (a part of chemical sensors) are electrochemical transducers with high specificity of biological detection systems. Electrochemical biosensors can be divided into two major categories based on the type of the biological recognition process that is biocatalytic devices and affinity sensors.^{90, 91} Electrochemical biosensors based devices contain a biological recognition element (proteins, enzymes, antibodies, nucleic acids, cells, tissues or receptors) that selectively responds with the specific analyte and generates an electrical signal that is connected to the concentration of the analyte being investigated. Electrochemical biosensors are recognized for the detection of glucose and lactose. Affinity sensors rely on a selective binding interaction between the analyte and a biological component such as an antibody (Figure7).^{89, 92-95}

1.3.1. Enzymes

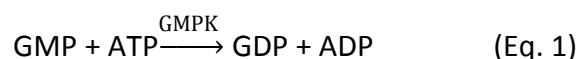
Enzymes are commonly used biocatalysts in biosensors. They have a task to speed up reactions by providing an alternative reaction pathway of lower activation energy. Similar to all catalysts, enzymes take part in the reaction. Enzymes do not undergo permanent changes and so remain unchanged at the end of the reaction. They can change the rate of reaction, not the position of the equilibrium. Most organic chemical catalysts catalyze a wide range of reactions. Numerous enzymes consist of a protein and a non-protein (called the coenzymes). Enzymes are generally highly selective due to the structure and catalyze specific reactions only. Ureases are highly specific for one type of compound.^{96, 97} Some of them are specific for one group of substrates. Alkaline Phosphatase (ALP) is specific for the phosphate group and can cleave it from a wide range of mono-phosphate esters.⁹⁸⁻¹⁰² The structure of enzymes consists of single peptide chain; the active molecule for selectivity can

Quantum Dots: Synthesis, characterization and electrochemical sensing for life sciences

be a separate molecule, attached with the polypeptide backbone. Some of the molecules are permitted to contact the active part, so that specificity of enzyme is mostly determined by access through the protein shell and the binding part, and not by the active part itself.^{98, 103-105}

1.3.1.1. Guanylate kinase (GMPK)

GMPK is crucial enzyme for the establishment of prodrugs used for the treatment of viral infections and cancers diseases¹⁰⁶ Thus, it is medically important to reveal its enzymatic mechanism and the structural foundation for its nucleotide specificity. GMPK could play a part in the design of enhanced antiviral and antineoplastic agents. Guanylate kinase is an enzyme that catalyzes the chemical reaction given in Equation 1.



Therefore, the two substrates of this enzyme are ATP (adenosine triphosphate) and GMP (guanosine monophosphate), where as its two products are ADP (adenosine diphosphate) and GDP (guanosine diphosphate). This enzyme belongs to the family of transferases (enzymes that enact the transfer of specific functional groups).¹⁰⁷⁻¹⁰⁹ The enzymatic activity of GMPK was measured by a standard NADH-dependent LDH/pyruvate kinase-coupled assay using a UV-Vis spectrophotometer.¹¹⁰

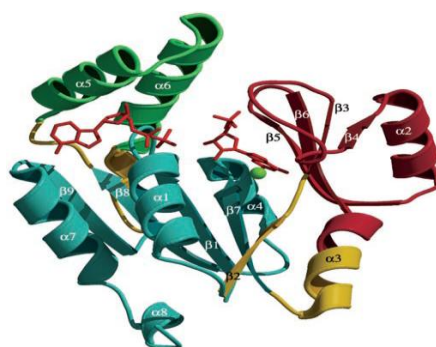


Figure 5: Ribbon diagram of $m\text{GMPK}_{\text{GMP-ADP}}$ (adopted from Sekulic et al.)¹⁰⁷

Quantum Dots: Synthesis, characterization and electrochemical sensing for life sciences

1.3.1.2. Guanylate monophosphate (GMP)

Guanylate monophosphate is a cofactor and belongs to a nucleotide, significant in metabolism and RNA synthesis. GMP consists of the phosphate group, the pentose sugar ribose, and the nucleobase guanine; therefore it is a ribonucleoside monophosphate. GMP and other nucleotide metabolites have traditionally been detected by assays based on the use of radiolabeled substrates, or *via* spectroscopic multi-step coupled-enzyme assays.¹¹⁰⁻¹¹³

1.3.1.3. Pyruvate kinase (PK)

Pyruvate kinase (PK) is an enzyme that converts glucose (C₆H₁₂O₆) into pyruvate (called glycolysis). It catalyzes the transfer of a phosphate group from phosphoenolpyruvate (PEP) to adenosine diphosphate (ADP), resulting in pyruvate and ATP.



PK deficiency is a genetic disorder (lack of the enzyme PK), which is used by red blood cells. Without this PK enzyme, red blood cells break down too easily, consequentially in low levels of these cells (hemolytic anemia).¹¹⁴ Pyruvate kinase (PK) deficiency and related disorders of the red cell glycolysis, initially diagnosed in the early 1960s¹¹⁵ is the most frequent enzyme irregularity of the glycolytic pathway, and the most common reason of inherited non-spherocytic haemolytic anaemia, mutually with class of glucose-6-phosphate dehydrogenase deficiency¹¹⁶. The disease is transmitted as an autosomal recessive trait, clinical symptoms usually occur in compound heterozygotes for two mutant alleles and in homozygotes.^{115, 117}

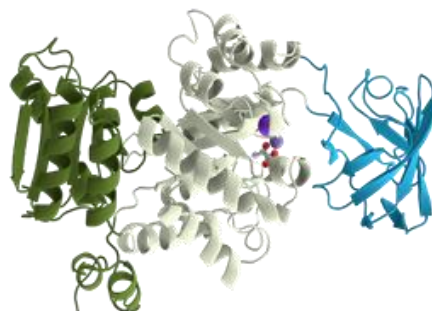


Figure 6: Pyruvate kinase diagram (taken from Cook et al.)¹¹⁴

Quantum Dots: Synthesis, characterization and electrochemical sensing for life sciences

1.3.1.4. Lactate dehydrogenase (LDH)

Lactate dehydrogenase (LDH) is a common and well-studied enzyme, which is found in all types of cells. LDH catalyzes the conversion of pyruvate to lactate and back, as it converts NADH to NAD⁺.^{118, 119}



Lactate dehydrogenase (LDH) is a LDH has been used as a marker enzyme to detect cell damage and cell toxicity induced by many diseases and hazardous exposures.⁹¹

1.3.1.5. Nicotinamide adenine dinucleotide hydrogen (NADH)

NADH is a significant coenzyme originates in vivo during dehydrogenase based enzymatic reactions and it has a number of essential parts in biological systems.¹²⁰ NADH is a dinucleotide, because it contains two nucleotides attached through their phosphate groups. First contains an adenine base and the second nicotinamide. Nicotinamide adenine dinucleotide exists in an oxidized and reduced form as NAD⁺ and NADH respectively.¹²¹ Consequently many researchers have consider the electrochemical oxidation of NADH to construct NAD⁺-dependent enzymatic electrochemical biosensors using for food and medical diagnosis.^{122, 123 124}

1.3.2. QD-Based Electrochemical biosensors

Quantum dots can be immobilized on gold (Au), silver (Ag) and platinum (Pt) substrate electrodes through covalent coupling (SAMs of dithiols¹²⁵) and electrostatic coupling (Layer by layer assembly)¹²⁶. In previous study, QD modified metal electrodes were used to detect different analytes and their corresponding enzymatic reactions with electrochemical methods like voltammetry etc.¹²⁷⁻¹²⁹ QDs play a very important role in this type of electrochemical detection system. They can be fabricated with different size and shape assisting the mediation of electrons from redox active group within the electrolyte. While their surfaces can be modified as well, they have become very useful technique for sensitive and selective recognition of specific species. With the incorporation of different

Quantum Dots: Synthesis, characterization and electrochemical sensing for life sciences

immobilization techniques (covalent or electrostatic) complex nanostructures can be fabricated. Since the selectivity to detect a particular analyte depends upon the material of the QD. Beside surface functionalization it is also feasible to synthesize hybrid structures of metals or magnetic semiconductor QDs.¹³⁰ For the electrochemical detections, QDs incorporated with metal electrodes are possible through light illumination.

Parak et al reported electrochemical biosensors based on modified electrode with quantum dots especially II_VI semiconductors (e.g., CdSe, CdS, ZnS, ZnSe) and FePt nanoparticles (NPs).^{127-129, 131, 132} They immobilized nanoparticles via self assembled monolayer (SAM) for the detection of hydrogen peroxide, glucose oxidase, nicotinamide adenine dinucleotide(NADH), p-aminophenyl phosphate (pAPP) with alkaline phosphatase (ALP).

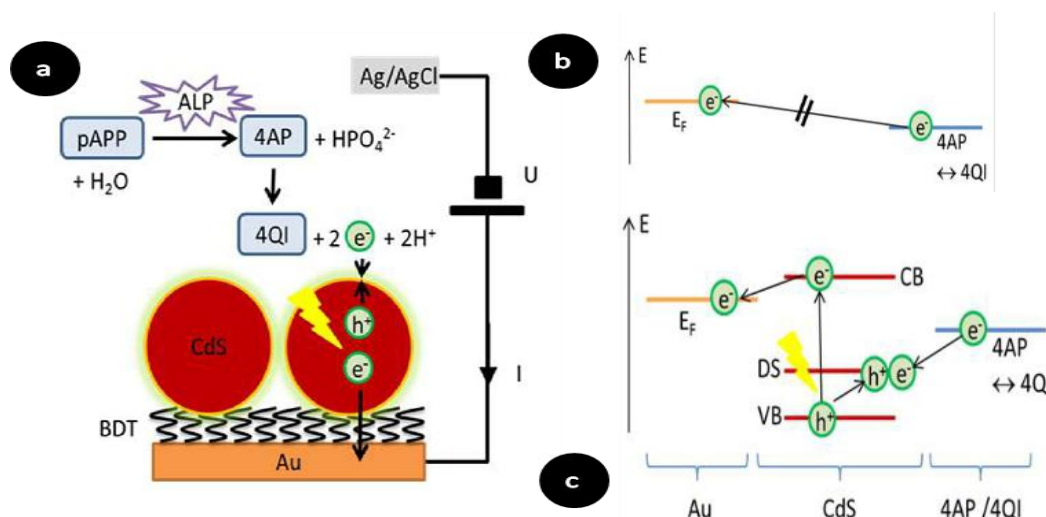


Figure 8: a) The CdS QDs immobilized on Au electrode via a BDT layer. pAPP is in solution degraded by ALP to 4AP. b) Without QDs Energy diagram c) Energy diagram with Illuminated QDs can act as redox mediator. (adopted from Khalid et al.)¹²⁸.

In a previous study, Khalid et al.¹²⁸ investigated the feasibility of a light controlled electrochemical biosensor for detection of the substrate p-aminophenyl phosphate (pAPP) with the enzyme alkaline phosphatase (ALP). QDs were immobilized on gold surfaces through 1,4-benzenedithiol (BDT) chains. Illumination of QDs promoted the oxidation of 4AP which could be detected through a corresponding photocurrent. Excited QDs conduction-band electrons can flow into an electrode or alternatively, to an electron acceptor in

Quantum Dots: Synthesis, characterization and electrochemical sensing for life sciences

solution. Electrons can also be transferred from an electrode or a solubilized electron donor to QDs valence-band holes. A bias voltage U is applied across Au electrode and an Ag/AgCl reference electrode in the electrochemical biosensor's bath solution. *p*-aminophenyl phosphate (pAPP) degraded into 4-aminophenol (4AP) in the presence of alkaline phosphatase (ALP) in the solution. Electron hole pairs are generated due to illumination of QDs. This directs to oxidation of 4AP to 4-quinoneimine (4QI) on the surface of QD, and here electrons are transferred to the QD. Electrons are transferred to the Au electrode and can be perceived as oxidation current I (figure 8(a)). Energy levels E are shown in figure 8(b). The absence of the QDs on the gold electrode as redox mediator oxidation of 4AP cannot happen in case the bias potential U is not sufficiently positive. For the condition of oxidation the Fermi level E_F of the Au electrode would need to be lower than the energy level at which electrons upon 4AP oxidation are released. In figure 8(c), illuminated QDs can act as redox mediator. Defect states (DS) on the surface of QD (which are vigorously above the valence band (VB)) avoid immediate recombination of the light generated electron hole pairs. In this way resulting electron from the oxidation of 4AP to 4QI can be transferred to the DS of the QD. The electrons from the conduction band (CB) can be passed through the BDT layer to the gold electrode, which is perceived as oxidation/photocurrent.¹²⁸

A light-addressable modified Au electrode with CdS@FePt nanoparticles was immersed via dithiol linker layer.¹²⁷ This study revealed that trans-stilbenedithiol provides high quality self-assembled monolayers (SAM) compared to benzene dithiol and biphenyl dithiol, in case they are formed at elevated temperatures. CdS QDs in good electrical contact with the electrode permit the generation of the current under appropriate illumination. FePt NPs have been used as catalytic sites for the reduction of hydrogen peroxide (H_2O_2) to water (H_2O). Either only CdS QDs or only FePt NPs immobilized at the Au electrode surface resultant no response of the photocurrent to H_2O_2 was found.¹²⁷

1.3.2.1. Guanosine Monophosphate detection

Recently, we show that photocurrent generation at QDs modified electrode can be effectively combined with a cascade enzymatic reaction to product in a light addressable

Quantum Dots: Synthesis, characterization and electrochemical sensing for life sciences

sensor for detecting the nucleotide GMP. Here, GMPK, which catalyzes the phosphoryl group transfer from ATP to GMP to form ADP and GDP, is an essential enzyme in the guanine nucleotide metabolism of cellular organisms.¹⁰⁷⁻¹⁰⁹ GMP is required for a variety of cellular metabolic processes, as well as for RNA and DNA formation.¹⁰⁶ Such metabolic processes include the recycling of GMP, products of RNA and DNA deterioration, and act as a second messenger cyclic GMP (cGMP) through the so-called cGMP cycle (cGMP → GMP → GDP → GTP → cGMP).¹³³

The first reaction (equation no.1) involves catalytic conversion of GMP by GMPK, which warrants for specificity. The reaction product ADP is a co-enzyme for the enzymatic conversion of phosphoenol pyruvate to pyruvate in a second reaction (equation no. 2) mediated by pyruvate kinase. Pyruvate in turn is co-enzyme for oxidation of NADH to NAD⁺. This third enzymatic reaction (equation no.3) mediated by LDH is then finally electrochemically detected.¹³³

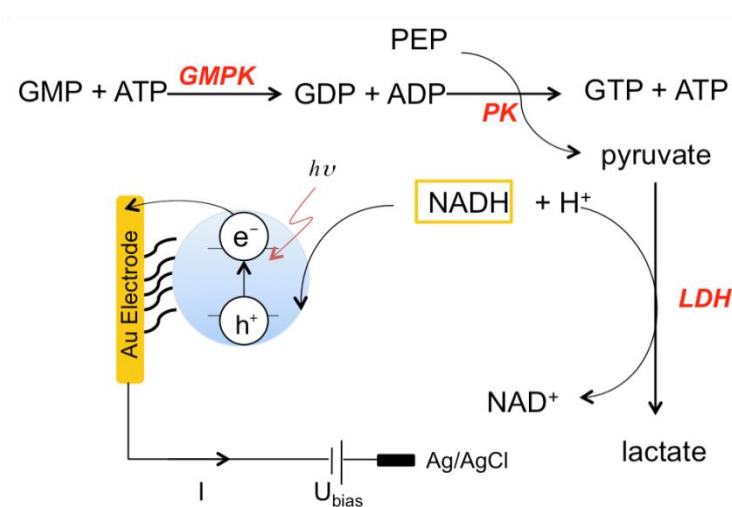


Figure 9: Detection of GMP using a NADH-dependent electrochemical assay.¹³³

Quantum Dots: Synthesis, characterization and electrochemical sensing for life sciences

2. Synthesis and Characterization of QDs

2.1. Synthesis of CdS QDs

Zinc-blend CdS nanocrystals were synthesized according to a previously published method.^{67, 134} In a typical synthesis, cadmium oxide (0.126 g, 0.98mmol), oleic acid (2.02 g, 7.1mmol), and 1-octadecene (ODE,12.0 mL) were loaded into a three-neck flask, degassed under vacuum for 10 minutes, and heated at 300 °C under nitrogen atmosphere. A solution of sulfur in ODE (0.25 M, 2.0 mL) was then injected into the mixture and the temperature dropped to 250 °C. After the injection, the solution was left for 5 minutes at 250 °C for the growth of the nanocrystals. The solution then was allowed to cool to room temperature by removing the heating mantle. The CdS QDs were precipitated with acetone and then precipitate was rinsed twice by dissolving and precipitating with chloroform and methanol. Finally, CdS nanocrystals were redispersed in chloroform for further use.

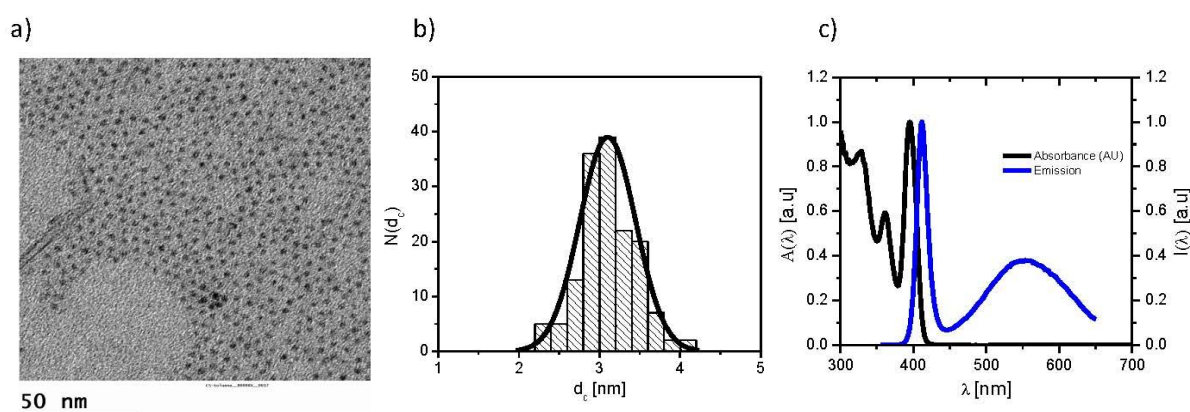


Figure 10: a) TEM image of CdS QDs. b) Typical CdS QD size (d_c) distribution, the mean diameter of QD is $d_c = 3.02 \pm 0.61$ nm. c) Normalized absorbance and emission spectra of CdS QDs. The higher emission narrow band is assigned to band edge emission, while the lower emission broad band comes from trap states.¹³⁵ This Figure was adapted and modified from Uwe et al. [A2].

The concentration of CdS quantum dots was determined by using the Beer-Lambert law as follows, $A = c \times \epsilon \times L$. Where A is the absorbance, ϵ is the molar extinction coefficient of the sample ($M^{-1} \cdot cm^{-1}$), L is the path length (cm) and c is the concentration of the sample. Here the value $\epsilon = 297788 M^{-1}cm^{-1}$ corresponding to their first exciton peak at 392 nm was

Quantum Dots: Synthesis, characterization and electrochemical sensing for life sciences

used.¹³⁶ The concentration is $c = (A / \epsilon / L)$ (dilution factor) = $(0.26638 / 297788 \text{ M}^{-1} \cdot \text{cm}^{-1} / 1 \text{cm})$ (50) = $44.72 \mu\text{M}$. The absorbance was obtained from the first exciton peak of the UV/Vis spectra. The UV/Vis spectra were recorded with an Agilent Tech. 8453UV/Vis spectrophotometer.

2.2. Synthesis of ZnS shell around CdS core (CdS/ZnS QDs)

Zinc-blend CdS quantum dots (QDs) were synthesized according to previously published methods^{67, 134}. The most significant reactions conditions are N_2 atmosphere and high temperature. Cadmium precursor and sulfur precursors are dissolved in surfactant (ODE, oleic acid). At high temperature, nucleation occurs and lowering temperature a little (around 250°C), growth starts and monodisperse quantum dots appear. Following 5min the injection of the stock solution(S:ODE) a “shoulder” at about 392 nm is clearly visible in the absorbance spectrum (Figure 5) and this shows the formation of the CdS QDs in solution. After washing steps, QDs were dissolved in chloroform for further used.

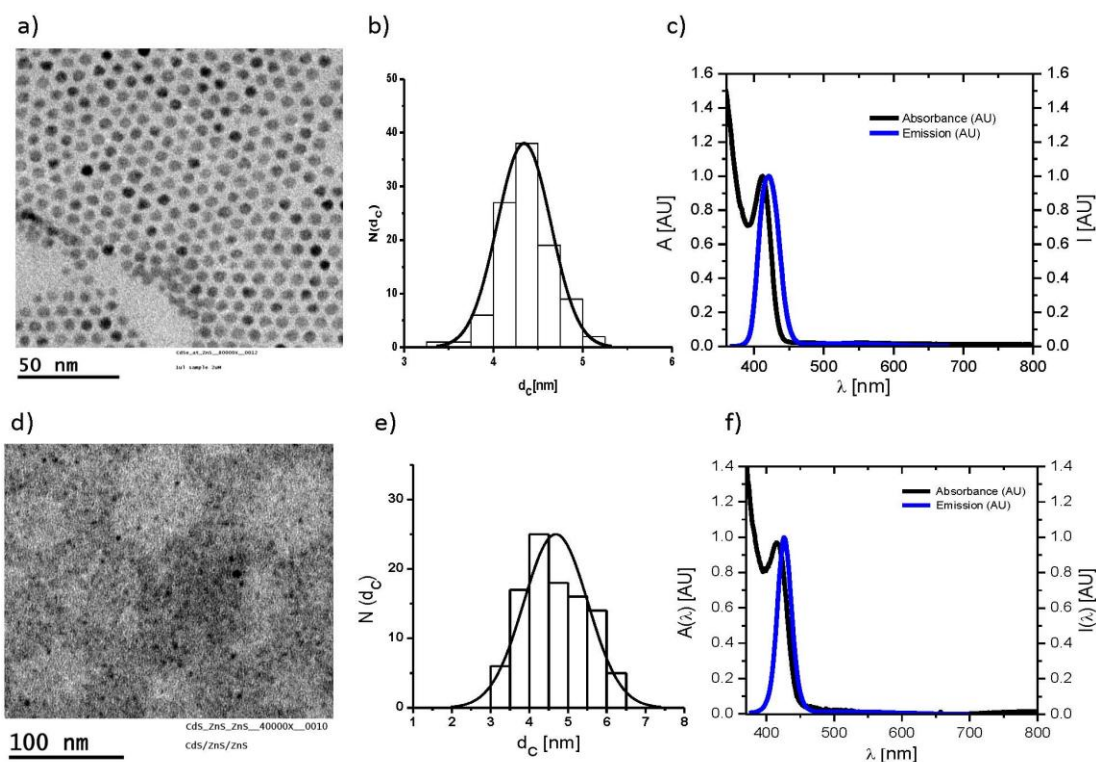


Figure 11: a) TEM image of CdS/ZnS QDs (2monolayer (ML) of ZnS Shells). b) Typical CdS/ZnS QD size (d_c) distribution, the mean diameter of CdS/ZnS QD (2 monolayer (ML) of ZnS Shells) is $d_c = 3.62 \pm 0.25 \text{ nm}$. c)

Quantum Dots: Synthesis, characterization and electrochemical sensing for life sciences

Normalized absorbance and emission spectra of CdS/ZnS NPs (2monolayer (ML) of ZnS shell). d) TEM image of CdS/ZnS QDs (6 monolayer (ML) of ZnS Shells). e) Typical CdS/ZnS QDs (6 monolayer (ML) of ZnS shell) size (dc) distribution, the mean diameter of QD is $d_c = 4.5 \pm 0.8$ nm. f) Normalized absorbance and emission spectra of CdS/ ZnS QDs (6 monolayer (ML) of ZnS shell). This Figure was adapted and modified from Uwe et al. [A2].

ZnS shells were grown around the CdS QDs to passivate the CdS QDs core and enhance their fluorescence using zinc stearate and sulfur as zinc (Zn) and sulfur (S) precursors.⁴⁶ The amount of the Zn/S precursor solution of shell was calculated according to the previously published methods.¹³⁷ The ZnS shells were grown monolayer by monolayer; by alternate injections of a solution of zinc stearate (40 mM) in ODE and sulfur in ODE (40 mM). Growth time was 10 minutes after each injection of zinc stearate or sulfur. When the desired shell thickness (6 monolayers) was attained, the temperature of the solution was reduced to room temperature. The resulting nanocrystals were further purified by three precipitation-redispersion cycles using methanol and chloroform. Finally, CdS/ZnS nanocrystals were redispersed in chloroform. The resulting size distribution as determined with TEM is shown in Figure 11(b).

2.3. Doping of Mn in ZnS shell of the CdS/ZnS QDs (CdS/Mn:ZnS QDs)

Mn²⁺ ions were introduced in the host ZnS shell. Briefly, CdS/ZnS NPs (25.2 μ M, 50.4 nmol, QDs concentration calculated as previously reported⁴⁶) dissolved in chloroform were added into a three neck flask to a mixture of 1-octadecene (ODE) and oleylamine (OAm) (8 ml, ODE/OAm: 3:1) and the chloroform was removed under vacuum. Under N₂ flow, the solution was heated to 250°C. The precursors for doping (220 μ l, 1.2 μ mol, Mn precursor (Mn(S₂CNEt₂)₂) was prepared according to the literature described by Yang et al.⁴⁶) were introduced into the solution by dropwise addition. After the addition, the mixture was stirred at 250 °C for 20 min. The reaction was stopped by removing the heating mantle and allowing the solution to cool at room temperature. The resulting CdS/Mn:ZnS NPs were purified *via* precipitation by adding acetone, and redispersed in chloroform.

Quantum Dots: Synthesis, characterization and electrochemical sensing for life sciences

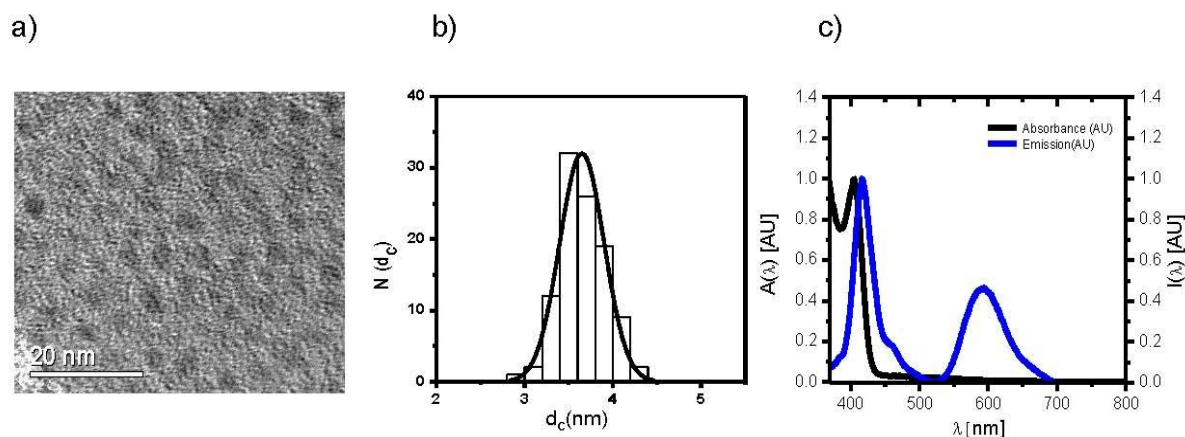


Figure 12: a) TEM image of CdS/Mn:ZnS QDs. b) Typical CdS QD size (d_c) distribution, the mean diameter of QD is $d_c = 3.65 \pm 0.3$ nm. c) Normalized absorbance and emission spectra of CdS/Mn:ZnS NPs.

2.4. Passivation of CdS/Mn:ZnS NPs with ZnS shell

Zinc-blend CdS quantum dots (QDs) were synthesized according to previously published methods.^{67, 134} Similarly two monolayers were grown around CdS cores as described in section 2.4.1. The dopant precursors ($\text{Mn}(\text{S}_2\text{CNET}_2)_2$, as described by Yang et al.), were introduced into the host ZnS Shell.⁴⁶ The precursors were added into the host solution dropwise at growth temperature. The solution was left stirring at this point for 20 minutes before removing the heating mantle to cool down the solution at room temperature. The resulting CdS/Mn:ZnS NPs were purified via precipitation method. Further four ML of ZnS shell were grown as described in above.

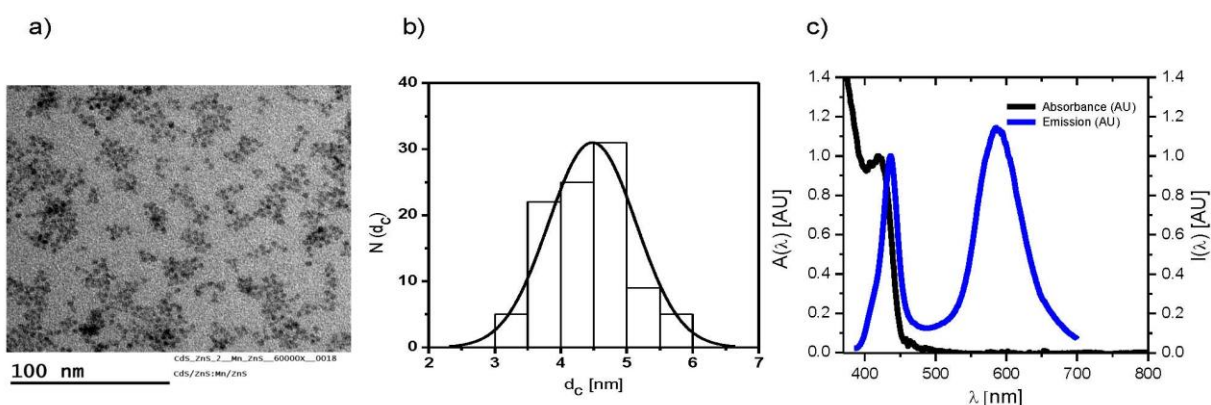
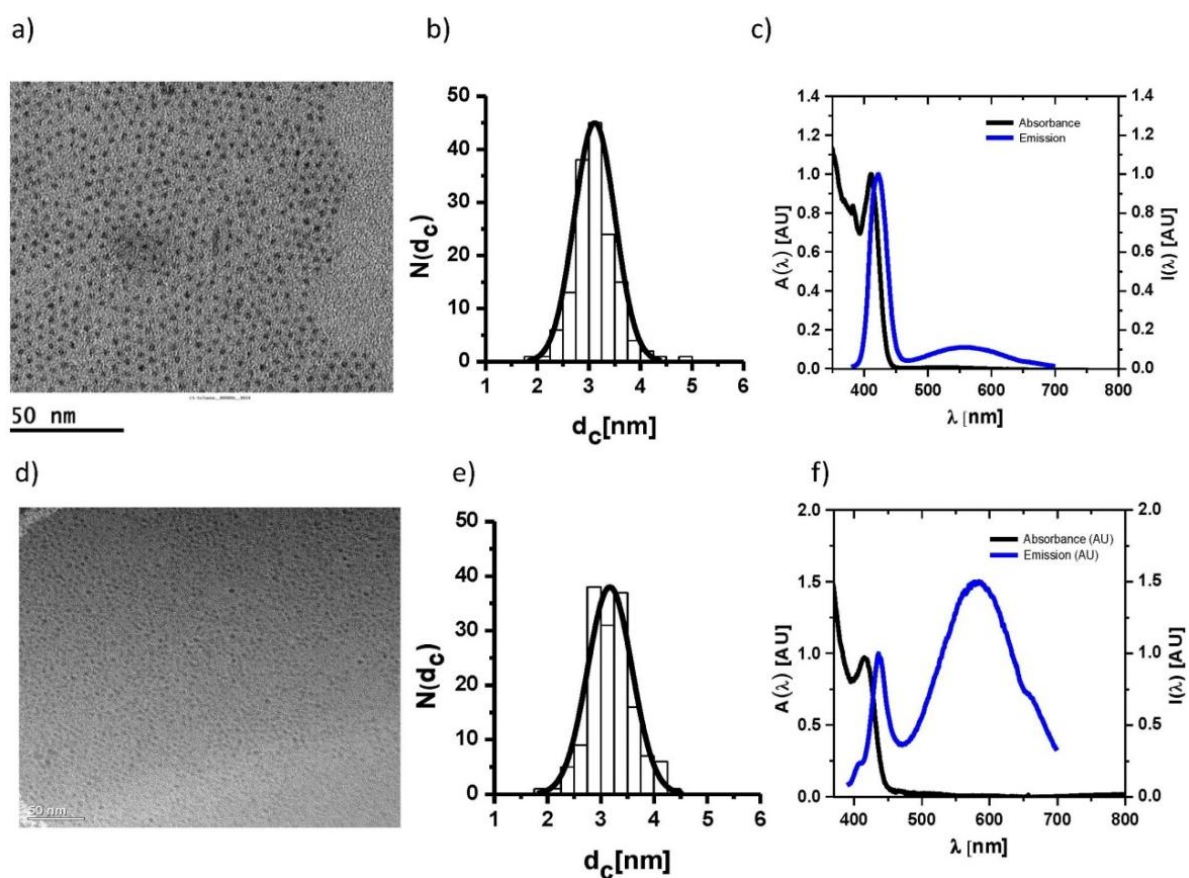


Figure 13: a) TEM image of CdS/Mn:ZnS/ZnS NPs. b) Typical CdS/Mn:ZnS/ZnS QD size (d_c) distribution, the mean diameter of QD is $d_c = 4.48 \pm 0.7$ nm. c) Normalized absorbance and emission spectra of CdS/Mn:ZnS/ZnS NPs. This Figure was adapted and modified from Uwe et al[A2].

Quantum Dots: Synthesis, characterization and electrochemical sensing for life sciences

2.5. Synthesis of Mn doped CdS quantum dots (CdS:Mn QDs)

The Mn^{2+} ions were incorporated into the CdS quantum dots using the previously published method developed by Yang *et al.* [5]. The CdS quantum dots suspended in chloroform solution of host particles, CdS (2 mL, 12.6 μM ; CdS QDs synthesis were explained in the section 2.1; QDs concentration calculated as previously reported [4]), was added into a mixture solution of 1-octadecene (ODE) and oleylamine (OAm) (8.0 mL, ODE:OAm 3:1) in a three-neck flask, and then chloroform was removed under vacuum. Under N_2 flow and with continuous stirring, the solution was heated to 250 $^\circ\text{C}$, and 0.22 mL of the doping precursor solution (5 mM, 1.2 μmol of Mn (S_2CNET_2)) were introduced into the solution by dropwise addition. After the addition, the mixture was stirred at 250 $^\circ\text{C}$ for 20 min, and then was allowed to cool to room temperature by removing the heating mantle. The resulting CdS:Mn nanocrystals were purified by precipitation by adding acetone, and re-dispersed in chloroform.



Quantum Dots: Synthesis, characterization and electrochemical sensing for life sciences

Figure 14: a) TEM image of CdS QDs. b) Typical CdS QD size (d_c) distribution, the mean diameter of QD is $d_c = 3.01 \pm 0.39$ nm. c) Normalized absorbance and emission spectra of CdS QDs. d) TEM image of CdS:Mn QDs. e) Typical CdS:Mn QD size (d_c) distribution, the mean diameter of doped QD is $d_c = 3.01 \pm 0.42$ nm. f) Normalized absorbance and emission spectra of CdS:Mn QDs.

2.6. Synthesis of the CdSe/ZnS core/shell QDs

CdSe QDS were synthesized according to a procedure previously described.^{138, 139} In a typical synthesis, 5.75 g of hexadecylamine (HDA, technical grade, Sigma-Aldrich #H7.40-8), 2.26 g of trioctylphosphine oxide (TOPO, 99%, Sigma-Aldrich #22.330-1), 2.20 g of dodecylphosphonic acid (DDPA 98%, Sigma-Aldrich) and 501 mg of CdO (99.99+%, Sigma-Aldrich #20.289-4) were added in a 50 ml 3-necked flask connected to an N₂ vacuum line assembled in an N₂ in the glove box. The mixture was degassed at 120 °C for 10 minutes and then heated to 300-320 °C until solution turned colorless and clear. 1 ml of TBP (tributylphosphine, 99%, ABC #15-5800) was then injected in to the solution and the temperature was lowered to 260 °C. Mean while, 320 mg of Se powder (99.99%, Sigma Aldrich #22.986-5) were dissolved in 1.28 g of TBP under vigorous stirring and the resulting solution was injected in the CdO/TOPO/HDA mixture. After injection, the temperature dropped but was allowed to recover to 260 °C and was then maintained at this level throughout the synthesis. 3-5 minutes after the injection the color of the solution turned from colorless to slightly yellow, indicating the nucleation of CdSe nanocrystals. This color turned yellow to light orange 2-5 minutes after the injection (first exciton absorption peak at 515 nm). The growth rate slightly varied from synthesis to synthesis, but it was always sufficiently low so that the synthesis could be stopped whenever the first exciton peak in the absorption spectrum reached at desired value. The synthesis was stopped by removing the heating mantle and by cooling the reaction mixture of the flask at room temperature. The resulting CdSe QDs were purified by precipitation by adding methanol, and redispersed in toluene.

Quantum Dots: Synthesis, characterization and electrochemical sensing for life sciences

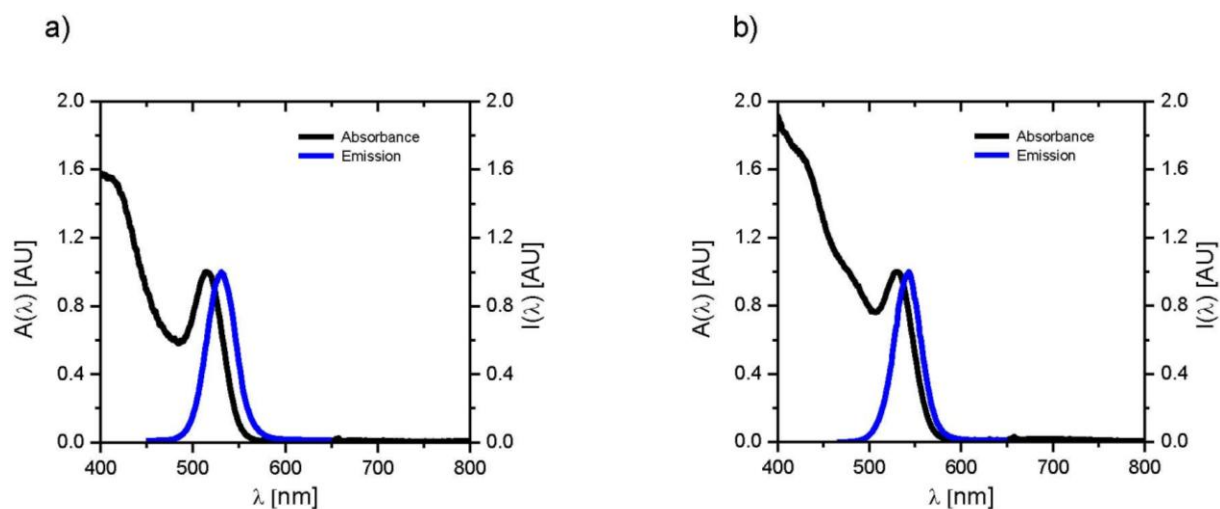


Figure 15: a) Normalized absorbance and emission spectra of CdSe QDs, absorbance of the QDs 515 nm and emission at 530nm. b) Normalized absorbance and emission spectra of CdSe/ZnS core-shell QDs, absorbance of the QDs 531 nm and emission at 543nm.

For the growth of the ZnS shell, 12 g of TOPO (technical grade, Alfa Aesar #14114) were added in a 50 ml 3-necked flask, switched to vacuum at 120 °C for 10 minutes. One ml of TOP (Trioctylphosphine, technical grade, Sigma-Aldrich #11.785-4) was injected into the flask. 60 mg of a dry QDs powder were dissolved in 3 mL of chloroform and the resulting solution was injected into the flask. The chloroform was removed by switching to vacuum for few minutes. The temperature of the solution was then increased to 160 °C. The ZnS shell precursor was freshly prepared by adding 0.647 g of a solution of diethylzinc ($C_4H_{10}Zn$, 1.0 M solution in heptane, Sigma-Aldrich #40.602-3) and 0.19 g of hexamethyldisilathiane ($C_6H_{18}Si_2S$) (Aldrich#28.313-4) in 4.73 g of TBP. Several drop-wise injections of the ZnS precursor were added (1 mL each) at 160 °C. The waiting time after each injection was of the order of 5-10 minutes. The injections were done dropwise, to permit a slow and uniform shell growth on the QDs and to prevent the nucleation of ZnS crystals. After the first few injections, the luminescence from the nanocrystals increased, indicating the growth of a ZnS shell. The luminescence then reached a maximum intensity, which was dependent on the particular QDs size. The best possible number of injections which maximized the final fluorescence quantum yield varied by synthesis, and ranged from 3-5 for the largest QDs sizes to 6-7 for the smallest QDs. After the injections were completed, the solution was

Quantum Dots: Synthesis, characterization and electrochemical sensing for life sciences

cooled to room temperature. The resulting CdSe/ZnS QDs were purified by precipitation by adding methanol and the mixture was centrifuged for 10 minutes at 300 rpm, and the precipitate was redispersed in chloroform.

Quantum Dots: Synthesis, characterization and electrochemical sensing for life sciences

3. Conclusions and outlook

Two amply different applications of semiconductor quantum dots have been discussed in this doctoral work mainly. In the first part it has been demonstrated that the incorporation of Mn ions as dopants within the ZnS shell of CdS/ZnS core-shell QDs leads to an efficient energy transfer from the excitonic QD states to the Mn states.[A2] A multistep growth of the ZnS shell was carried out to control the location of the Mn ions. The effective incorporation of the Mn ions into the QD core-shell structure was confirmed by a clearly observable PL band around 585 nm, which is due to the typical Mn transition.[A2] This PL band showed a mono-exponential decay with a lifetime of about 4.6 ms. These Mn-doped CdS/Mn:ZnS/ZnS QDs were further functionalized with an organic dye decorated amphiphilic polymer leading to a third fluorescence emitter centre, and therefore to a third PL band. Continuous wave spectra indicated a complex interaction of the different energy states within the QD system. Investigation of the decay characteristics of the respective PL bands through time resolved spectroscopy revealed the non-radiative energy pathways. It was concluded that the QD states act as an energy donor for the Mn as well as for the dye states. Interestingly, the Mn states have a two-fold transfer characteristic, as they also worked as an acceptor from the QD states and as a donor for the dye states. Especially the feeding of the dye states from the Mn excitation led to tremendous increase of the dye PL lifetime. By choosing a certain dye and thereby a certain spectral overlap it was able to control the lifetime of the dye PL in range of a few milliseconds.

In the second part it was demonstrated that photocurrent generation at QD electrodes can be effectively combined with a sequential enzymatic reaction cascade to result in a light-triggered sensor. Such a system can be used for detecting and quantifying the nucleotide guanosine monophosphate (GMP), which is a physiological metabolite generated by nucleic acid degradation, or by *de novo* biosynthesis in all cells. Here, three enzymes have been coupled in a reaction system where the last step is a redox reaction that was detected by photocurrent measurement. Whereas the enzyme GMPK catalyzing the first step ensured selectivity of the detection, NADH was consumed in the last enzyme reaction step, and this was subsequently detected at the QD electrode by an oxidation reaction at rather low

Quantum Dots: Synthesis, characterization and electrochemical sensing for life sciences

potential. It has to be emphasized that GMP detection can categorically provide access to the analysis of biochemical processes that produce or consume this nucleotide, e.g. GMPK activity, and in a more general context, we anticipate that adapted similar sensing platforms can be used for detection of almost any physiologically occurring nucleoside and nucleotide metabolite, and even nucleoside analogues used as drugs, which can be phosphorylated by kinases.

Hybrid NPs can be immobilized on gold substrate electrodes with dithiols (covalent coupling) and LbL assembly (electrostatic coupling). Hybrid NPs modified Au electrodes can be used to detect different analytes and their subsequent enzymatic reaction with photo electrochemical techniques. Hybrid NPs not only provide the selectivity but also allow constructing a unique system.

Quantum Dots: Synthesis, characterization and electrochemical sensing for life sciences

4. Publications

[A1] N. Sabir, N. Khan, J. Völkner, F. Widdascheck, P. Del Pino, G. Witte, M. Riedel, F. Lisdat, M. Konrad, W. J. Parak. Photo-electrochemical Bioanalysis of Guanosine Monophosphate Using Coupled Enzymatic Reactions at a CdS/ZnS Quantum Dot Electrode. *Small*. 2015 Sep 23. doi: 10.1002/smll.201501883.

In this paper, CdS/ZnS core/shell QDs modified gold electrode was used to detect the Guanosine Monophosphate using the three steps cascaded enzymatic reactions via electrochemical setup.

The author contributed to all the experiments of QDs synthesis, characterization, electrode preparation (attachment of enzymes and QDs via layer by layer assembly on thiol modified gold electrode) and data evaluation.

[A2] U. Kaiser, N. Sabir, C. Carrillo-Carrion, P. del Pino, M. Bossi, W. Heimbrodt, W. J. Parak. Förster resonance energy transfer mediated enhancement of the fluorescence lifetime of organic fluorophores to the millisecond range by coupling to Mn-doped CdS/ZnS quantum dots. *Nanotechnology* 27 (2016) 055101.

In this paper, the Mn ions doped and undoped CdS/ZnS core-shell QDs were produced and functionalized with the ATTO590/ATTO633/ATTO655 organic dyes. Förster resonance energy transfer (FRET) scheme studied in Manganese-doped CdS/ZnS QDs. Doped QDs could be used to enhance the effective lifetime of organic fluorophores up to millisecond.

The author contributed to the experiments of Mn doped NPs synthesis, characterization and their data evaluation.

[A3] B. Pelaz, N. Sabir, J. Hühn, C. Carrillo-Carrion, K. Kantner, P. del Pino, N. Feliu, I. Gounko, Vito, I. nelissen, W. J. Parak. Can doping reduce the cytotoxicity of cadmium containing quantum dots? In preparation.

In this paper, the Mn doped CdS and ZnS QDs were produced and functionalized. We characterized and analyzed the toxicity of the doped and undoped QDs.

Quantum Dots: Synthesis, characterization and electrochemical sensing for life sciences

The author contributed to the experiments of Mn doped CdS NPs synthesis, characterization and their data evaluation.

[A4] Z. Yue, F. Lisdat, W. J. Parak, S. G. Hickey, L. Tu, N. Sabir, D. Dorfs, and N. C. Bigall. Quantum-Dot-Based Photoelectrochemical Sensors for Chemical and Biological Detection. *ACS Appl. Mater. Interfaces* 5(8) (2013), pp. 2800 – 2814.

This review article is regarding the Quantum dots based photoelectrochemical sensors. Although, QD-based photoelectrochemical sensors are still in their formative years, this review paper summarizes the fabrication methods, improvements, and applications of QDs based sensors for biochemical detection.

The author contributed in the literature survey, manuscript writing and edition.

[A5] K. Kantner, S. Ashraf, S. Carregal-Romero, C. Carillo-Carrion, M. Collot, P. del Pino, W. Heimbrod, D. Jimenez de Aberasturi, U. Kaiser, L. I. Kazakova, M. Lelle, N. Martinez de Baroja, J. M. Montenegro, M. Nazarenus, B. Pelaz, K. Peneva, P. R. Gil, N. Sabir, L. M. Schneider, L. I. Shabarchina, G. B. Sukhorukov, M. Vasquez, F. Yang, and W. J. Parak. Particle-Based Optical Sensing of Intracellular Ions at the Example of Calcium – What Are the Experimental Pitfalls? *Small* 11(8) (2015), pp. 896 - 904.

This review illustrates that particle-based intracellular ion-sensing is insignificant and involves several drawbacks. Some prominent problems are delivery, intracellular location, crosstalk of fluorescence readout under the influence of pH, analytes, and spectral overlap of emission spectra of different fluorophores. These problems have been discussed by virtue of experimental examples and a potential future perspective for particle-based intracellular ion sensing has been proposed.

The author contributed in the literature research and in the manuscript writing and edition.

Quantum Dots: Synthesis, characterization and electrochemical sensing for life sciences

6. Bibliography

1. Hoet, P. H.; Bruske-Hohlfeld, I.; Salata, O. V., Nanoparticles - known and unknown health risks. *J Nanobiotechnology* **2004**, 2, (1), 12.
2. Wang, Z.; Lee, J.; Cossins, A. R.; Brust, M., Microarray-Based Detection of Protein Binding and Functionality by Gold Nanoparticle Probes. *Anal. Chem.* **2005**, 77, (17), 5770-5774.
3. Corato, R. D.; Quarta, A.; Piacenza, P.; Ragusa, A.; Figuerola, A.; Buonsanti, R.; Cingolani, R.; Manna, L.; Pellegrino, T., Water solubilization of hydrophobic nanocrystals by means of poly(maleic anhydride-alt-1-octadecene). *Journal of Materials Chemistry* **2008**, 18, 1991-1996.
4. Shevchenko, E. V.; Talapin, D. V.; Rogach, A. L.; Kornowski, A.; Haase, M.; Weller, H., Colloidal Synthesis and Self-Assembly of CoPt₃ Nanocrystals. *JACS* **2002**, 124, 11480-11485.
5. Semmler-Behnke, M.; Kreyling, W. G.; Lipka, J.; Fertsch, S.; Wenk, A.; Takenaka, S.; Schmid, G.; Brandau, W., Biodistribution of 1.4- and 18-nm Gold Particles in Rats. *Small* **2008**, 4, (12), 2108-2111.
6. Brust, M.; Walker, M.; Bethell, D.; Schiffrin, D. J.; Whyman, R., Synthesis of Thiol-Derivatized Gold Nanoparticles in a 2-Phase Liquid-Liquid System. *Journal of the Chemical Society-Chemical Communications* **1994**, (7), 801-802.
7. Zhang, F.; Ali, Z.; Amin, F.; Feltz, A.; Oheim, M.; Parak, W. J., Ion and pH sensing with colloidal nanoparticles: influence of surface charge on sensing and colloidal properties. *ChemPhysChem* **2010**, 11, 730-735.
8. Chen, M. S.; Goodman, D. W., The structure of catalytically active gold on titania. *Science* **2004**, 306, (5694), 252-255.
9. Valden, M.; Lai, X.; Goodman, D. W., Onset of catalytic activity of gold clusters on titania with the appearance of nonmetallic properties. *Science* **1998**, 281, (5383), 1647-1650.
10. Rai, M.; Yadav, A.; Gade, A., Silver Nanoparticles as a New Generation of Antimicrobials. *Biotechnology Advances* **2009**, 27, (1), 76-83.

Quantum Dots: Synthesis, characterization and electrochemical sensing for life sciences

11. Morones, J.; Elechiguerra, J.; Camacho, A.; Holt, K.; Kouri, J.; Ram, J.; Yacaman, M., The Bactericidal Effect of Silver Nanoparticles. *Nanotechnology* **2005**, *16*, 2346-2352.
12. Jiang, Z.-J.; Liu, C.-Y.; Sun, L.-W., Catalytic Properties of Silver Nanoparticles Supported on Silica Spheres. *Journal of Physical Chemistry B* **2005**, *109*, (5), 1730-1735.
13. Zhou, Q.; Qian, G. Z.; Li, Y.; Zhao, G.; Chao, Y. W.; Zheng, J. W., Two-dimensional assembly of silver nanoparticles for catalytic reduction of 4-nitroaniline. *Thin Solid Films* **2008**, *516*, (6), 953-956.
14. Klimov, V. I.; Mikhailovsky, A. A.; Xu, S.; Malko, A.; Hollingsworth, J. A.; Leatherdale, C. A.; Eisler, H.-J.; Bawendi, M. G., Optical Gain and Stimulated Emission in Nanocrystal Quantum Dots. *Science* **2000**, *290*, (13 October), 314-317.
15. El-Sayed, M. A., Some interesting properties of metals confined in time and nanometer space of different shapes. *Accounts of Chemical Research* **2001**, *34*, (4), 257-264.
16. Daniel, M. C.; Astruc, D., Gold Nanoparticles: Assembly, Supramolecular Chemistry, Quantum-Size-Related Properties, and Applications toward Biology, Catalysis, and Nanotechnology. *Chemical Reviews* **2004**, *104*, (1), 293-346.
17. Reiss, P.; Protiere, M.; Li, L., Core/Shell Semiconductor Nanocrystals. *Small* **2009**, *5*, (2), 154-168.
18. Xu, S.; Ziegler, J.; Nann, T., Rapid synthesis of highly luminescent InP and InP/ZnS nanocrystals. *Journal of Materials Chemistry* **2008**, *18*, (23), 2653-2656.
19. Xu, S.; Klama, F.; Ueckermann, H.; Hoogewerff, J.; Clayden, N.; Nann, T., Optical and Surface Characterisation of Capping Ligands in the Preparation of InP/ZnS Quantum Dots. *Science of Advanced Materials* **2009**, *1*, (2), 125-137.
20. Xu, S.; Kumar, S.; Nann, T., Rapid synthesis of high-quality InP nanocrystals. *Journal of the American Chemical Society* **2006**, *128*, (4), 1054-1055.
21. Parak, W. J.; Pellegrino, T.; Plank, C., Labelling of cells with quantum dots. *Nanotechnology* **2005**, *16*, R5-R25.
22. Bruchez, M. J.; Moronne, M.; Gin, P.; Weiss, S.; Alivisatos, A. P., Semiconductor Nanocrystals as Fluorescent Biological Labels. *Science* **1998**, *281*, (5385), 2013-2016.
23. Resch-Genger, U.; Grabolle, M.; Cavaliere-Jaricot, S.; Nitschke, R.; Nann, T., Quantum dots versus organic dyes as fluorescent labels. *Nat Meth* **2008**, *5*, (9), 763.

Quantum Dots: Synthesis, characterization and electrochemical sensing for life sciences

24. Bimberg, D., Quantum dots for lasers, amplifiers and computing. *Journal of Physics D-Applied Physics* **2005**, 38, (13), 2055-2058.
25. Park, N. M.; Kim, T. S.; Park, S. J., Band gap engineering of amorphous silicon quantum dots for light-emitting diodes. *Applied Physics Letters* **2001**, 78, (17), 2575-2577.
26. Nozik, A. J., Quantum dot solar cells. *Physica E* **2002**, 14, 115-120.
27. Kamat, P. V., Quantum Dot Solar Cells. Semiconductor Nanocrystals as Light Harvesters. *Journal of physical chemistry C* **2008**, 112, (48), 18737-18753.
28. Haynes, C. L.; Van Duyne, R. P., Nanosphere lithography: A versatile nanofabrication tool for studies of size-dependent nanoparticle optics. *Journal of Physical Chemistry B* **2001**, 105, (24), 5599-5611.
29. Ming, L. Z., J. and Liwei, S., Top-Down Fabrication of Nanostructures. **2010**.
30. Thompson, "An Introduction to Lithography," Introduction to Microlithography, Second Edition, Ed. L.F. Thompson, C.G. Willson, and M.J. Bowden. *Washington, DC: American Chemical Society* **1994**, 1.
31. Moreau, W. M., Semiconductor Lithography: Principles, Practices and Materials. *New York: Plenum Press* **1988**, 473.
32. Katsumi, S. S., M. and Yukinori, O., Sub-Half-Micron Lithography for ULSIs. *Cambridge University Press, Cambridge* **2000**.
33. Gentili, M., Giovannella, C., and Selci, S., Nanolithography: A Borderland between STM, EB, IB, and X-Ray Lithographies. *Kluwer, Dordrecht, The Netherlands*. **1993**.
34. Brambley, D., Martin, B., and Prewett, F.D., Microlithography: An Overview. *Adv. Mater: Opt. Electron.*, **1994**, 4, (2), 55-74.
35. Goesmann, H.; Feldmann, C., Nanoparticulate Functional Materials. *Angewandte Chemie, International Edition* **2010**, 49, (8), 1362-1395.
36. Zhang, J. Z., Interfacial charge carrier dynamics of colloidal semiconductor nanoparticles. *Journal of Physical Chemistry B* **2000**, 104, (31), 7239-7253.
37. Shen, G. Z.; Cho, J. H.; Yoo, J. K.; Yi, G. C.; Lee, C. J., Synthesis of single-crystal CdS microbelts using a modified thermal evaporation method and their photoluminescence. *Journal of Physical Chemistry B* **2005**, 109, (19), 9294-9298.

Quantum Dots: Synthesis, characterization and electrochemical sensing for life sciences

38. Alivisatos, A. P.; Colvin, V. Electroluminescent devices formed using semiconductor nanocrystals as an electron transport media and method of making such electroluminescent devices. US patent 5,537,000, 1994.
39. Alivisatos, A. P.; Colvin, V. L. Semiconductor nanocrystals covalently bound to solid inorganic surfaces using self-assembled monolayers. US patent 5,751,018, 1994.
40. Klein, D. L.; Roth, R.; Lim, A. K. L.; Alivisatos, A. P.; McEuen, P. L., A single-electron transistor made from a cadmium selenide nanocrystal. *Nature* **1997**, 389, 699-701.
41. Schlamp, M. C.; Peng, X.; Alivisatos, A. P., Improved efficiencies in light emitting diodes made with CdSe(CdS) core/shell type nanocrystals and a semiconducting polymer. *Journal of Applied Physics* **1997**, 82, (11), 5837-5842.
42. Alivisatos, A. P., Nano letters after one year. *Nano Letters* **2002**, 2, (1), 1-1.
43. Woo, W.-K.; Jarosz, K. T. S. V.; Neuhauser, R. G.; Leatherdale, C. A.; Rubner, M. A.; Bawendi, M. G., Reversible Charging of CdSe Nanocrystals in a Simple Solid-State Device. *Advanced Materials* **2002**, 14, (15), 1068-1071.
44. Chan, W. C. W.; Nie, S., Quantum Dot Bioconjugates for Ultrasensitive Nonisotopic Detection. *Science* **1998**, 281, 2016-2018.
45. Yang, Y.; Chen, O.; Angerhofer, A.; Cao, Y. C., Radial-position-controlled doping in CdS/ZnS core/shell nanocrystals. *J Am Chem Soc* **2006**, 128, (38), 12428-9.
46. Yang, Y.; Chen, O.; Angerhofer, A.; Cao, Y. C., On doping CdS/ZnS core/shell nanocrystals with Mn. *J Am Chem Soc* **2008**, 130, (46), 15649-61.
47. Shi, X.; Han, S.; Sanedrin, R. J.; Zhou, F.; Selke, M., Synthesis of Cobalt Oxide Nanotubes from Colloidal Particles Modified with a Co(III)-Cysteinato Precursor. *Chemistry of Materials* **2002**, 14, (4), 1897-1902.
48. Osorio-Cantillo, C.; Santiago-Miranda, A. N.; Perales-Perez, O.; Xin, Y., Size-and phase-controlled synthesis of cobalt nanoparticles for potential biomedical applications. *Journal of Applied Physics* **2012**, 111, (7), 07B324.
49. Hanif, K. M.; Meulenberg, R. W.; Strouse, G. F., Magnetic ordering in doped Cd(1-x)Co(x)Se diluted magnetic quantum dots. *J Am Chem Soc* **2002**, 124, (38), 11495-502.

Quantum Dots: Synthesis, characterization and electrochemical sensing for life sciences

50. Schwartz, D. A.; Norberg, N. S.; Nguyen, Q. P.; Parker, J. M.; Gamelin, D. R., Magnetic quantum dots: synthesis, spectroscopy, and magnetism of Co²⁺ - and Ni²⁺-doped ZnO nanocrystals. *J Am Chem Soc* **2003**, 125, (43), 13205-18.
51. Kumar, P.; Singh, K., Ferromagnetism in Cu-doped ZnSe semiconducting quantum dots. *Journal of Nanoparticle Research* **2011**, 13, (4), 1613-1620.
52. Duan, L. B.; Zhao, X. R.; Liu, J. M.; Wang, T.; Rao, G. H., Room-temperature ferromagnetism in lightly Cr-doped ZnO nanoparticles. *Applied Physics a-Materials Science & Processing* **2010**, 99, (3), 679-683.
53. Zanella, M.; Abbasi, A. Z.; Schaper, A. K.; Parak, W. J., Discontinuous Growth of II-VI Semiconductor Nanocrystals from Different Materials. *Journal Of Physical Chemistry C* **2010**, 114, (14), 6205-6215.
54. Panda, S. K.; Hickey, S. G.; Demir, H. V.; Eychmuller, A., Bright White-Light Emitting Manganese and Copper Co-Doped ZnSe Quantum Dots. *Angewandte Chemie-International Edition* **2011**, 50, (19), 4432-4436.
55. Smith, B. A.; Zhang, J. Z.; Joly, A.; Liu, J., Luminescence decay kinetics of Mn²⁺-doped ZnS nanoclusters grown in reverse micelles. *Physical Review B* **2000**, 62, (3), 2021-2028.
56. Sun, L. D.; Yan, C. H.; Liu, C. H.; Liao, C. S.; Li, D.; Yu, J. Q., Study of the optical properties of Eu³⁺-doped ZnS nanocrystals. *Journal of Alloys and Compounds* **1998**, 275, 234-237.
57. Vitaly, P. Y., D., Long-lived emission in Mn doped CdS, ZnS, and ZnSe diluted magnetic semiconductor quantum dots. *Chemical Physics* **2015**.
58. Chen, O.; Shelby, D. E.; Yang, Y.; Zhuang, J.; Wang, T.; Niu, C.; Omenetto, N.; Cao, Y. C., Excitation-intensity-dependent color-tunable dual emissions from manganese-doped CdS/ZnS core/shell nanocrystals. *Angewandte Chemie - International Edition* **2010**, 49, (52), 10132-10135.
59. Wang, Y.; Herron, N.; Moller, K.; Bein, T., 3-Dimensionally Confined Diluted Magnetic Semiconductor Clusters - Zn₁-Xm_nxs. *Solid State Communications* **1991**, 77, (1), 33-38.
60. Bhargava, R. N.; Gallagher, D.; Hong, X.; Nurmikko, A., Optical-Properties of Manganese-Doped Nanocrystals of Zns. *Physical Review Letters* **1994**, 72, (3), 416-419.

Quantum Dots: Synthesis, characterization and electrochemical sensing for life sciences

61. Norris, D. J.; Yao, N.; Charnock, F. T.; Kennedy, T. A., High-quality manganese-doped ZnSe nanocrystals. *Nano Letters* **2001**, 1, (1), 3-7.
62. Suyver, J. F.; Wuister, S. F.; Kelly, J. J.; Meijerink, A., Luminescence of nanocrystalline ZnSe: Mn²⁺. *Physical Chemistry Chemical Physics* **2000**, 2, (23), 5445-5448.
63. Furdyna, J. K., Diluted Magnetic Semiconductors. *Journal Of Applied Physics* **1988**, 64, (4), R29-R64.
64. Schmechel, R.; Winkler, H.; Li, X. M.; Kennedy, M.; Kolbe, M.; Benker, A.; Winterer, M.; Fischer, R. A.; Hahn, H.; von Seggern, H., Photoluminescence properties of nanocrystalline Y2O3: Eu³⁺ in different environments. *Scripta Materialia* **2001**, 44, (8-9), 1213-1217.
65. Bol, A. A.; Meijerink, A., Doped semiconductor nanoparticles - a new class of luminescent materials? *Journal Of Luminescence* **2000**, 87-9, 315-318.
66. Artemyev, M. V.; Gurinovich, L. I.; Stupak, A. P.; Gaponenko, S. V., Luminescence of CdS Nanoparticles Doped with Mn. *Physica Status Solidi B* **2001**, 224, (1), 191-194.
67. Chen, H. Y.; Maiti, S.; Son, D. H., Doping Location-Dependent Energy Transfer Dynamics in Mn-Doped CdS/ZnS Nanocrystals. *Acs Nano* **2012**, 6, (1), 583-591.
68. Viswanatha, R.; Brovelli, S.; Pandey, A.; Crooker, S. A.; Klimov, V. I., Copper-Doped Inverted Core/Shell Nanocrystals with "Permanent" Optically Active Holes. *Nano Letters* **2011**, 11, (11), 4753-4758.
69. Norris, D. J.; Efros, A. L.; Erwin, S. C., Doped nanocrystals. *Science* **2008**, 319, (5871), 1776-1779.
70. Förster, T., *Delocalized excitation and excitation transfer*. ed.; Academic Press Inc: New York, 1965; 'Vol.' 3, p.
71. Lakowicz, J. R., *Principles of Fluorescence Spectroscopy*. 2nd ed.; Plenum Publishing Corp: New York, 1999; 'Vol.' p.
72. Geissler, D.; Linden, S.; Liermann, K.; Wegner, K. D.; Charbonniere, L. J.; Hildebrandt, N., Lanthanides and Quantum Dots as Forster Resonance Energy Transfer Agents for Diagnostics and Cellular Imaging. *Inorganic Chemistry* **2014**, 53, (4), 1824-1838.

Quantum Dots: Synthesis, characterization and electrochemical sensing for life sciences

73. Hildebrandt, N.; Wegner, K. D.; Algar, W. R., Luminescent terbium complexes: Superior Förster resonance energy transfer donors for flexible and sensitive multiplexed biosensing. *Coordination Chemistry Reviews* **2014**, 273, 125-138.
74. Gill, R.; Willner, I.; Shweky, I.; Banin, U., Fluorescence resonance energy transfer in CdSe/ZnS-DNA conjugates: Probing hybridization and DNA cleavage. *Journal Of Physical Chemistry B* **2005**, 109, (49), 23715-23719.
75. Medintz, I. L.; Uyeda, H. T.; Goldman, E. R.; Mattoussi, H., Quantum Dot Bioconjugates for Imaging, Labelling and Sensing. *Nat. Mater.* **2005**, 4, (6), 435-446.
76. Clapp, A. R.; Medintz, I. L.; Mauro, J. M.; Fisher, B. R.; Bawendi, M. G.; Mattoussi, H., Fluorescence Resonance Energy Transfer Between Quantum Dot Donors and Dye-Labeled Protein Acceptors. *Journal of the American Chemical society* **2004**, 126, (1), 301-310.
77. Niebling, T.; Zhang, F.; Ali, Z.; Parak, W. J.; Heimbrod, W., Excitation dynamics in polymer-coated semiconductor quantum dots with integrated dye molecules: The role of reabsorption. *Journal of Applied Physics* **2009**, 106, 104701.
78. Medintz, I. L.; Clapp, A. R.; Melinger, J. S.; Deschamps, J. R.; Mattoussi, H., A Reagentless Biosensing Assembly Based on Quantum Dot-Donor Förster Resonance Energy Transfer. *Advanced Materials* **2005**, 17, 2450-2455.
79. Clapp, A. R.; Medintz, I. L.; Mattoussi, H., Förster Resonance Energy Transfer Investigations Using Quantum-Dot Fluorophores. *ChemPhysChem* **2006**, 7, 47-57.
80. Algar, W. R.; Ancona, M. G.; Malanoski, A. P.; Susumu, K.; Medintz, I. L., Assembly of a concentric Förster resonance energy transfer relay on a quantum dot scaffold: characterization and application to multiplexed protease sensing. *ACS Nano* **2012**, 6, (12), 11044-11058.
81. Geißler, D.; Stuffer, S.; Löhmansröben, H.-G.; Hildebrandt, N., Six-color time-resolved Förster resonance energy transfer for ultrasensitive multiplexed biosensing. *Journal of the American Chemical Society* **2012**, 135, (3), 1102-1109.
82. Algar, W. R.; Kim, H.; Medintz, I. L.; Hildebrandt, N., Emerging non-traditional Förster resonance energy transfer configurations with semiconductor quantum dots: investigations and applications. *Coordination Chemistry Reviews* **2014**, 263, 65-85.

Quantum Dots: Synthesis, characterization and electrochemical sensing for life sciences

83. Kaiser, U.; Aberasturi, D. J. d.; Malinowski, R.; Amin, F.; Parak, W. J.; Heimbrodt, W., Multiplexed measurements by time resolved spectroscopy using colloidal CdSe/ZnS quantum dots. *Applied Physics Letters* **2014**, 104, 41901-41904.
84. Kaiser, U.; Aberasturi, D. J. d.; Vazquez-Gonzalez, M.; Carrillo-Carrion, C.; Niebling, T.; Parak, W. J.; Heimbrodt, W., Determining the exact number of dye molecules attached to colloidal CdSe/ZnS quantum dots in Förster resonant energy transfer assemblies. *JOURNAL OF APPLIED PHYSICS* **2015**, 117, 024701.
85. Busse, W.; Gumlich, H. E.; Meissner, B.; Theis, D., Time Resolved Spectroscopy of ZnS:Mn by Dye-Laser Technique. *Journal of Luminescence* **1976**, 12, (1), 693-700.
86. Donega, C. D.; Bol, A. A.; Meijerink, A., Time-resolved luminescence of ZnS: Mn²⁺ nanocrystals. *Journal of Luminescence* **2002**, 96, (2-4), 87-93.
87. Clark, L. C.; Lyons, C., Electrode Systems for Continuous Monitoring in Cardiovascular Surgery. *Annals of the New York Academy of Sciences* **1962**, 102, (1), 29-&.
88. Brian, R. E., *Chemical Sensors and Biosensors*. ed.; John Wiley & Sons, West Sussex, England: 2002; 'Vol.' p.
89. Ronkainen, N. J.; Halsall, H. B.; Heineman, W. R., Electrochemical biosensors. *Chemical Society Reviews* **2010**, 39, (5), 1747-1763.
90. Wang, J., *Analytical Electrochemistry*. **2006**.
91. Zanella, A.; Fermo, E.; Bianchi, P.; Valentini, G., Red cell pyruvate kinase deficiency: molecular and clinical aspects. *British Journal of Haematology* **2005**, 130, (1), 11-25.
92. Frew, J. E.; Hill, H. A. O., Electrochemical Biosensors. *Analytical Chemistry* **1987**, 59, (15), 933A-944A.
93. Thévenot, D. R.; Toth, K.; Durst, R. A.; Wilson, G. S., Electrochemical biosensors: recommended definitions and classification. *Biosensors and Bioelectronics* **2001**, 16, (1-2), 121-131.
94. Guo, S. J.; Dong, S. J., Biomolecule-Nanoparticle Hybrids for Electrochemical Biosensors. *TrAC Trends In Analytical Chemistry* **2009**, 28, (1), 96-109.
95. Golub, E.; Niazov, A.; Freeman, R.; Zatspein, M.; Willner, I., Photoelectrochemical Biosensors Without External Irradiation: Probing Enzyme Activities and DNA Sensing Using

Quantum Dots: Synthesis, characterization and electrochemical sensing for life sciences

- Hemin/G-Quadruplex-Stimulated Chemiluminescence Resonance Energy Transfer (CRET) Generation of Photocurrents. *Journal of Physical Chemistry C* **2012**, 116, (25), 13827-13834.
96. Volotovskiy, V.; Jaffrezic-Renault, N.; Martelet, C.; Soldatkin, A. P. In *Improvements of Sensitivity of Urease-Based Biosensor for Heavy Metal Ions Determination*, Eurosensors XI, Warschau, Polen, 1997; Jachowicz, R. S., 'Ed.' 'Eds.' Warschau, Polen, 1997; pp 1201-1204 (abstract 3P1-1).
97. Soldatkin, A. P.; Montoriol, J.; Sant, W.; Martelet, C.; Jaffrezic-Renault, N., A novel urea sensitive biosensor with extended dynamic range based on recombinant urease and ISFETs. *Biosensors and Bioelectronics* **2003**, 19, (2), 131-135.
98. Xie, Q.; Alpers, D. H., The two isozymes of rat intestinal alkaline phosphatase are products of two distinct genes. *Physiological Genomics* **2000**, 3, (1), 1-8.
99. Schrenkhammer, P.; Rosnizeck, I. C.; Duerkop, A.; Wolfbeis, O. S.; Schaferling, M., Time-resolved fluorescence-based assay for the determination of alkaline phosphatase activity and application to the screening of its inhibitors. *Journal Of Biomolecular Screening* **2008**, 13, (1), 9-16.
100. Bagel, O.; Limoges, B.; Schollhorn, B.; Degrand, C., Subfemtomolar determination of alkaline phosphatase at a disposable screen-printed electrode modified with a perfluorosulfonated ionomer film. *Analytical Chemistry* **1997**, 69, (22), 4688-4694.
101. Kreuzer, M. P.; O'Sullivan, C. K.; Guilbault, G. G., Alkaline phosphatase as a label for immunoassay using amperometric detection with a variety of substrates and an optimal buffer system. *Analytica Chimica Acta* **1999**, 393, (1-3), 95-102.
102. Ruan, C. M.; Wang, W.; Gu, B. H., Detection of alkaline phosphatase using surface-enhanced Raman spectroscopy. *Analytical Chemistry* **2006**, 78, (10), 3379-3384.
103. Neumann, H.; Vanvreed, M., An Improved Alkaline Phosphatase Determination With P-Nitrophenyl Phosphate. *Clinica Chimica Acta* **1967**, 17, (2), 183-&.
104. Nistor, C.; Emneus, J., An enzyme flow immunoassay using alkaline phosphatase as the label and a tyrosinase biosensor as the label detector. *Analytical Communications* **1998**, 35, (12), 417-419.
105. Freeman, R.; Finder, T.; Gill, R.; Willner, I., Probing Protein Kinase (CK2) and Alkaline Phosphatase with CdSe/ZnS Quantum Dots. *Nano Letters* **2010**, 10, (6), 2192-2196.

Quantum Dots: Synthesis, characterization and electrochemical sensing for life sciences

106. Van Rompay, A.; Johansson, M.; Karlsson, A., Phosphorylation of nucleosides and nucleoside analogs by mammalian nucleoside monophosphate kinases. *PHARMACOLOGY & THERAPEUTICS* **2000**, *87*, (2-3), 189-198.
107. Sekulic, N.; Shuvalova, L.; Spangenberg, O.; Konrad, M.; Lavie, A., Structural characterization of the closed conformation of mouse guanylate kinase. *Journal of Biological Chemistry* **2002**, *277*, (33), 30236-30243.
108. Beck, B.; Huelsmeyer, M.; Paul, S.; Downs, D., A mutation in the essential gene gmk (encoding guanylate kinase) generates a requirement for adenine at low temperature in *Salmonella enterica*. *JOURNAL OF BACTERIOLOGY* **2003**, *185*, (22), 6732-6735.
109. Choi, B.; Zocchi, G., Guanylate kinase, induced fit, and the allosteric spring probe. *BIOPHYSICAL JOURNAL* **2007**, *92*, (5), 1651-1658.
110. Konrad, M., Cloning and Expression of the Essential Gene for Guanylate Kinase from Yeast. *Journal of Biological Chemistry* **1992**, *267*, (36), 25652-25655.
111. Hazra, S.; Ort, S.; Konrad, M.; Lavie, A., Structural and Kinetic Characterization of Human Deoxycytidine Kinase Variants Able To Phosphorylate 5-Substituted Deoxycytidine and Thymidine Analogues. *Biochemistry* **2010**, *49*, (31), 6784-6790.
112. MILLER, L.; WELLS, R., NUCLEOSIDE DIPHOSPHOKINASE ACTIVITY ASSOCIATED WITH DNA POLYMERASES. *PROCEEDINGS OF THE NATIONAL ACADEMY OF SCIENCES OF THE UNITED STATES OF AMERICA* **1971**, *68*, (9), 2298-&.
113. Kochius, S.; Magnusson, A.; Hollmann, F.; Schrader, J.; Holtmann, D., Immobilized redox mediators for electrochemical NAD(P)(+) regeneration. *APPLIED MICROBIOLOGY AND BIOTECHNOLOGY* **2012**, *93*, (6), 2251-2264.
114. Cook, W. J.; Senkovich, O.; Aleem, K.; Chattopadhyay, D., Crystal structure of *Cryptosporidium parvum* pyruvate kinase. *PLoS One* *7*, (10), e46875.
115. Valentine, W. N.; Tanaka, K. R.; Miwa, S., A specific erythrocyte glycolytic enzyme defect (pyruvate kinase) in three subjects with congenital non-spherocytic hemolytic anemia. *Trans Assoc Am Physicians* **1961**, *74*, 100-10.
116. Glader, B., Hereditary hemolytic anemias due to enzyme disorders. In: Wintrobe's Clinical Hematology. In 11th ed.; Mentzer, W. C.; and Wagner, G. H., 'Ed.'^'Eds.' Philadelphia, 2004; 'Vol.' p^pp.

Quantum Dots: Synthesis, characterization and electrochemical sensing for life sciences

117. Harvey, J. W., Congenital erythrocyte enzyme deficiencies. *Vet Clin North Am Small Anim Pract* **1996**, 26, (5), 1003-11.
118. Adams, M. J.; Buehner, M.; Chandrasekhar, K.; Ford, G. C.; Hackert, M. L.; Liljas, A.; Rossmann, M. G.; Smiley, I. E.; Allison, W. S.; Everse, J.; Kaplan, N. O.; Taylor, S. S., Structure-function relationships in lactate dehydrogenase. *Proc Natl Acad Sci U S A* **1973**, 70, (7), 1968-72.
119. Tarloff, J. B.; Kendig, D. M., Inactivation of lactate dehydrogenase by several chemicals: Implications for in vitro toxicology studies. *Toxicology in Vitro* **2007**, 21, (1), 125-132.
120. Zare, H. R.; Nasirizadeh, N.; Mazloun-Ardakani, M.; Namazian, M., Electrochemical properties and electrocatalytic activity of hematoxylin modified carbon paste electrode toward the oxidation of reduced nicotinamide adenine dinucleotide (NADH). *Sensors and Actuators B-Chemical* **2006**, 120, (1), 288-294.
121. Shlyahovsky, B.; Katz, E.; Xiao, Y.; Pavlov, V.; Willner, I., Optical and Electrochemical Detection of NADH and of NAD⁺-Dependent Biocatalyzed Processes by the Catalytic Deposition of Copper on Gold Nanoparticles. *Small* **2005**, 1, (2), 213-216.
122. Limoges, B.; Marchal, D.; Mavre, F.; Saveant, J. M., Electrochemistry of immobilized redox enzymes: Kinetic characteristics of NADH oxidation catalysis at diaphorase monolayers affinity immobilized on electrodes. *Journal of the American Chemical Society* **2006**, 128, (6), 2084-2092.
123. Huang, T.; Warsinke, A.; Kuwana, T.; Scheller, F. W., Determination of L-phenylalanine based on an NADH-detecting biosensor. *Analytical Chemistry* **1998**, 70, (5), 991-997.
124. Banks, C.; Compton, R., Exploring the electrocatalytic sites of carbon nanotubes for NADH detection: an edge plane pyrolytic graphite electrode study. *ANALYST* **2005**, 130, (9), 1232-1239.
125. Xu, H.; Hong, R.; Lu, T. X.; Uzun, O.; Rotello, V. M., Recognition-directed orthogonal self-assembly of polymers and nanoparticles on patterned surfaces. *Journal of the American Chemical Society* **2006**, 128, (10), 3162-3163.

Quantum Dots: Synthesis, characterization and electrochemical sensing for life sciences

126. Kotov, N. A.; Dekany, I.; Fendler, J. H., Layer-by-Layer Self-Assembly of Polyelectrolyte-Semiconductor Nanoparticle Composite Films. *The Journal of Physical Chemistry* **1995**, *99*, (35), 13065-13069.
127. Khalid, W.; Helou, M. E.; Murböck, T.; Yue, Z.; Montenegro, J.-M.; Schubert, K.; Göbel, G.; Lisdat, F.; Witte, G.; Parak, W. J., Immobilization of Quantum Dots via Conjugated Self-Assembled Monolayers and Their Application as a Light-Controlled Sensor for the Detection of Hydrogen Peroxide. *ACS Nano* **2011**, *5*, (12), 9870-9876.
128. Khalid, W.; Göbel, G.; Hühn, D.; Montenegro, J.-M.; Rivera Gil, P.; Lisdat, F.; Parak, W. J., Light Triggered Detection of Aminophenyl Phosphate with a Quantum Dot Based Enzyme Electrode. *J. Nanobiotechnol.* **2011**, *9*, 46.
129. Tanne, J.; Schafer, D.; Khalid, W.; Parak, W. J.; Lisdat, F., Light-Controlled Bioelectrochemical Sensor Based on CdSe/ZnS Quantum Dots. *Analytical Chemistry* **2011**, *83*, (20), 7778-7785.
130. Zanella, M.; Falqui, A.; Kudera, S.; Manna, L.; Casula, M. F.; Parak, W. J., Growth of Colloidal Nanoparticles of Group II-VI and IV-VI Semiconductors on Top of Magnetic Iron-Platinum Nanocrystals. *Journal of Materials Chemistry* **2008**, *18*, 4311-4317.
131. Schubert, K.; Khalid, W.; Yue, Z.; Parak, W. J.; Lisdat, F., Quantum-Dot-Modified Electrode in Combination with NADH-Dependent Dehydrogenase Reactions for Substrate Analysis. *Langmuir* **2010**, *26*, (2), 1395-1400.
132. Yue, Z.; Khalid, W.; Zanella, M.; Abbasi, A. Z.; Pfreundt, A.; Rivera_Gil, P.; Schubert, K.; Lisdat, F.; Parak, W. J., Evaluation of Quantum Dots Applied as Switchable Layer in a Light-Controlled Electrochemical Sensor. *Analytical and Bioanalytical Chemistry* **2010**, *396*, (3), 1095-1103.
133. Sabir, N.; Khan, N.; Volkner, J.; Widdascheck, F.; Del Pino, P.; Witte, G.; Riedel, M.; Lisdat, F.; Konrad, M.; Parak, W. J., Photo-electrochemical Bioanalysis of Guanosine Monophosphate Using Coupled Enzymatic Reactions at a CdS/ZnS Quantum Dot Electrode. *Small* **2015**.
134. Yu, W. W.; Peng, X., Formation of High-Quality CdS and Other II-VI Semiconductor Nanocrystals in Noncoordinating Solvents: Tunable Reactivity of Monomers. *Angewandte Chemie International Edition* **2002**, *41*, (13), 2368-2371.

Quantum Dots: Synthesis, characterization and electrochemical sensing for life sciences

135. Veamatahau, A.; Jiang, B.; Seifert, T.; Makuta, S.; Latham, K.; Kanehara, M.; Teranishi, T.; Tachibana, Y., Origin of surface trap states in CdS quantum dots: relationship between size dependent photoluminescence and sulfur vacancy trap states. *Physical Chemistry Chemical Physics* **2015**, *17*, (4), 2850-2858.
136. Yu, W. W.; Qu, L.; Guo, W.; Peng, X., Experimental Determination of the Extinction Coefficient of CdTe, CdSe, and CdS Nanocrystals. *Chemistry of Materials* **2003**, *15*, (14), 2854-2860.
137. Chen, D.; Zhao, F.; Qi, H.; Rutherford, M.; Peng, X., Bright and Stable Purple/Blue Emitting CdS/ZnS Core/Shell Nanocrystals Grown by Thermal Cycling Using a Single-Source Precursor. *CHEMISTRY OF MATERIALS* **2010**, *22*, (4), 1437-1444.
138. Reiss, P.; Bleuse, J.; Pron, A., Highly Luminescent CdSe/ZnSe Core/Shell Nanocrystals of Low Size Dispersion. *Nano Letters* **2002**, *2*, (7), 781-784.
139. Pellegrino, T.; Manna, L.; Kudera, S.; Liedl, T.; Koktysh, D.; Rogach, A. L.; Keller, S.; Rädler, J.; Natile, G.; Parak, W. J., Hydrophobic Nanocrystals Coated with an . Amphiphilic Polymer Shell: A General Route to Water Soluble Nanocrystals. *Nano Letters* **2004**, *4*, (4), 703-707.

Appendix

Photo-electrochemical Bioanalysis of Guanosine Monophosphate Using Coupled Enzymatic Reactions at a CdS/ZnS Quantum Dot Electrode

Nadeem Sabir, Nazimuddin Khan, Johannes Völkner, Felix Widdascheck, Pablo del Pino, Gregor Witte, Marc Riedel, Fred Lisdat,* Manfred Konrad,* and Wolfgang J. Parak*

A photo-electrochemical sensor for the specific detection of guanosine monophosphate (GMP) is demonstrated, based on three enzymes combined in a coupled reaction assay. The first reaction involves the adenosine triphosphate (ATP)-dependent conversion of GMP to guanosine diphosphate (GDP) by guanylate kinase, which warrants substrate specificity. The reaction products ADP and GDP are co-substrates for the enzymatic conversion of phosphoenolpyruvate to pyruvate in a second reaction mediated by pyruvate kinase. Pyruvate in turn is the co-substrate for lactate dehydrogenase that generates lactate via oxidation of nicotinamide adenine dinucleotide (reduced form) NADH to NAD⁺. This third enzymatic reaction is electrochemically detected. For this purpose a CdS/ZnS quantum dot (QD) electrode is illuminated and the photocurrent response under fixed potential conditions is evaluated. The sequential enzyme reactions are first evaluated in solution. Subsequently, a sensor for GMP is constructed using polyelectrolytes for enzyme immobilization.

N. Sabir, J. Völkner, F. Widdascheck, Prof. G. Witte,
Prof. W. J. Parak

Fachbereich Physik, Philipps-Universität Marburg
Renthof 5, D-35032 Marburg, Germany
E-mail: wolfgang.parak@physik.uni-marburg.de

N. Khan, Prof. M. Konrad
Max Planck Institute for Biophysical Chemistry
Am Fassberg 11, D-37077 Göttingen, Germany
E-mail: mkonrad@mpiibpc.mpg.de

Dr. P. del Pino, Prof. W. J. Parak
CIC biomaGUNE
Parque Tecnológico de San Sebastián
Pº Miramón 182 – Ed. Empresarial C, 20009 San Sebastian, Spain

M. Riedel, Prof. F. Lisdat
Biosystems Technology
Institute of Applied Life Sciences
Technical University Wildau
Hochschulring 1, D-15745 Wildau, Germany
E-mail: flisdat@th-wildau.de

DOI: 10.1002/sml.201501883



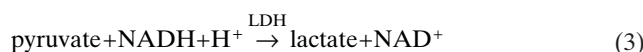
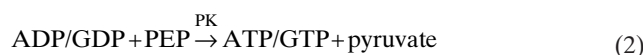
1. Introduction

Guanylate kinase (GMPK), which catalyzes the easily reversible phosphoryl group transfer from adenosine triphosphate (ATP) to (deoxy) guanosine monophosphate (GMP, dGMP) to form adenosine diphosphate (ADP) and (deoxy) guanosine diphosphate (GDP, dGDP), is an essential enzyme in the guanine nucleotide metabolism of unicellular and multicellular organisms.^[1–3] Guanine nucleotides are required for a variety of cellular metabolic processes, as well as for RNA and DNA synthesis.^[4] Such metabolic processes include the recycling of GMP and dGMP, products of RNA and DNA degradation, and of the second messenger cyclic GMP (cGMP) through the so-called cGMP cycle (cGMP → GMP → GDP → GTP → cGMP), thus providing guanine nucleotides to signal transduction pathways.^[5–8] Moreover, cellular GMPK is a critical and rate-limiting enzyme for metabolic activation of a number of guanine analogs (e.g., 6-thioguanine, mercaptopurine) that are used in anticancer therapy.^[1,9–13] GMP and other nucleotide metabolites have

traditionally been detected by assays based on the use of radio-labeled substrates, or via spectroscopic multi-step coupled-enzyme assays.^[14–17] In the coupled assays, the enzymes usually are free in solution. Here, we report on the electrochemical detection of GMP with GMPK, whereby the enzyme is either free in solution or immobilized on the surface of quantum dots (QD) electrodes, coupled to the oxidation of NADH. For the selective recognition of GMP we harness the natural selectivity of enzymes for their substrates. Thus, for GMP detection we utilize GMPK. The enzymatic reaction is given by:



However, as neither reaction product is particularly well suited for electrochemical detection, two subsequent reactions need to be linked to the first one, as follows:



In this coupled-enzyme system, the two auxiliary enzymes, pyruvate kinase (PK) and lactate dehydrogenase (LDH), are involved. In the second reaction, ADP (and GDP, though with less kinetic efficiency) and phosphoenolpyruvate (PEP) are converted to ATP (and GTP, though with less kinetic efficiency) and pyruvate, respectively. In the third reaction, pyruvate and the reduced form of nicotinamide adenine dinucleotide (NADH) are converted to lactate and NAD^+ . Thus, the consumption of NADH is proportional to the GMPK activity, thereby indirectly detecting the presence of GMP.

Based on the reaction scheme shown above, NADH-dependent spectroscopic assays were developed, which monitor the absorbance change at 340 nm (extinction coefficient $\epsilon = 6.2 \text{ mM}^{-1} \text{ cm}^{-1}$) due to NADH oxidation. This allows for studying the steady-state kinetics of nucleoside/nucleotide kinases, in particular GMPK.^[1,6,14] However, due to the cost of enzymes discarded after each measurement, investigations in solution are unfavorable, and a fixation of the whole enzyme system to a sensor surface would be beneficial for the analysis. The third reaction is a redox reaction and, thus, is also suited for electrochemical detection, whereby the detection relies on the analysis of the NADH concentration. NADH electrochemistry on metal electrodes is, however, rather ill-defined, and thus surface modifications have been shown to be necessary.^[18–20]

One possibility for NADH detection, as we have demonstrated previously, applies quantum dot (QD)-modified electrodes, and uses the oxidation of NADH at a rather low potential.^[21] The electrodes hereby are fabricated by coupling QDs to gold (Au) electrodes via dithiols.^[22] The advantage of such a measurement scheme lies in the light-addressability of the detection, with a photocurrent as the analytical signal.^[23,24] Upon illumination, electron–hole pairs are generated in the

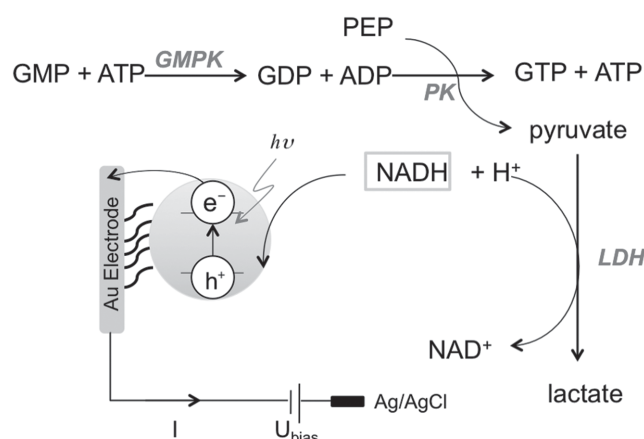


Figure 1. Detection of GMP using an NADH-dependent electrochemical assay.

QDs. A redox reaction at the QD surface attracts electrons across the solution interface to the QDs, from where they flow to the Au electrode or vice versa.^[25] Without light, there are no light-generated electron–hole pairs, and no photocurrent can flow. Cycles of illumination and darkness thus serve to switch the photocurrent on and off, which can be recorded for example by a lock-in-amplifier-based detection scheme.^[26] The amplitude of the photocurrent (at fixed bias voltage) then depends on the concentration of the redox couple in solution. This principle has been applied for analyzing a redox protein,^[27] but also different enzymatic reactions.^[25,28–30] Similar photoelectrochemical detection schemes have been recently published by several groups.^[31–33]

In the present study, we combined an enzymatic reaction cycle with the sensitive detection of NADH at a QD electrode. **Figure 1** illustrates the general scheme: For the selective detection of GMP, the enzyme GMPK is used. It catalyzes the first, rate-limiting step in the reaction pathway. The subsequent two reactions, catalyzed by PK and LDH, are limited only by the formation of products in the GMPK-catalyzed reaction. Reactions 1 and 2 are phosphorylation reactions that involve a phosphoryl group transfer from a donor (ATP or PEP) to an acceptor molecule (GMP or ADP). In contrast, reaction 3 is a redox reaction that results in the formation of NAD^+ . As outlined before, NADH can serve as electron donor to light-excited quantum dots.^[21] Light-generated holes (h^+) in the QDs hereby react with NADH, thereby oxidizing the molecule.

Thus, we detect the LDH-catalyzed reaction (Equation (3)) via the concentration change of NADH. Upon addition of pyruvate and LDH to the reaction mixture, the enzymatic conversion of pyruvate to lactate takes place causing NADH depletion, and consequently those electrons are no longer available for transfer to the QDs. In this way, an increase in pyruvate concentration reduces the photocurrent. Involving all three reactions (Equations (1)–(3)), the presence of GMP reduces the equilibrium current due to the oxidation of NADH, which was experimentally demonstrated in this work as proof-of-concept study for GMP sensing.

2. Results and Discussion

In this study, we first investigated the possibility to use the QD electrode arrangement for the detection of pyruvate, as the LDH-catalyzed conversion of pyruvate to lactate is the signal-generating reaction. For this purpose CdS/ZnS QDs (see the Supporting Information for more details) were fixed on thin-film gold electrodes with the help of stilbenedithiol (StDT), resulting in a defined photocurrent.

Based on NADH sensitivity studies reported previously,^[21] we first tested the photoelectrochemical response of the QD/StDT/Au/Si electrode in the presence of NADH and pyruvate, as well as after addition of the NADH-consuming enzyme, LDH. In the absence of LDH the photocurrent remained stable as there is no conversion. After enzyme addition, the catalytic activity could be followed by measuring the decrease in photocurrent. This can be attributed to the competition between the QD electrode and LDH for NADH and provides the basis for the subsequent GMP detection. As there was no significant change in the magnitude of the NADH-dependent photocurrent when applying a constant potential of around 0 mV vs. Ag/AgCl, for all ensuing measurements we used a constant bias of +50 mV vs. Ag/AgCl, in agreement with a previous study.^[21] For details of the bias dependence of the photocurrent, we refer to the Supporting Information.

The photocurrent was found to depend on the pyruvate concentration. As can be seen in **Figure 2**, the amplitude of the photocurrent ΔI_{\max} decreased with increasing pyruvate concentrations due to the oxidation of NADH by LDH (Equation (3)). By analyzing the concentration-dependent photocurrent changes, pyruvate could be detected in the range from 0.05 mM to 1 mM (see Figure 2). At higher pyruvate concentrations, the photocurrent was saturated under the present conditions. This was due to the limiting concentration of the co-substrate NADH, which was fixed to 1.2 mM. These data demonstrate that the electrode system allowed for pyruvate detection by measuring the consumption of NADH. This implicates that any reaction that changes the pyruvate concentration can be detected via coupling to the reaction given by Equation (3), that is, through electrochemical detection of the light-triggered current response.

In a second set of experiments, controls were carried out to demonstrate that the reactions according to Equations (1) and (2) do not interfere with the electrochemical readout. The results showed that the presence of all individual components used in the first two enzymatic reactions, namely, the enzymes GMPK and PK, and the substrates GMP (varied from 0.05 mM to 1.6 mM), ATP (4 mM), and PEP (2 mM), did not change the photocurrent. This was analyzed for reaction 1 alone (see Supporting Information) and then for both, reactions 1 and 2. The results of the latter experiments are

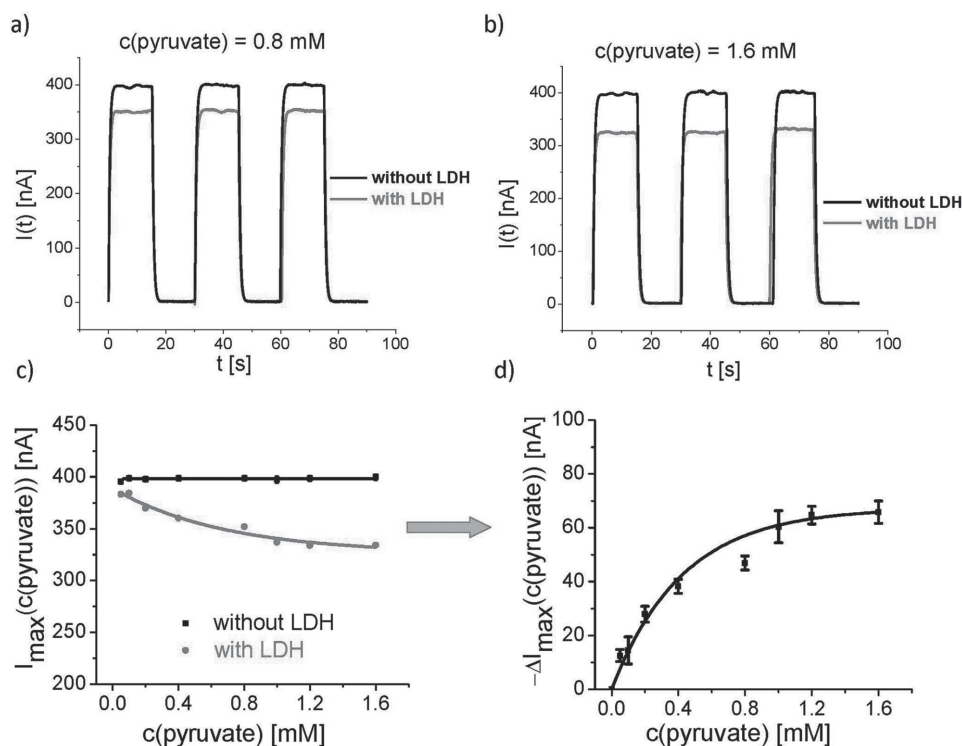


Figure 2. Examples of photocurrent measurements $I(t)$ of a QD-coated Au electrode with the following reaction conditions for Equation (3): 1.2 mM NADH and optionally 15 units mL^{-1} LDH in solution upon addition of: a) 0.8 mM pyruvate and b) 1.6 mM pyruvate. In all studies, the bias voltage U_{bias} was fixed to +50 mV. Illumination was switched on and off in cycles of 30 s. During periods of illumination, a photocurrent with amplitude I_{\max} flowed. c) Dependence of the photocurrent amplitude on the pyruvate concentration, with (“w”) or without (“wo”) 15 unit mL^{-1} LDH in solution. d) Plot of the photocurrent difference with and without LDH: $\Delta I_{\max} = I_{\max}^{\text{wLDH}} - I_{\max}^{\text{woLDH}}$, showing a response depending on the pyruvate concentration. All data points of I_{\max} and $-\Delta I_{\max}$ (c and d panels) result from mean values of I_{\max} taken during three ON/OFF cycles of illumination and the corresponding standard deviations are given as error bars.

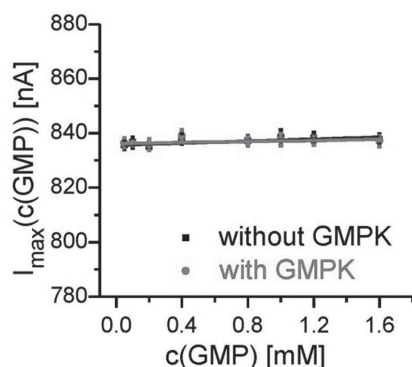


Figure 3. Photocurrent response of a CdS/ZnS-modified gold electrode in dependence of varying GMP concentrations and in the presence of 4 mM ATP, 2 mM PEP, 12 units mL⁻¹ PK in 100 mM HEPES, pH 7.5, 100 mM KCl, 20 mM MgCl₂, measured at $U_{\text{bias}} = +50$ mV, $T = 25$ °C. GMPK was optionally added at a concentration of 18 nM. All data points of I_{max} were the mean value of I_{max} taken during three ON/OFF cycles of illumination and the corresponding standard deviations are given as error bars.

compiled in **Figure 3**. These control measurements clearly demonstrate that all these substances do not disturb the read-out based on NADH oxidation. Changes in the photocurrent are thus mediated only by the reaction described in Equation (3) upon changes in the pyruvate concentration due to NADH oxidation. As the reactions according to Equations (1) and (2) alone did not lead to changes in the photocurrent, an important precondition for the application of a sequential enzymatic reaction cascade is fulfilled with this transduction system.

In the next step for developing a GMP-detecting sensor, we combined all three enzymatic reactions with the detection at the QD electrode. In a first approach, all enzymes (GMPK, PK, LDH) were added directly to the electrolyte. Photocurrent measurements were performed with varying concentrations of GMP, but with fixed activities of the three enzymes and fixed concentrations of ATP, PEP,

and NADH. Furthermore, a control experiment was performed in which no GMPK was added to the solution, yet all other substances were retained as in the previous experiment. No signal change was detected for this control series, thus verifying the selectivity of the signal originating from the enzymatic reaction chain. The difference in photocurrent $\Delta I_{\text{max}} = I_{\text{max}}^{\text{wGMPK}} - I_{\text{max}}^{\text{woGMPK}}$ (with and without GMPK) was used as the final electrode read-out. The results shown in **Figure 4** indicate that the photocurrent response was dependent on the concentration of added GMP. This demonstrates that a signal chain was established from the GMPK reaction in the first step through the PK and LDH-dependent reactions and finally to the NADH oxidation at the QD electrode. The dependency of the response on the GMP concentration, as shown in Figure 3 for the coupled-enzyme reaction system, verified that GMP can be detected photoelectrochemically.

By comparing the response of the QD electrode to pyruvate (Figure 2) with its response to GMP (Figure 4) it becomes evident that the sensing behavior of the three-enzyme system is determined by the response of the QD electrode to NADH. The GMP is quantitatively converted by the used enzymes and thus the presence of GMP is “translated” into a decrease of NADH at the QD electrode. This also means that reaction 2 and 3 are not rate limiting and that they can convert all the produced intermediates. Reaction 1 is consequently the reaction which governs the coupled enzymatic reaction cascade.

In the ultimate step of the GMP sensor development, the enzymes PK, LDH, and GMPK were immobilized on top of the QD electrode. To do so, the enzymes were first adsorbed and then covered by two bilayers of the polyelectrolytes poly(sodium-4-styrene sulfonate) (PSS) and poly(allylamine) hydrochloride (PAH). Such polyelectrolyte multilayer systems have been shown to provide a beneficial matrix for protein immobilization, as well as to improve the stability of enzymes and preserve their activity, but also the photocurrent behavior of QD electrodes.^[26,34]

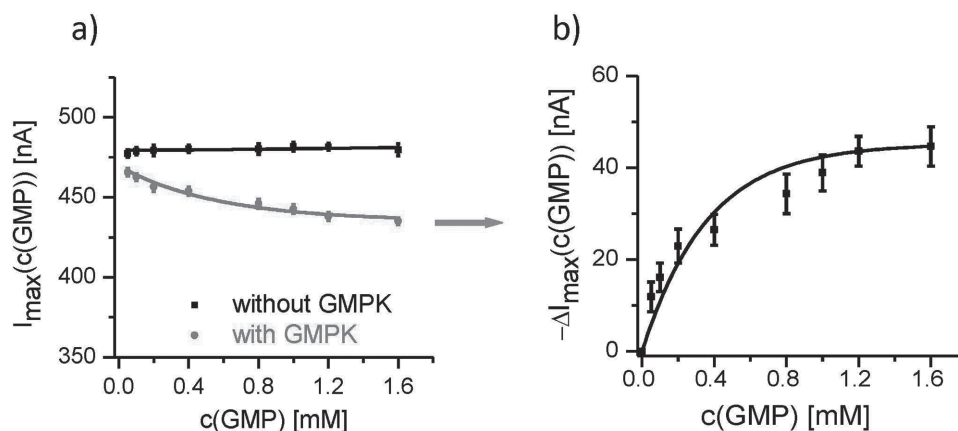


Figure 4. a) Amplitude of the photocurrent I_{max} versus the GMP concentration with all enzymes directly added to the solution. Reaction conditions for Equations (1)–(3): 1.2 mM NADH, 4 mM ATP, 2 mM PEP, 12 units mL⁻¹ PK, 15 units mL⁻¹ LDH, 100 mM HEPES, pH 7.5, 100 mM KCl, 20 mM MgCl₂, $U_{\text{bias}} = +50$ mV, $T = 25$ °C. GMPK was optionally added at a concentration of 18 nM. The GMP concentration was varied. b) The difference in photocurrent amplitude with (“w”) and without (“wo”) GMPK is plotted: $\Delta I_{\text{max}}(c(\text{GMP})) = I_{\text{max}}^{\text{wGMPK}}(c(\text{GMP})) - I_{\text{max}}^{\text{woGMPK}}(c(\text{GMP}))$. All data points of I_{max} and $-\Delta I_{\text{max}}$ (c and d panels) represent the mean values of I_{max} during three ON/OFF illumination cycles and the corresponding standard deviations are given as error bars.

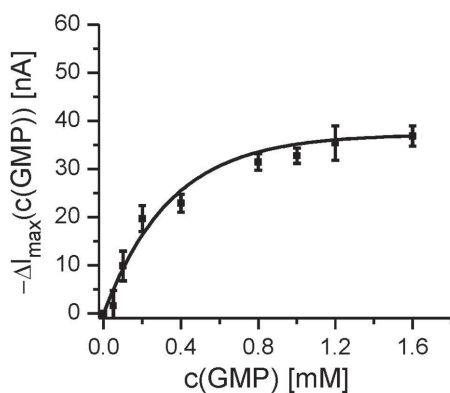


Figure 5. Sensitivity plot of the photobioelectrochemical sensor: Amplitude of the photocurrent change ΔI_{\max} versus GMP concentration with PK, LDH, and GMPK immobilized on top of the CdS/ZnSAu electrode. (Solution: 1.2 mM NADH, 4 mM ATP, 2 mM PEP, 100 mM HEPES, pH 7.5, 100 mM KCl, 20 mM CaCl_2 ; $U_{\text{bias}} = +50$ mV, $T = 25$ °C). All data points of $-\Delta I_{\max}$ were obtained from the mean values of I_{\max} during three ON/OFF cycles of illumination and the corresponding standard deviations are given as error bars.

As GMPK was now bound to the electrode, reference measurements without GMPK (such as shown in Figure 4) could not be performed, and therefore photocurrent measurements without added GMP were used as reference: $\Delta I_{\max}(c(\text{GMP})) = I_{\max}^{\text{wGMP}}(c(\text{GMP})) - I_{\max}^{\text{woGMP}}$. The change in current was detected by the sensor within a few minutes after mixing the reactants. A stable photocurrent signal was always obtained. In **Figure 5**, the changes in photocurrent are plotted against the GMP concentration, resulting in a well-defined response curve verifying the sensitivity in the concentration range from 0.05 to 1 mM.

The current change ΔI_{\max} recorded in the system with the immobilized enzymes was similar to that detected with the enzymes in solution. This demonstrates that GMP can also be detected with a completely prefabricated electrode in which all enzymes have been readily incorporated and do not have to be added separately into the solution. The concentration range and sensitivity is rather similar to some other electrochemical systems based on the direct oxidation of GMP at modified electrode surfaces.^[35–37] However, such systems need a rather high working potential, which also increases the susceptibility for interfering reactions with other molecules (e.g., ascorbic acid or other nucleotides), and are therefore less beneficial for GMP sensing. In contrast, the sensor illustrated in this study combines a low operation potential of the QD electrode-based NADH detection with a high selectivity of the enzymatic reactions, resulting in superior electrochemical GMP detection. Furthermore, the construction of such enzymatic reaction cascades on QD electrodes has great potential for the detection of other nucleotides by simply replacing the nucleotide-consuming substrate-specific enzyme. In particular, our system can easily be adapted to monitoring ATPase, GTPase, and protein kinase reactions that generate ADP or GDP. Thus, the combination of the light-triggered read-out by spatially resolved illumination and spatially resolved immobilization of the corresponding enzymes may allow for the parallel analysis of different nucleotides in solution. However, the defined fixation of

small enzyme spots on the QD electrodes needs further investigation.

3. Conclusions

This study demonstrates that photocurrent generation at QD electrodes can be effectively combined with a sequential enzymatic reaction cascade to result in a light-triggered sensor for detecting and quantifying the nucleotide guanosine monophosphate (GMP, dGMP), which is a physiological metabolite generated by nucleic acid degradation, or by de novo biosynthesis in all cells. Here, three enzymes were coupled in a reaction system where the last step is a redox reaction that is detected by photocurrent measurements. The enzyme GMPK catalyzes the first step and thus ensures the selectivity of the detection. NADH is then consumed in the last enzyme reaction step, which is subsequently detected at the QD electrode by an oxidation reaction at rather low potential. We have shown that all three enzymes required in this system of GMP detection can be co-immobilized on top of the QD electrodes by making use of protein adsorption and a layer-by-layer deposition method to fix the enzymes with the help of the polyelectrolytes PSS and PAH. The sensor operated at rather low potential and could be read-out using short illumination pulses. This bio-hybrid electrode combined nanoparticles and enzymes which resulted in a new functional system. It showed a distinct concentration-dependent response, which is absent when GMPK is not present. Importantly, the signal generation was not disturbed by auxiliary enzymes and co-substrates necessary for the sequential enzymatic conversion of GMP.

Such a light-triggered read-out would particularly be beneficial in a non-structured electrode setup with spatially separated immobilized enzymes for analyzing different substrates in parallel. Localized illumination then allows for individual sensor read-out. As many enzymatic assays rely on a dehydrogenase reaction with participation of NADH, or NADPH, as the co-substrate, good prospects are expected for such kind of photoelectrochemical sensing schemes. We emphasize that sensorial GMP detection can also provide access to the analysis of biochemical processes that produce or consume this nucleotide, for instance GMPK activity, and in a more general context, we anticipate to develop sensor systems for detection of almost any physiologically occurring nucleoside and nucleotide metabolites, and even nucleoside analogs used as drugs, which can be phosphorylated by kinases.

4. Experimental Section

QDs Synthesis: CdS QDs were synthesized using established protocols.^[38,39] The CdS QDs were surrounded by a ZnS shell.^[40] The average diameter of the inorganic core of the CdS/ZnS QDs was 4.38 nm, as calculated from transmission electron microscopy (TEM), and the wavelength of the first excitation peak was $\lambda_{\text{abs}} = 399$ nm. For details we refer to the Supporting Information.

Electrode Preparation: The CdS/ZnS QDs were immobilized on the stilbenedithiol (StDT)-coated Au/Si substrates acting as

working electrodes. The method has been explained in a previously published protocol.^[22] The StDT-coated Au/Si electrodes were mounted on the vacuum holder of a spin coater, and a solution of CdS/ZnS QDs (dissolved in toluene at a QD concentration of 12.6 μM) was added while rotating the electrode at 6000 rpm for 1 minute. This type of electrode was used for the studies with the enzymes in solution, or as the basis for the enzyme immobilization during sensor development.

Enzyme Immobilization: Enzymes were immobilized on the surface of a QDs-modified Au electrode (surface area of 1 cm^2) using a layer-by-layer (LbL) assembly technique.^[41] For this, 18 nM of human guanylate kinase GMPK (purified as highly pure recombinant fusion protein with His₆-SUMO tag,^[1] 8 μL of pyruvate kinase PK (12 units mL^{-1} solution; Sigma-Aldrich), and 10 μL of lactate dehydrogenase LDH (15 units mL^{-1} solution; Sigma-Aldrich) were adsorbed on the surface of each electrode, followed by application of a 20 to 30 μL solution containing the strong poly-anion poly(sodium-4-styrene sulfonate) (PSS, $M_w = 70$ kDa, 59 μM ; Sigma-Aldrich) on top of the enzyme solution. After incubation for 15 minutes, without letting the solution dry, the electrodes were spun for 1 minute at 6000 rpm in order to remove the non-attached macromolecules. The electrodes were rinsed with water, and once they were dried, 20 to 30 μL of a solution containing the weak poly-cation poly(allylamine) hydrochloride (PAH, $M_w = 56$ kDa, 33 μM ; Sigma-Aldrich) was added to the PSS layer. After rinsing, another PSS/PAH bilayer was deposited following the same procedure. This resulted in two PSS/PAH bilayers, with PAH forming the outermost layer. The overall structure of the assembled electrode can be expressed as (PSS/PAH)₂/LDH/PK/GMPK/QD/StDT/Au/Si.

Photocurrent Measurements: The homebuilt set-up for recording the photocurrents has been described in previous publications.^[22,25,26] A Xe arc lamp (emission spectrum $\lambda = 300 - 700$ nm) controlled by a lamp power supply LPS 220 (Photon Technology International) was used as the light source. An optical chopper (Scitec instruments) was introduced in the light path ahead of the lens, which focused the light onto the working electrode, thus allowing us to modulate the incident light at a desired frequency. A plano-convex lens and a 45° mirror (Linos Germany) were used to focus light from the Xe arc lamp on the working electrode in the electrochemical cell. The illumination was periodically modulated with a chopper. The electrochemical cell (1 mL solution volume) with the three-electrode arrangement was connected to a potentiostat. In this arrangement, the working electrode (WE, i.e., the CdS@ZnS/StDT/Au/Si chip) was set to ground potential. The fixed potential $U_{\text{bias}} = +50$ mV was controlled via the reference electrode (RE, i.e., the Ag/AgCl electrode) using an operational amplifier (OP), which supplied the required voltage through the counter electrode (CE, i.e., a platinum wire). In order to improve the signal-to-noise ratio for the photocurrent measurements $I(t)$, a lock-in amplifier (EG&G Model # 5210) was used. All measurements were performed at room temperature in 100 mM HEPES buffer, pH 7.5, containing 100 mM KCl and 20 mM MgCl₂. A modulation frequency of 17.3 Hz was applied for the lock-in of the chopper. The time constant was set to 300 ms during the measurements. The modulated illumination was switched on and off for fixed periods of 30 s with a shutter (15 s on, 15 s off). The output of the lock-in amplifier, namely, the rectified mean amplitude $I = \langle |I| \rangle$ of the photocurrent, was recorded through the serial port interface using a personal computer (PC).

Supporting Information

Supporting Information is available from the Wiley Online Library or from the author.

Acknowledgements

N. Sabir and N. Khan contributed equally to this work. This work was supported by the German Research Foundation (grant PA794/15–1 to WJP, grant WI 1361/6–1 to GW, and grant Li 706/8–1 to FL). NS acknowledges the Higher Education Commission (HEC) of Pakistan and GC University Faisalabad (GCUF) of Pakistan. NK's doctoral thesis work has been funded by a DAAD scholarship. MK and NK acknowledge continuous support by the Max Planck Society.

- [1] N. Sekulic, L. Shuvalova, O. Spangenberg, M. Konrad, A. Lavie, *J. Biol. Chem.* **2002**, *277*, 30236.
- [2] B. J. Beck, M. Huelsmeyer, S. Paul, D. M. Downs, *J. Bacteriol.* **2003**, *185*, 6732.
- [3] B. Choi, G. Zocchi, *Biophys. J.* **2007**, *92*, 1651.
- [4] A. R. Van Rompay, M. Johansson, A. Karlsson, *Pharmacol. Ther.* **2000**, *87*, 189.
- [5] S. W. Hall, H. Kühn, *Eur. J. Biochem.* **1986**, *161*, 551.
- [6] M. Konrad, *J. Biol. Chem.* **1992**, *267*, 25652.
- [7] W. A. Brady, M. S. Kokoris, M. Fitzgibbon, M. E. Black, *J. Biol. Chem.* **1996**, *271*, 16734.
- [8] J. Fitzgibbon, N. Katsanis, D. Wells, J. Delhanty, W. Vallins, D. M. Hunt, *FEBS Lett.* **1996**, *385*, 185.
- [9] B. G. Gentry, S. N. Gentry, T. L. Jackson, J. Zemlicka, J. C. Drach, *Biochem. Pharmacol.* **2011**, *81*, 43.
- [10] P. Karran, *Br. Med. Bull.* **2006**, *79–80*, 153.
- [11] P. Karran, N. Attard, *Nat. Rev. Cancer* **2008**, *8*, 24.
- [12] F. Zhang, L. Fu, Y. Wang, *Mol. Cell. Proteomics* **2013**, *12*, 3803.
- [13] B. Yuan, T. R. O'Connor, Y. Wang, *ACS Chem. Biol.* **2010**, *5*, 1021.
- [14] K. C. Agarwal, R. P. Miech, R. E. Parks, Jr., *Methods Enzymol.* **1978**, *51*, 483.
- [15] S. Hazra, S. Ort, M. Konrad, A. Lavie, *Biochemistry* **2010**, *49*, 6784.
- [16] L. K. Miller, R. D. Wells, *Proc. Natl. Acad. Sci. USA* **1971**, *68*, 2298.
- [17] M. Staeben, K. M. Kleman-Leyer, A. L. Kopp, T. A. Westermeyer, R. G. Lowery, *Assay Drug Dev. Technol.* **2010**, *8*, 344.
- [18] L. Gorton, E. Domínguez, *Rev. Mol. Biotechnol.* **2002**, *82*, 371.
- [19] C. E. Banks, R. G. Compton, *Analyst* **2005**, *130*, 1232.
- [20] S. Kochius, A. O. Magnusson, F. Hollmann, J. Schrader, D. Holtmann, *Appl. Microbiol. Biotechnol.* **2012**, *93*, 2251.
- [21] K. Schubert, W. Khalid, Z. Yue, W. J. Parak, F. Lisdat, *Langmuir* **2010**, *26*, 1395.
- [22] W. Khalid, M. El Helou, T. Murböck, Z. Yue, J.-M. Montenegro, K. Schubert, G. Göbel, F. Lisdat, G. Witte, W. J. Parak, *ACS Nano* **2011**, *5*, 9870.
- [23] C. Stoll, S. Kudera, W. J. Parak, F. Lisdat, *Small* **2006**, *2*, 741.
- [24] E. Katz, M. Zayats, I. Willner, F. Lisdat, *Chem. Commun.* **2006**, *13*, 1395.
- [25] W. Khalid, G. Göbel, D. Hühn, J.-M. Montenegro, P. Rivera Gil, F. Lisdat, W. J. Parak, *J. Nanobiotechnol.* **2011**, *9*, 46.
- [26] Z. Yue, W. Khalid, M. Zanella, A. Z. Abbasi, A. Pfreundt, P. Rivera Gil, K. Schubert, F. Lisdat, W. J. Parak, *Anal. Bioanal. Chem.* **2010**, *396*, 1095.

- [27] C. Stoll, C. Gehring, K. Schubert, M. Zanella, W. J. Parak, F. Lisdat, *Biosens. Bioelectron.* **2008**, *24*, 260.
- [28] J. Tanne, D. Schäfer, W. Khalid, W. J. Parak, F. Lisdat, *Anal. Chem.* **2011**, *83*, 7778.
- [29] M. Riedel, G. Göbel, A. M. Abdelmonem, W. J. Parak, F. Lisdat, *ChemPhysChem* **2013**, *14*, 2338.
- [30] X. Xu, J. Qian, J. Yu, Y. Zhang, S. Liu, *Chem. Commun.* **2014**, *50*, 7607.
- [31] W.-W. Zhao, J.-J. Xu, H.-Y. Chen, *Chem. Rev.* **2014**, *114*, 7421.
- [32] W.-W. Zhao, J.-J. Xu, H.-Y. Chen, *Chem. Soc. Rev.* **2015**, *44*, 729.
- [33] Y.-T. Long, C. Kong, D.-W. Li, Y. Li, S. Chowdhury, H. Tian, *Small* **2011**, *7*, 1624.
- [34] F. Caruso, D. Trau, H. Möhwald, R. Renneberg, *Langmuir* **2000**, *16*, 1485–1488.
- [35] H. Xie, D. Yang, A. Heller, Z. Gao, *Biophys. J.* **2007**, *92*, L70.
- [36] R. N. Goyal, B. K. Puri, N. Jain, *J. Chem. Soc., Perkin Trans. 2* **2001**, 832.
- [37] J. X. He, K. Kobayashi, Y. M. Chen, G. Villemure, A. Yamagishi, *Electrochem. Commun.* **2001**, *3*, 473.
- [38] W. W. Yu, X. Peng, *Angew. Chem. Int. Ed.* **2002**, *41*, 2368.
- [39] H. Y. Chen, S. Maiti, D. H. Son, *ACS Nano* **2012**, *6*, 583.
- [40] C.-A. J. Lin, R. A. Sperling, J. K. Li, T.-Y. Yang, P.-Y. Li, M. Zanella, W. H. Chang, W. J. Parak, *Small* **2008**, *4*, 334.
- [41] G. Decher, *Science* **1997**, *277*, 1232.

Received: June 28, 2015
Revised: August 10, 2015
Published online:

NANO MICRO
small

Supporting Information

for *Small*, DOI: 10.1002/smll.201501883

Photo-electrochemical Bioanalysis of Guanosine
Monophosphate Using Coupled Enzymatic Reactions at a
CdS/ZnS Quantum Dot Electrode

*Nadeem Sabir, Nazimuddin Khan, Johannes Völkner, Felix
Widdascheck, Pablo del Pino, Gregor Witte, Marc Riedel,
Fred Lisdat,* Manfred Konrad,* and Wolfgang J. Parak**

Photoelectrochemical bioanalysis of guanosine monophosphate via the use of coupled enzymatic reactions at a CdS/ZnS quantum dot electrode

Nadeem Sabir^{1§}, Nazimuddin Khan^{2§}, Johannes Völkner¹, Felix Widdascheck¹, Pablo del Pino³, Gregor Witte¹, Marc Riedel⁴, Fred Lisdat^{4*}, Manfred Konrad^{2*}, Wolfgang J. Parak^{1,3*}

¹ Fachbereich Physik, Philipps Universität Marburg, Marburg, Germany

² Max Planck Institute for Biophysical Chemistry, Göttingen, Germany

³ CIC biomaGUNE, San Sebastian, Spain

⁴ Biosystems Technology, Institute of Applied Life Sciences, Technical University Wildau, Wildau, Germany

* corresponding authors: flisdat@th-wildau.de, mkonrad@mpibpc.mpg.de,
wolfgang.parak@physik.uni-marburg.de

§ contributed equally

Supporting Information

I) Materials and Methods

I.1) Reagents

I.2) Quantum dot synthesis

I.3) Preparation of the Au electrode and immobilization of dithiol on Au

I.4) Electrochemical cell and measurement set-up

II) Measurements

II.1) Photocurrent measurements of the QD electrode following the pyruvate conversion (third reaction)

II.2) Photocurrent measurements of the QD electrode with the reactants of the first enzyme reaction

II.3) Photocurrent measurements of the QD electrode in solutions with the reactants of the first and second enzyme reaction

II.4) Photocurrent measurements of the QD electrode with all the three enzymes in solution

II.5) Photocurrent measurements of the QD sensor electrode immobilized enzymes

III) References

I) Materials and Methods

I.1) Reagents

Cadmium oxide (99.99%), sulfur powder (99.99%), trioctylphosphine oxide (TOPO, 99%), hexadecylamine (HDA, technical grade 90%), diethyl zinc solution ($C_4H_{10}Zn$, 1.0 M solution in heptane), hexamethyldisilathiane ($C_6H_{18}Si_2S$), 1-octadecene (ODE, technical grade 90%), oleylamine (OA, technical grade 70%), poly(sodium 4-styrenesulfonate) (PSS, $M_w \approx 70$ kDa, #243051) and poly(allylamine hydrochloride) (PAH, $M_w \approx 56$ kDa, #283223), Adenosine 5'-triphosphate (ATP), guanosine-5'-monophosphate (GMP), pyruvic acid, pyruvate kinase (PK), lactate dehydrogenase (LDH), and 4,4'-dimercaptostilbene (StDT, >96%) were purchased from Sigma-Aldrich; zinc stearate (count as $ZnO\% \approx 14\%$) from Alfa Aesar; tri-n-butylphosphine (TBP, 99%) from ABCR GmbH & Co. KG; $MgCl_2$ and KCl from Merck (Darmstadt, Germany); methanol, acetone, toluene, hexane and HEPES from Carl Roth GmbH + Co. KG (Karlsruhe, Germany); nicotinamide adenine dinucleotide reduced (NADH) and phosphoenolpyruvate (PEP) from Roche Diagnostic GmbH (Mannheim, Germany). Human guanylate kinase (GMPK) was expressed and purified as highly pure recombinant fusion protein with His₆-SUMO tag^[1].

I.2) Quantum dot synthesis

Synthesis of CdS nanoparticle (NP) cores, *i.e.* quantum dots (QDs), was carried out by using the procedure reported by Yu and Chen.^[2,3] Briefly, cadmium oxide (0.126 g), oleic acid (2.02 g), and ODE (12.0 mL) were added in a three-neck flask. The system was heated to 300 °C under nitrogen atmosphere after degassing. At this temperature, sulfur dissolved in ODE (0.25 M, 2.0 mL) was swiftly injected into the mixture. After the injection, the temperature was reduced to 240 °C for 3.5 minutes. For the precipitation of the QDs, toluene (10 mL) was added followed by 20-30 mL of acetone. The resulting solution was then centrifuged at 2000 rounds per minute (rpm) for 5 minutes, and the precipitate was re-dispersed in toluene. One more washing step was performed by adding 20-30 mL of methanol. The precipitate (after discarding of the supernatant) containing the CdS NPs was re-dispersed in hexane.

Growth of a ZnS shell on top of the CdS cores. A previously described protocol was used for the growth of a ZnS shell onto the CdS QDs.^[4] For this purpose, 4 g of TOPO and 1 g of HDA were weighed in a 50 mL 3-necked flask. The temperature of this mixture was increased under vacuum up to 120 °C for 20 minutes under stirring. After switching the vacuum to argon flow, an appropriate amount of CdS QD solution (NP concentration *ca* $c_{NP} = 4 \mu M$, NP concentrations were determined by UV/Vis absorption spectra according to Yu *et al.*^[5]) was injected into the TOPO/HDA mixture, and the chloroform was then removed under vacuum. After switching the vacuum to nitrogen, the temperature was raised to 170 °C according to published procedures^[6]. A stock solution for the ZnS shell growth was prepared by dissolving 0.31 g of diethylzinc solution and 0.45 g of hexamethyldisilathiane in 20.0 g TBP. The stock solution was added dropwise to the CdS/TOPO/HAD mixture. The amount of added stock

solution for growing the ZnS shell was calculated according to a previously published protocol.^[6] After adding the ZnS precursor, the temperature was reduced to 100 °C, and the solution was kept stirring for 2 hours. Then the reaction was stopped by removing the heating mantle, and the CdS/ZnS NPs were precipitated by adding methanol. After discarding of the supernatant, the NPs were re-dispersed in toluene. UV/Vis absorption and fluorescence spectra, as well as transmission electron microscopy (TEM) images of the resulting CdS/ZnS QDs are shown in Figure SI-I.2.1.

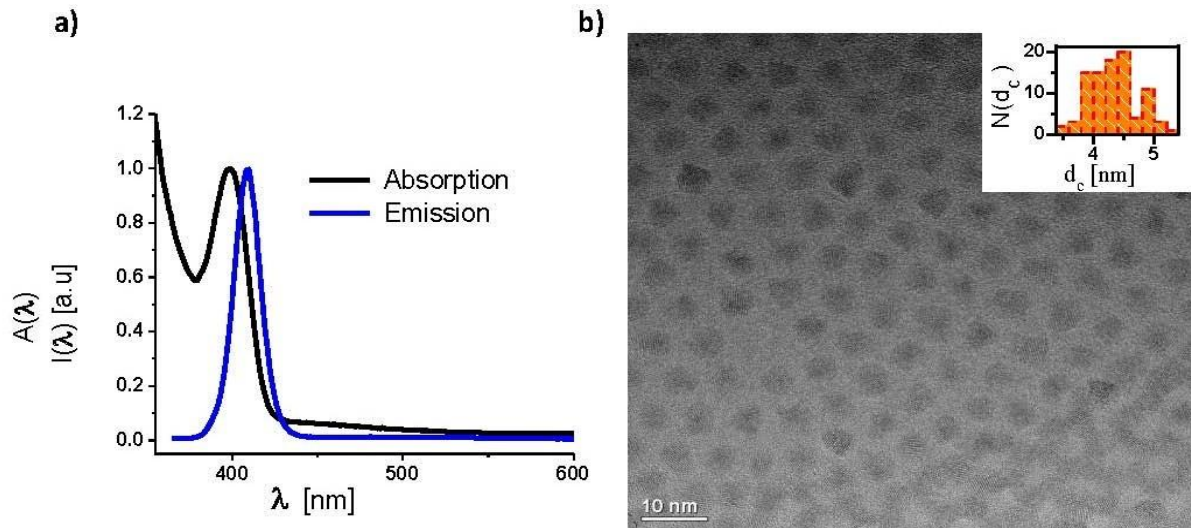


Figure SI-I.2.1: a) Normalized absorption $A(\lambda)$ (black line) and fluorescence $I(\lambda)$ spectra (blue line, emission at 409 nm) of CdS/ZnS QDs dissolved in toluene. The wavelengths of the first excitation peak in the absorption spectrum and of the maximum of the fluorescence emission of the CdS/ZnS NPs are $\lambda = 399$ nm and $\lambda = 409$ nm, respectively. The wavelengths of the first excitation peak in the absorption spectrum and of the maximum of the fluorescence emission of the underlying, original CdS NPs were $\lambda = 390$ nm and $\lambda = 398$ nm, respectively. b) TEM image of the CdS/ZnS QDs. The scale bar corresponds to 10 nm. The mean core diameter d_c of the CdS/ZnS NPs as determined from the size distribution $N(d_c)$ is $d_c = 4.4 \pm 0.4$ nm.

1.3) Preparation of the Au electrode and immobilization of dithiol on Au

Polished silicon wafers covered with a native oxide layer (SilchemHgbmh) were cut into pieces of 1 cm², rinsed with 2-propanol and ethanol and subsequently dried in a nitrogen stream. Gold was deposited *via* sputter deposition in argon plasma yielding a homogeneous film with a thickness of about 15 nm (Au/SiO₂).

Self-assembling monolayers (SAMs) of stilbenedithiol were prepared following previously established protocol.^[7] Au/SiO₂ substrates were immersed in a 100 nM solution of StDT in toluene for 24 hours at 75 °C, followed by subsequent rinsing with toluene and drying in a nitrogen stream to remove excess molecules. For daily experiments, individual solutions were prepared from a 100 μM stock solution in toluene which was renewed every month and stored refrigerated in the dark to avoid aging.

Please note that in this study instead of a massive Au electrode a thin Au film deposited on a Si chip was used as working electrode (Au/Si substrate). While for linking off the StDT layer to the surface of the working electrode the underlying Si substrate does not play a role, it may well influence details of signal generation. As Si is a semiconductor, electron-hole pairs may be also generated in the Si chip upon illumination, which can contribute to the photocurrent. In this way the underlying Si chip may be involved in the photocurrent in addition to the photocurrent originating from the QDs. However, the detailed source of the basic photocurrent is not of importance for the here described sensor assay.

I.4) Electrochemical cell and measurement set-up

The electrochemical measurement set-up consisted of five main parts: A light source, a chopper, an electrochemical cell, a three-electrode system, and a lock-in amplifier. This set up was described in previously published protocols.^[7-9]

Light Source: A Xe arc lamp (emission spectrum $\lambda_{em} = 300 - 700$ nm), controlled by a lamp power supply (LPS 220 by Photon Technology International), was used as a light source. The light from the arc lamp to the electrochemical cell was focused through a convex and a plano-convex lens coupled to a 45° mirror, as shown in the schematic diagram Figure SI-I.4.3. All the optical parts were purchased from Linos Germany. The illumination power (P_{illum}) of the resulting light spot of approximately 6 mm diameter was measured with a photometer (Fieldmaster photometer, Coherent). An illumination power of $P_{illum} = 23$ mW was used for electrochemical measurements reported in this work.

Optical chopper: An optical chopper (Scitec instruments) was used in the light prior to the convex lens to modulate the incident light at a desired frequency.

Electrochemical measurement cell: The electrochemical measurement cell harboring the Au chips is shown in Figure SI-I.4.3. It comprised a rectangular container which contained the buffer solution of up to 2 mL, and built a support for both, the reference and the counter electrode. Light entered the chamber from the top to hit the gold electrode on the bottom. At the bottom, the rectangular container contained a small hole of 6 mm diameter. The electrochemical cell was tightly sealed with screws as shown in Figure SI-I.4.1.

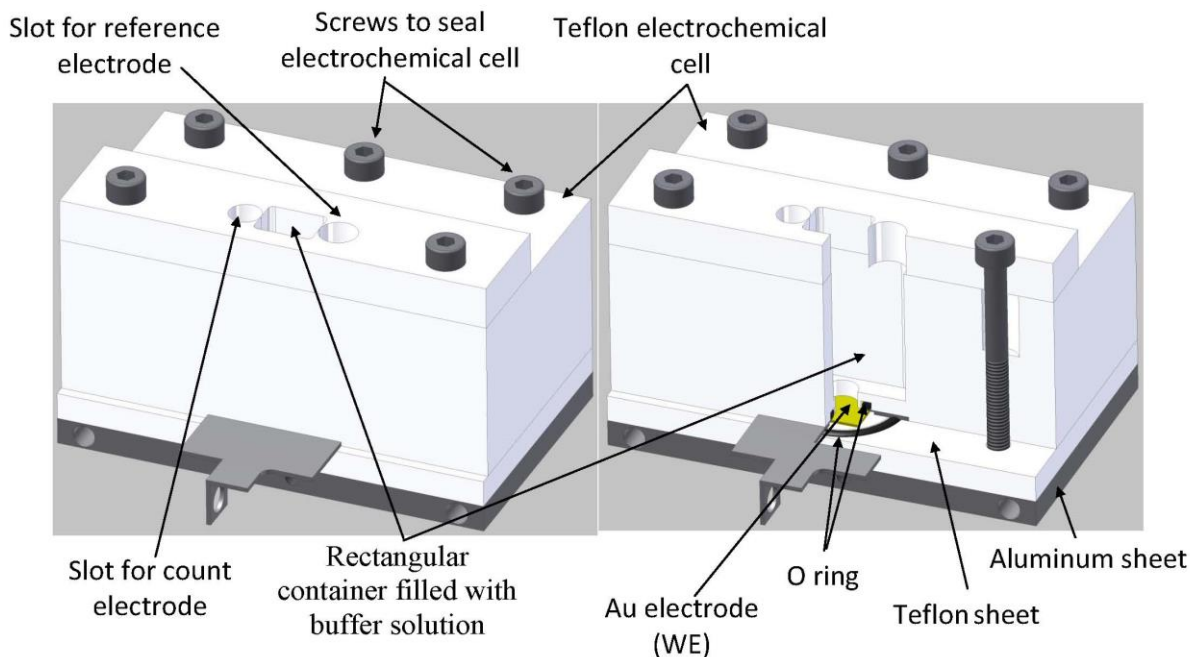


Figure SI-I.4.1: a) Complete view of the electrochemical cell showing the arrangement of the counter and reference electrode. b) Intersection view of the electrochemical cell. The Au electrode (working electrode) lies on the gold plated holder which is squeezed between the Teflon rectangular container and Teflon sheet with the help of an O-ring.

Three-electrode system: The important components of the three-electrode system were three electrodes and a microcomputer with an interface card for digital-to-analog (DAC) and analog-to-digital (ADC) conversion. An Ag/AgCl-saturated reference electrode (RE), a spiral wire of platinum as counter electrode (CE), and a gold chip as working electrode (WE) were assembled within the electrochemical cell as shown in Figure SI-I.4.3. The operational amplifiers OP1, OP2, and OP3 were mounted within the three-electrode arrangement as shown in Figure SI-I.4.2. The voltage U_{Ext} was applied by the DAC at the positive input of OP1 through OP3. The operational amplifier OP3 acted as an inverter and gave stable input. The RE was connected with the negative input of OP1. The resultant current I_{OP1} is zero, according to the characteristics of an OP (all input currents = 0), and thus no current flows through the RE. The potential difference between the RE and WE remains constant. To adjust the sensitivity of the instrument, a variable resistor was R_2 introduced in the circuit around OP2 between the negative input and the output of the OP2. This setup is called current-to-voltage converter. The output U_{out} of OP2 was measured by a lock-in amplifier followed by the ADC.

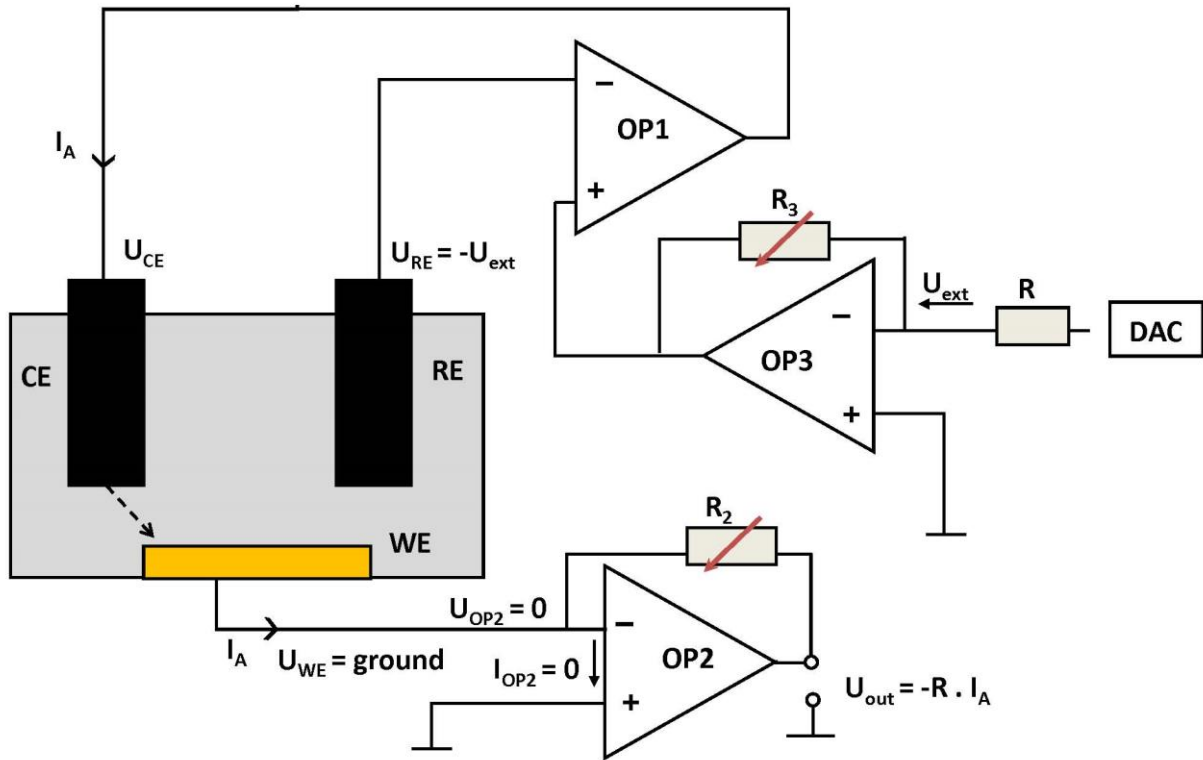


Figure SI-I.4.2: Schematics of a three-electrode system.

Lock-in amplifier: A lock-in amplifier (EG&G, Model # 5210) was used to improve the signal-to-noise ratio.^[9] A modulation frequency of 17.3 Hz for the chopper was used as a reference frequency for the lock-in. The lock-in amplifier filtered out all additional frequencies and amplified only the part of the input signal at the reference frequency. Throughout the experiment, for all the measurements, a time constant of 30 ms was used. The output of the lock-in amplifier was read by a serial port interface (DAC).

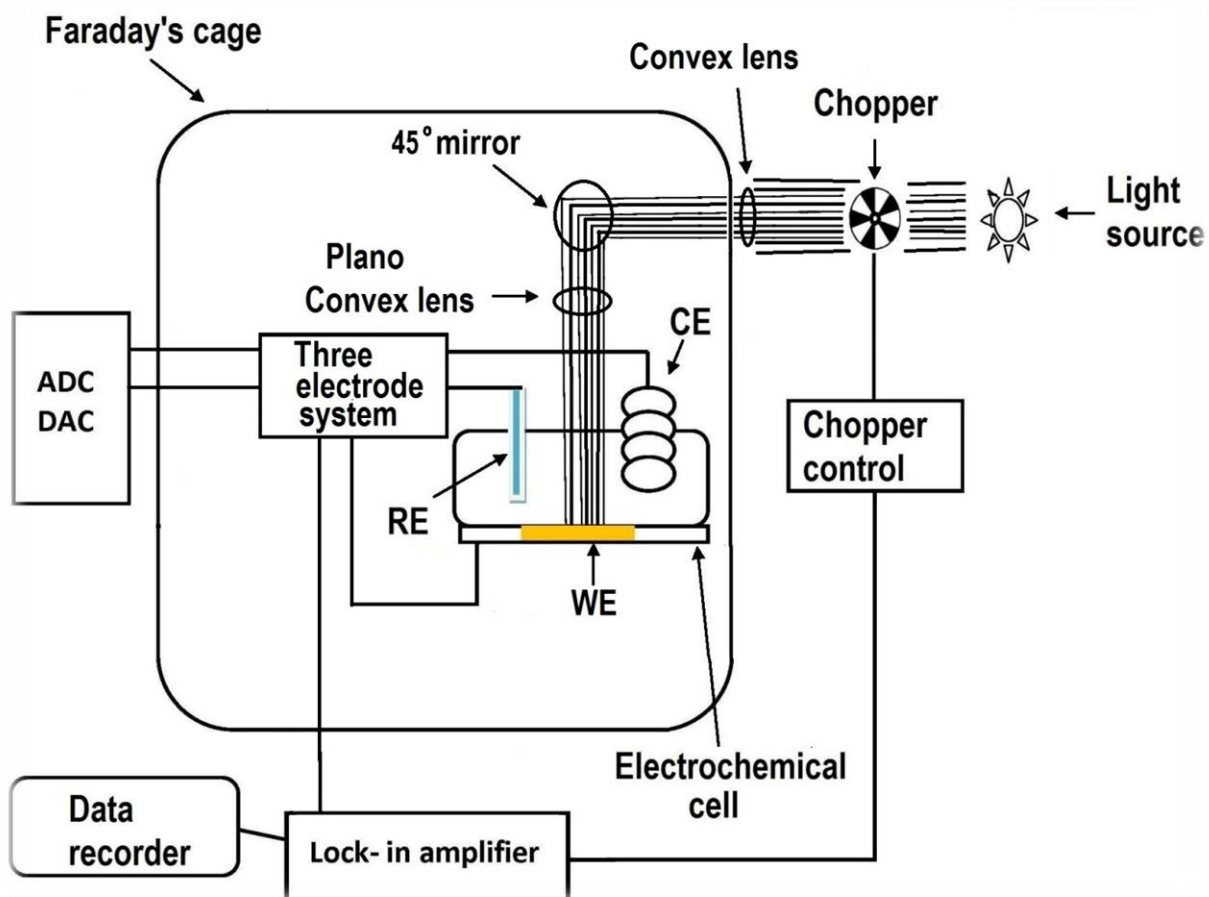


Figure SI-I.4.3: Schematic diagram of the set-up of the electronics to connect the electrochemical cell.

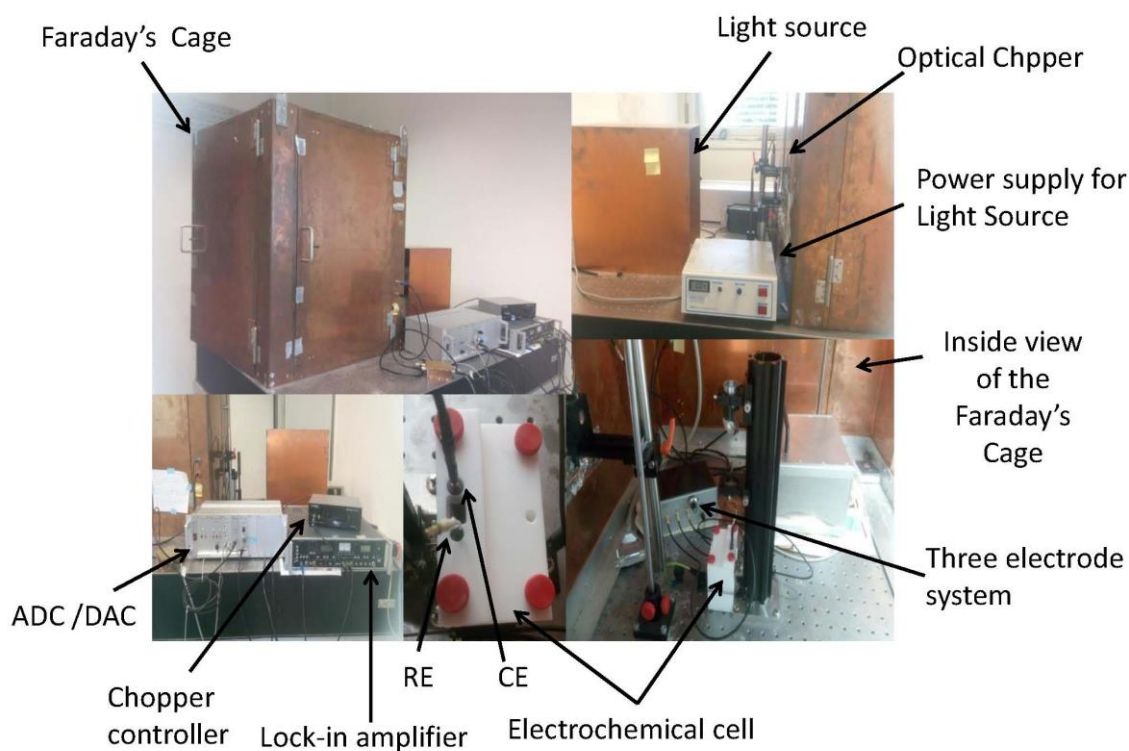


Figure SI-I.4.4: Photographs of the set-up.

II) Measurements

II.1) Photocurrent measurements of the QD electrode following the pyruvate conversion (third reaction)

The reaction according to Eq. 3 in the main text is sketched in Figure SI-II.1.1. Photocurrent measurements $I(t)$ in the presence of NADH, with and without LDH, and variable pyruvate concentrations, are shown in Figure SI-II.1.2. The modulated light was switched on and off in cycles of 30 s, and photocurrent only flew upon illumination. The concentration dependence is shown in Figure 2 of the paper. Enzymes (here LDH) were free in solution.

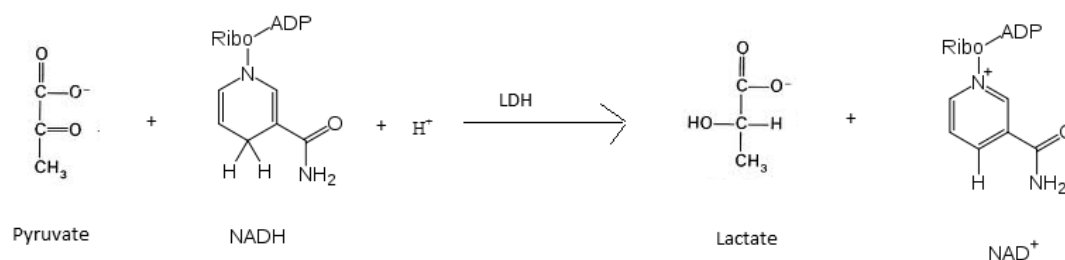


Figure SI-II.1.1: Schematic of the 3rd reaction catalyzed by lactate dehydrogenase.

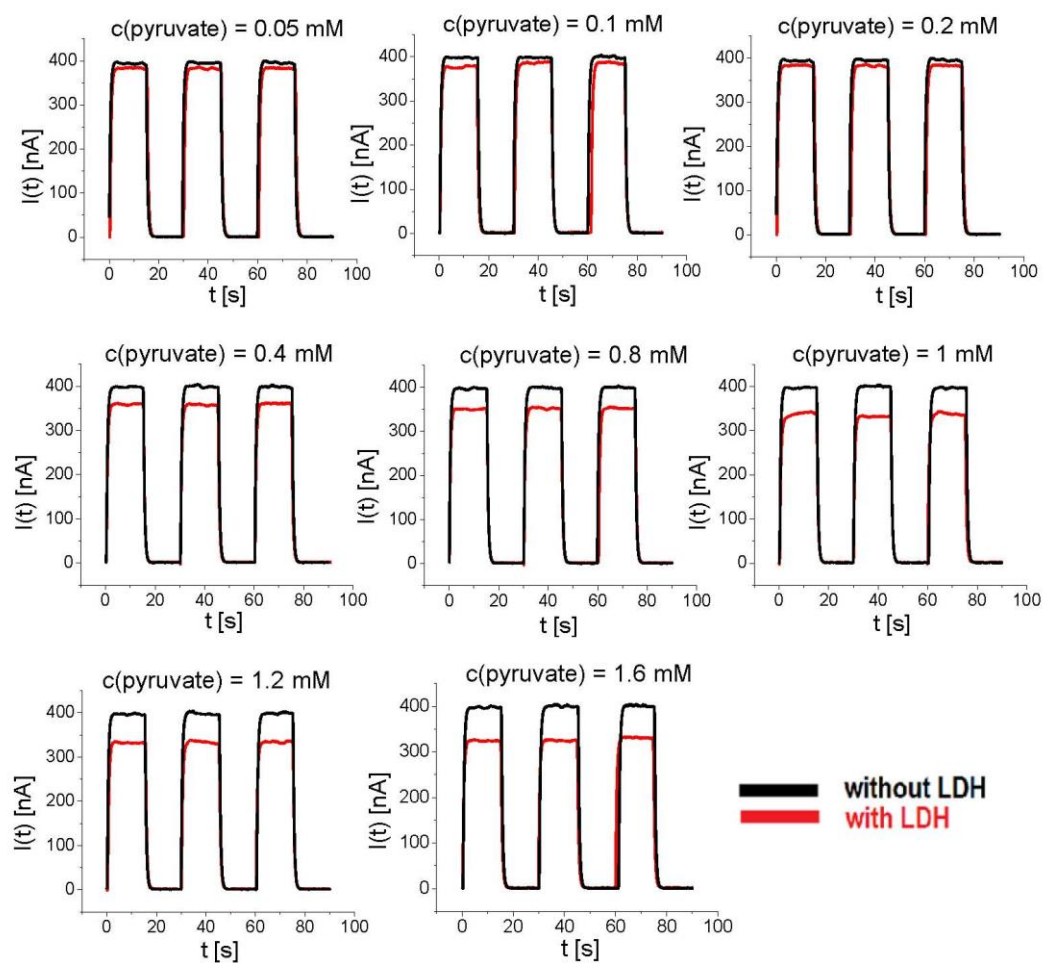


Figure SI-II.1.2: Photocurrent measurements $I(t)$ following the reaction of Eq. 3 with the following conditions: 1.2 mM NADH, 100 mM HEPES pH 7.5, 100 mM KCl, 20 mM MgCl₂,

$U_{bias} = +50 \text{ mV}$, $T = 25 \text{ }^\circ\text{C}$. LDH was optionally added (15 units/mL). Pyruvate concentrations $c(\text{pyruvate})$ were varied from 0.05 mM to 1.6 mM. The resulting amplitudes of the photocurrent versus the pyruvate concentration $I_{max}(c(\text{pyruvate}))$ are displayed in Figure SI-II.1.3. In Figure 2 of the main text, the amplitude of the photocurrent I_{max} versus the pyruvate concentration $c(\text{pyruvate})$ is plotted as the difference in photocurrent amplitude with (“w LDH”) and without LDH (“wo LDH”): $\Delta I_{max}(c(\text{pyruvate})) = I_{max}^{w LDH}(c(\text{pyruvate})) - I_{max}^{wo LDH}(c(\text{pyruvate}))$.

Photocurrent measurements $I(t)$ for the reaction given in Eq. 3 and Figure SI-II.1.1 were also carried out for different bias voltages U_{bias} , cf. Figure SI-II.1.3 and Figure SI-II.1.4. U_{bias} is the applied voltage of the working electrode versus a homemade Ag/AgCl electrode. As in the investigated range there was no significant dependence from U_{bias} , in all following measurements U_{bias} was fixed to $U_{bias} = +50 \text{ mV}$.

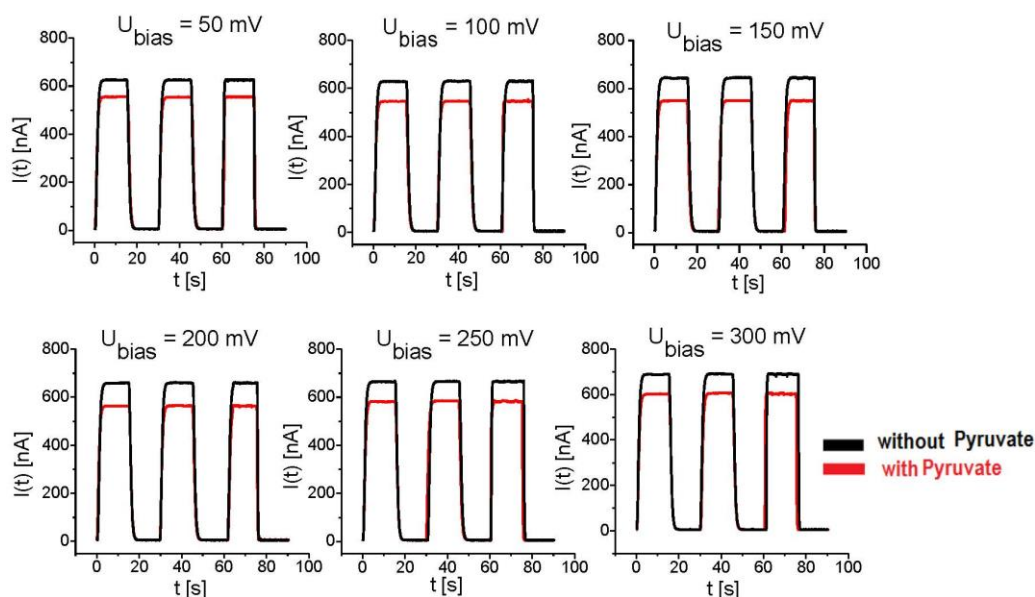


Figure SI-II.1.3: Photocurrent measurements $I(t)$ following the reaction of Eq. 3 with the following conditions: 1.2 mM NADH, 15 units/mL LDH, 100 mM HEPES pH 7.5, 20 mM MgCl_2 , $T = 25 \text{ }^\circ\text{C}$. Measurements without and with 1.2 mM pyruvate were carried out. The bias voltage U_{bias} was varied. The resulting amplitudes of the photocurrent versus the bias voltage are displayed in Figure SI-II.1.4.

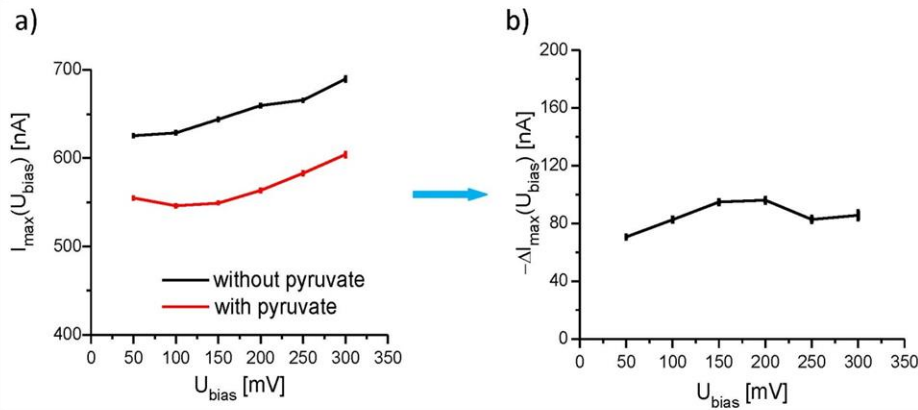


Figure SI-II.1.4: a) Amplitude of the photocurrent I_{\max} versus the applied bias U_{bias} , as derived from the data shown in Figure SI-II.1.3. The reaction according to Eq. 3 was carried out using the following conditions: 1.2 mM NADH, 15 units/mL LDH, 100 mM HEPES pH 7.5, 100 mM KCl, 20 mM MgCl_2 , $T = 25^\circ\text{C}$. Measurements without and with 1.2 mM pyruvate were performed. The bias voltage U_{bias} was varied. b) The difference in photocurrent amplitude with and without pyruvate is plotted: $\Delta I_{\max}(U_{\text{bias}}) = I_{\max}^{\text{with pyruvate}}(U_{\text{bias}}) - I_{\max}^{\text{without pyruvate}}(U_{\text{bias}})$.

II.2) Photocurrent measurements of the QD electrode with the reactants of the first enzyme reaction

The guanylate kinase reaction is sketched in Figure SI-II.2.1. Photocurrent measurements $I(t)$ in the presence of ATP, with and without GMPK, and variable GMP concentration are shown in Figure SI-II.2.2. The concentration dependence is shown in Figure SI-II.2.3. Enzymes (here GMPK) were free in solution.

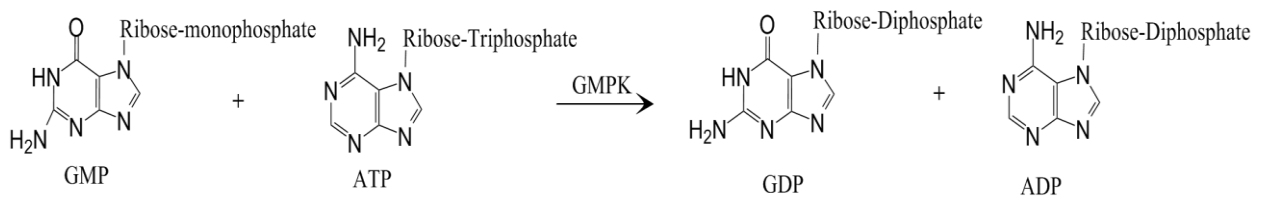


Figure SI-II.2.1: Schematic of the 1st reaction representing phosphoryl group transfer from ATP to GMP catalyzed by the enzyme guanylate kinase.

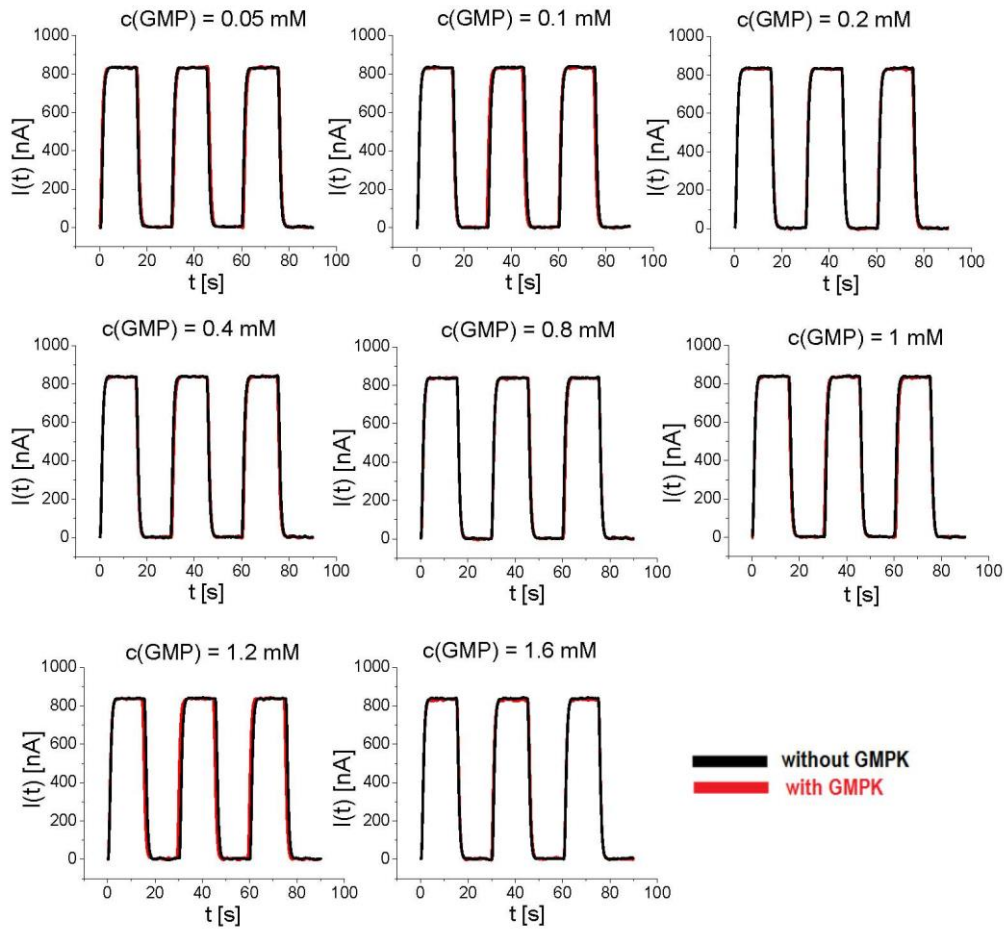


Figure SI-II.2.2: Photocurrent measurements $I(t)$ following the reaction of Eq. 1 with the following conditions: 4 mM ATP, 100 mM HEPES, pH 7.5, 100 mM KCl, 20 mM MgCl₂, $U_{bias} = +50$ mV, $T = 25$ °C. GMPK was optionally added at 18 nM. The GMP concentrations were varied from 0.05 mM to 1.6 mM. The resulting amplitudes of the photocurrent versus the GMP concentration $I_{max}(c(\text{GMP}))$ are displayed in Figure SI-II.2.3.

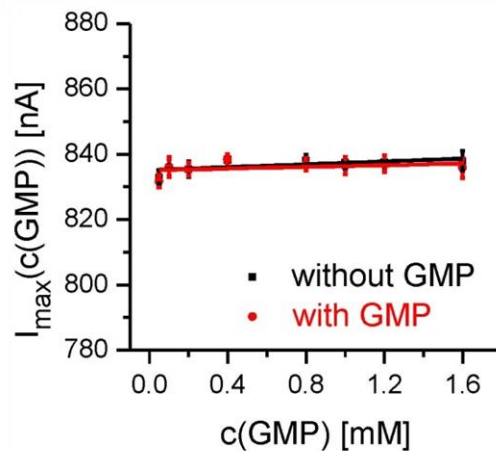


Figure SI-II.2.3: Amplitude of the photocurrent I_{max} versus GMP concentration, as derived from the data shown in Figure SI-II.2.2.

II.3) Photocurrent measurements of the QD electrode in solutions with the reactants of the first and second enzyme reaction

The pyruvate kinase reaction is sketched in Figure SI-II.3.1. Photocurrent measurements $I(t)$ in the presence of ATP, with and without GMPK, and variable GMP concentration are shown in Figure SI-II.3.2, *i.e.* reactions combining steps 1 and 2. The concentration dependence is shown in Figure SI-II.3.3. Enzymes (here PK and GMPK) were free in solution.

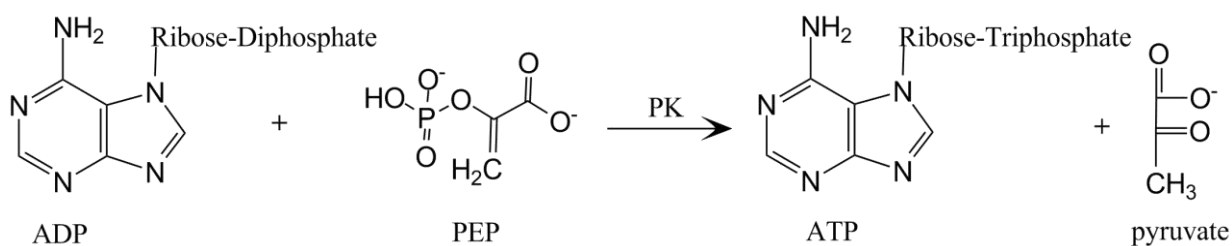


Figure SI-II.3.1: Schematic of the 2nd reaction catalyzed by pyruvate kinase.

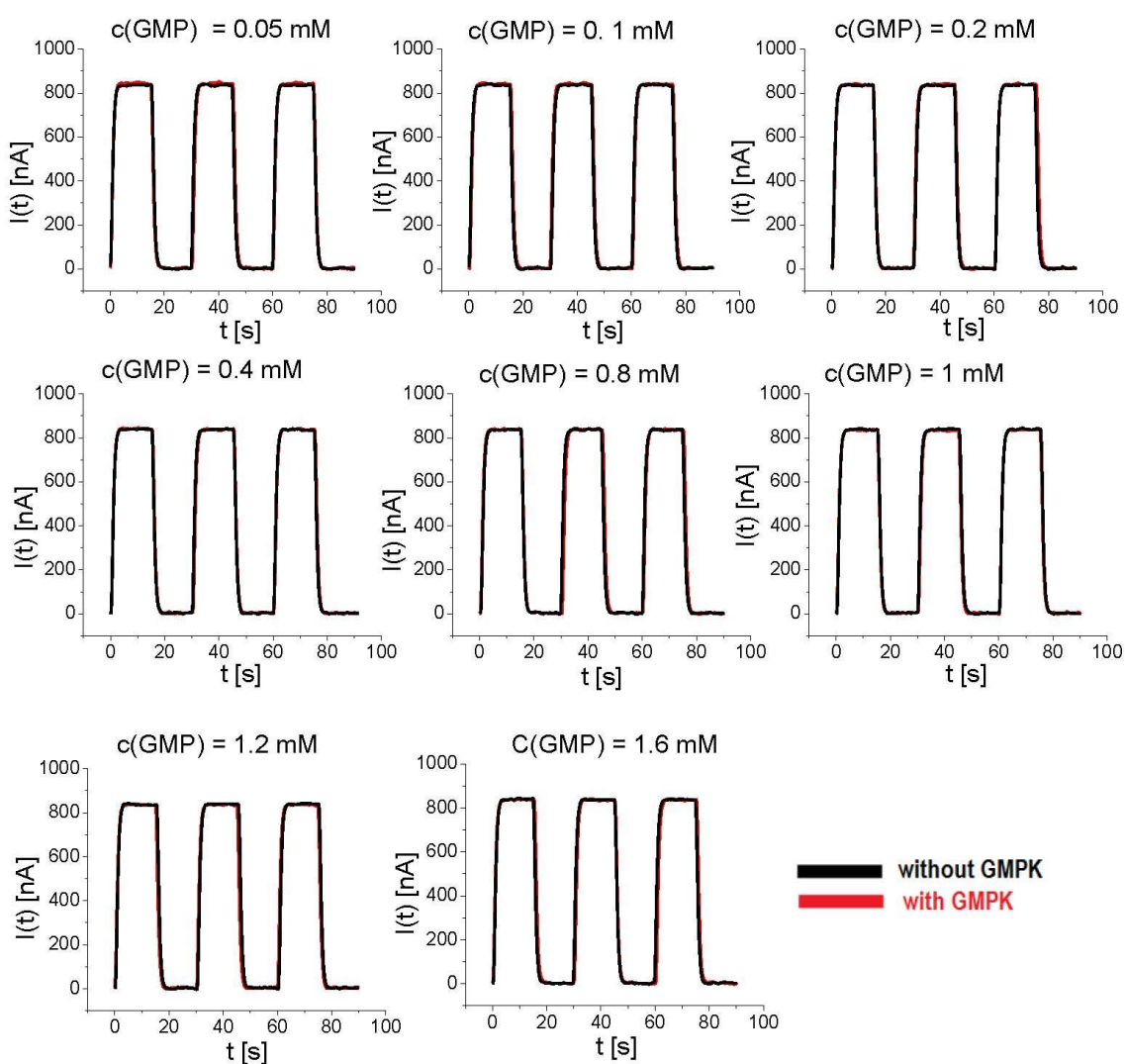


Figure SI-II.3.2: Photocurrent measurements $I(t)$ following the combined reactions of Eq. 1 and Eq. 2 with the following conditions: 4 mM ATP, 2 mM PEP, 12 units/mL PK, 100 mM

HEPES, pH 7.5, 100 mM KCl, 20 mM MgCl₂, $U_{bias} = +50$ mV, $T = 25$ °C. GMPK was optionally added at 18 nM. The GMP concentrations were varied from 0.05 mM to 1.6 mM. The resulting amplitudes of the photocurrent versus the GMP concentration $I_{max}(c(GMP))$ are displayed in Figure SI-II.3.3.

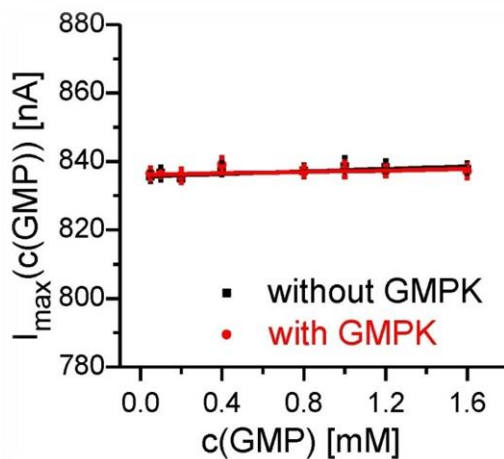


Figure SI-II.3.3: Amplitude of the photocurrent I_{max} versus GMP concentration, as derived from the data shown in Figure SI-II.3.2.

II.4) Photocurrent measurements of the QD electrode with all the three enzymes in solution

In this paragraph, results for the combination of all three reactions according to equations 1-3 are shown. Enzymes (*i.e.* PK, LDH, and GMPK) were free in solution. Photocurrent measurements $I(t)$ in the presence of ATP, PEP, NADH, PK, LDH, with and without GMPK, and variable GMP concentration are shown in Figure SI-II.4.1. The concentration dependence is shown in Figure 4 of the main text.

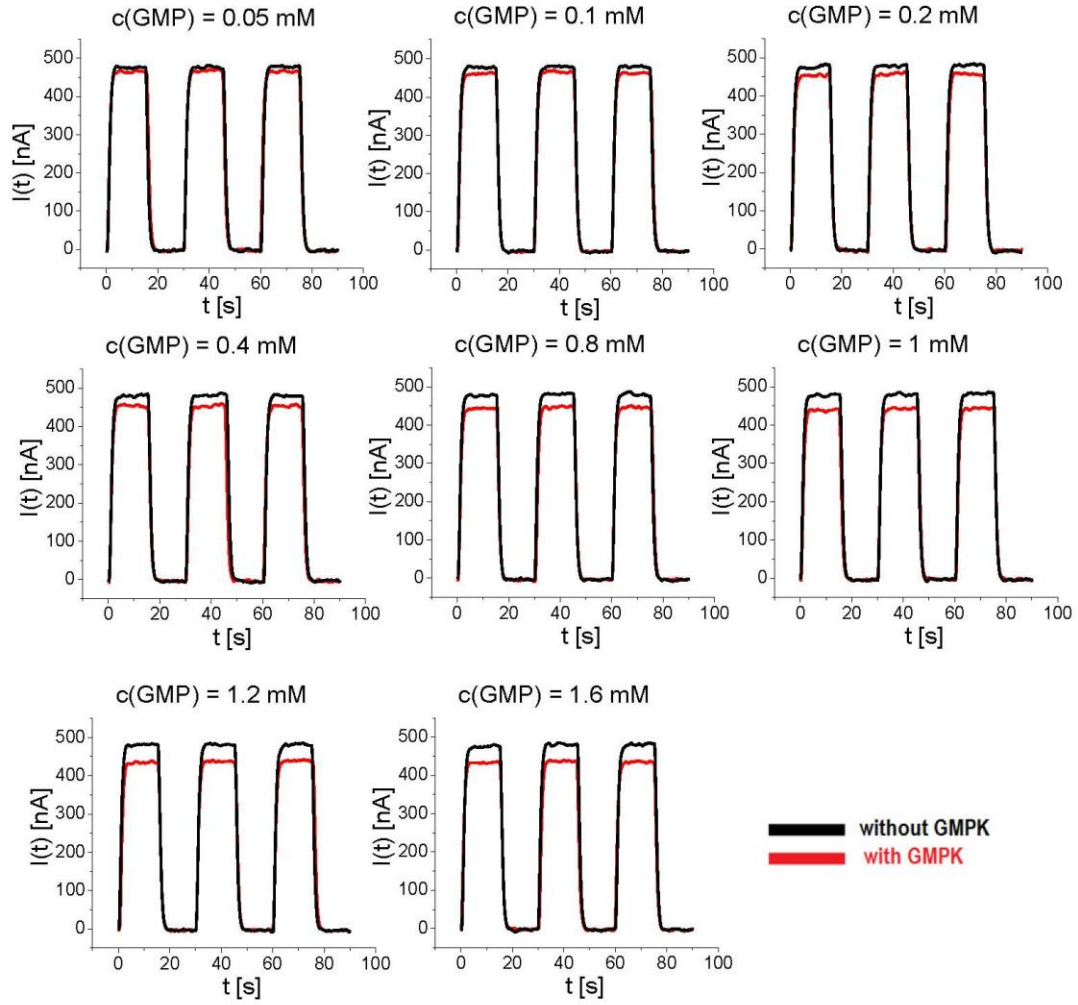


Figure SI-II.4.1: Photocurrent measurements $I(t)$ following the combined reactions of Eq. 1, Eq. 2, and Eq. 3 with the following conditions: : 1.2 mM NADH, 4 mM ATP, 2 mM PEP, 12 units/mL PK, 15 units/mL LDH, 100 mM HEPES, pH 7.5, 100 mM KCl, 20 mM $MgCl_2$, $U_{bias} = +50$ mV, $T = 25$ °C. GMPK was optionally added at 18 nM. The GMP concentrations were varied from 0.05 mM to 1.6 mM. The resulting amplitudes of the photocurrent versus the GMP concentration $I_{max}(c(GMP))$ are displayed in Figure 3 of the main text.

II.5) Photocurrent measurements of the QD sensor electrode immobilized enzymes

In this paragraph, results for the combination of all three reactions according to equations 1-3 are shown. Here, LDH, PK and GMPK were immobilized on the QD-modified electrode. Photocurrent measurements $I(t)$ in the presence of ATP, PEP, NADH, LDH, PK, GMPK and with/ without variable GMP concentration are shown in Figure SI-II.5.1. The concentration dependence is shown in Figure 5 of the main text.

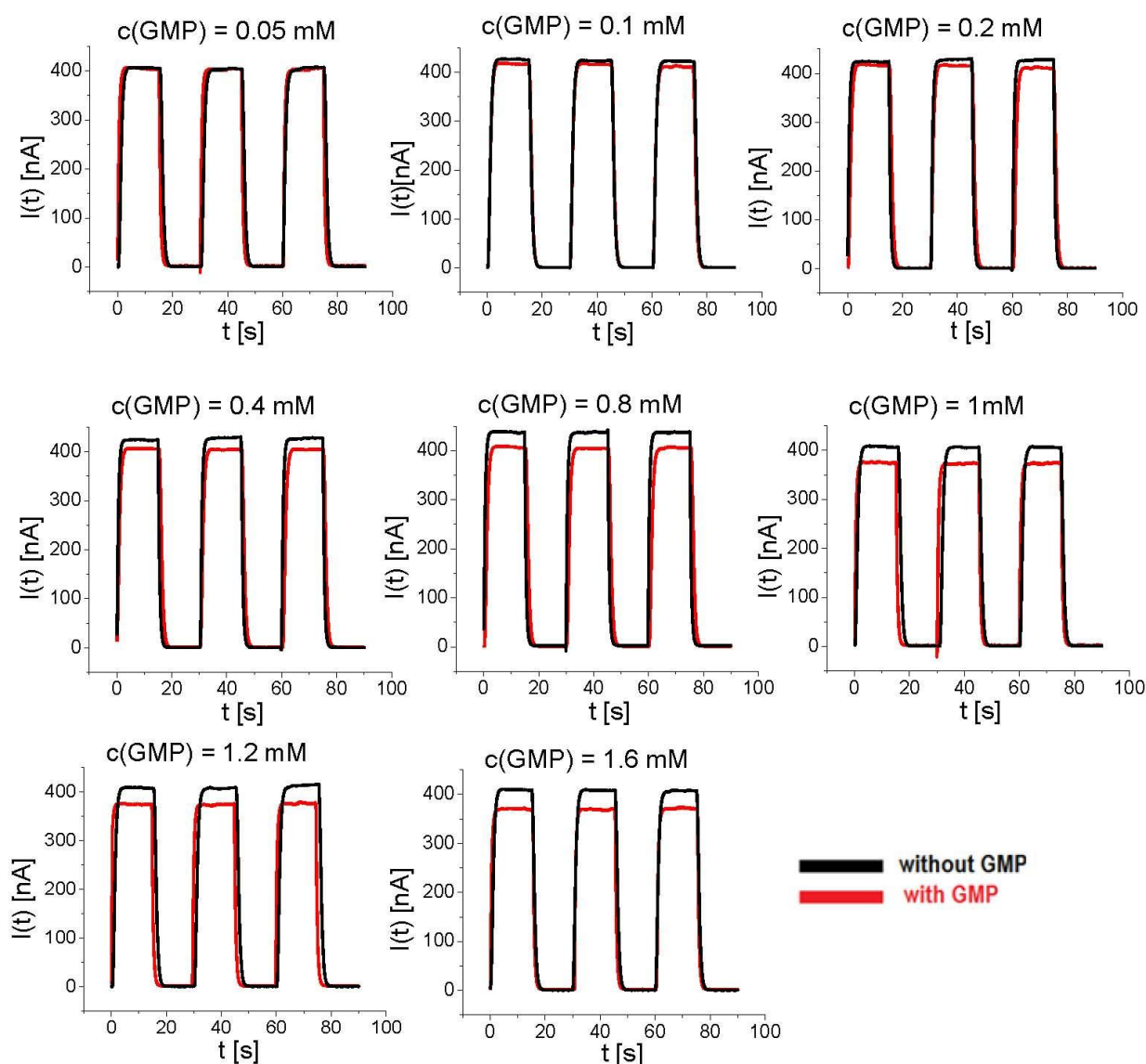


Figure SI-II.5.1: Photocurrent measurements $I(t)$ following the combined reactions of Eq. 1, Eq. 2, and Eq. 3 with the following conditions: 1.2 mM NADH, 4 mM ATP, 2 mM PEP, 100 mM HEPES, pH 7.5, 100 mM KCl, 20 mM MgCl₂, $U_{bias} = +50$ mV, $T = 25$ °C. Here, 6 μ L of 18 nM GMPK, 12 units PK and 15 units LDH were immobilized on the QDs layer. The GMP concentrations were varied from 0.05 mM to 1.6 mM. The resulting amplitudes of the photocurrent versus the GMP concentration $I_{max}(c(GMP))$ are displayed in Figure 5 of the main text.

As in all coupled enzymatic test systems the presence of intermediates such as ADP or GDP in the conversion cycle would change the response of the read-out of the coupled three reactions. However the three-step coupled-enzyme assay as presented in this work has the advantage of being a modular setup allowing for independent detection of each reaction. Therefore, in the absence of guanylate kinase, the pyruvate kinase-catalyzed reaction can be monitored to first detect the presence of ADP and/or GDP, thus excluding interference with the detection of GMP, and this applies even to cellular extracts.

III) References

- [1] N. Sekulic, L. Shuvalova, O. Spangenberg, M. Konrad, A. Lavie, *J. Biol. Chem.* **2002**, 277 (33), 30236-30243.
- [2] W. W. Yu, X. Peng, *Angew. Chem. Int. Ed.* **2002**, 41 (13), 2368-2371.
- [3] H. Y. Chen, S. Maiti, D. H. Son, *ACS Nano* **2012**, 6 (1), 583-591.
- [4] C.-A. J. Lin, R. A. Sperling, J. K. Li, T.-Y. Yang, P.-Y. Li, M. Zanella, W. H. Chang, W. J. Parak, *Small* **2008**, 4 (3), 334-341.
- [5] W. W. Yu, L. Qu, W. Guo, X. Peng, *Chem. Mater.* **2003**, 15 (14), 2854-2860.
- [6] B. O. Dabbousi, J. Rodriguez-Viejo, F. V. Mikulec, J. R. Heine, H. Mattoussi, R. Ober, K. F. Jensen, M. G. Bawendi, *J. Phys. Chem. B* **1997**, 101 (46), 9463-9475.
- [7] W. Khalid, M. E. Helou, T. Murböck, Z. Yue, J.-M. Montenegro, K. Schubert, G. Göbel, F. Lisdat, G. Witte, W. J. Parak, *ACS Nano* **2011**, 5 (12), 9870-9876.
- [8] W. Khalid, G. Göbel, D. Hühn, J.-M. Montenegro, P. Rivera Gil, F. Lisdat, W. J. Parak, *J. Nanobiotechnol.* **2011**, 9, 46.
- [9] Z. Yue, W. Khalid, M. Zanella, A. Z. Abbasi, A. Pfreundt, P. Rivera_Gil, K. Schubert, F. Lisdat, W. J. Parak, *Anal. Bioanal. Chem.* **2010**, 396 (3), 1095-1103.

Förster resonance energy transfer mediated enhancement of the fluorescence lifetime of organic fluorophores to the millisecond range by coupling to Mn-doped CdS/ZnS quantum dots

Uwe Kaiser¹, Nadeem Sabir¹, Carolina Carrillo-Carrion¹, Pablo del Pino², Mariano Bossi³, Wolfram Heimbrot¹ and Wolfgang J Parak^{1,2}

¹ Department of Physics and Material Sciences Center (WZMW), Philipps-University Marburg, Renthof 5, D-35032 Marburg, Germany

² CIC biomaGUNE, Paseo de Miramón 182, 20009, Donostia—San Sebastián, Spain

³ CONICET, Pabellón 2, Piso3, Ciudad Universitaria, Buenos Aires, Argentina

E-mail: Wolfram.Heimbrot@physik.uni-marburg.de and Wolfgang.Parak@physik.uni-marburg.de

Received 7 September 2015

Accepted for publication 10 November 2015


Published 16 December 2015



CrossMark

Abstract

Manganese-doped CdS/ZnS quantum dots have been used as energy donors in a Förster-like resonance energy transfer (FRET) process to enhance the effective lifetime of organic fluorophores. It was possible to tune the effective lifetime of the fluorophores by about six orders of magnitude from the nanosecond (ns) up to the millisecond (ms) region. Undoped and Mn-doped CdS/ZnS quantum dots functionalized with different dye molecules were selected as a model system for investigating the multiple energy transfer process and the specific interaction between Mn ions and the attached dye molecules. While the lifetime of the free dye molecules was about 5 ns, their linking to undoped CdS/ZnS quantum dots led to a long effective lifetime of about 150 ns, following a non-exponential transient. Manganese-doped core-shell quantum dots further enhanced the long-lasting decay time of the dye to several ms. This opens up a pathway to analyse different fluorophores in the time domain with equal spectral emissions. Such lifetime multiplexing would be an interesting alternative to the commonly used spectral multiplexing in fluorescence detection schemes.

 Online supplementary data available from stacks.iop.org/NANO/27/055101/mmedia

Keywords: energy transfer, time-resolved fluorescence, quantum dots

(Some figures may appear in colour only in the online journal)

1. Introduction

Using quantitative fluorescence [1, 2] for the detection of fluorophores is a common method for quantifying the concentration of analytes in a solution, e.g. via fluorescence-labelled antibodies which selectively bind to the analyte [3], or by using analyte-sensitive fluorophores [4, 5]. By using several fluorophores in parallel, in principle the concentration

of different analytes can be determined simultaneously. This is possible by using fluorophores with a different colour of emission, although this is hampered by spectral overlap as determined by the bandwidth of the emission of the different fluorophores [1]. Alternatively, discriminating the fluorescence emission of different fluorophores can also be achieved in the time domain [6]. In cases where fluorophores possess different emission lifetimes, their emission can be

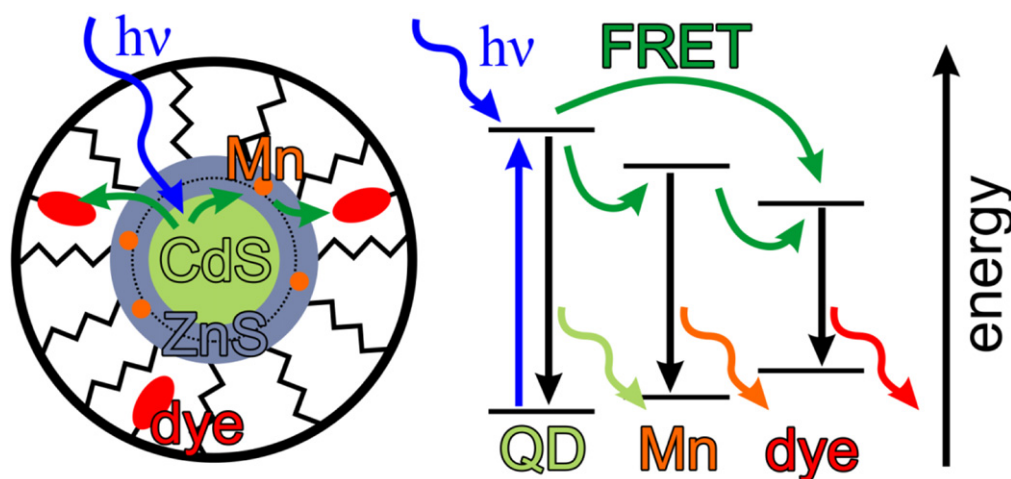


Figure 1. On the left, a sketch of the Mn-doped CdS/ZnS QDs with attached dye molecules is shown. The Mn ions are incorporated within the ZnS shell. A scheme of the different energetic states is depicted on the right. The excitation of the CdS core is indicated by the blue wavy arrow. The green arrows show the possible energy transfer pathways. The QD, the Mn ions, and the dye can all undergo radiative recombination to the respective ground state under the emission of photons.

distinguished via time-dependent fluorescence measurements. This principle is used for fluorescence lifetime imaging, for example, in which the lateral distribution of different fluorophores is detected by the deconvolution of the respective recorded emissions in the time domain [7]. Unfortunately, variation in the fluorescence lifetime of organic fluorophores is limited, typically within a range of a few nanoseconds. This lies within the same region as the autofluorescence lifetimes of biological samples such as cells [8]. The use of inorganic fluorophores based on quantum dots (QDs) allows for slightly higher fluorescence lifetimes. QDs can be combined with other fluorophores in Förster-like resonance energy transfer (FRET) schemes. In cases where lanthanides are used as donors and QDs as acceptors, a multiplexed read-out of fluorescence with long lifetimes is possible [9, 10]. Alternatively, QDs can be used as donors for organic fluorophores as acceptors [11, 12]. Based on the last detection scheme, we have recently shown that lifetime multiplexing is an interesting alternative to spectral multiplexing. In this previous work, ATTO590 dye molecules bound to gold nanoparticles (NPs) exhibited a mono-exponential decay with a lifetime of a few ns (equivalent to the lifetime of free dye molecules), whereas dye molecules bound to CdSe/ZnS QDs showed a non-exponential decay with a slow component of more than 100 ns due to the FRET from the QDs to the dye. We demonstrated the fundamental possibility of determining the mixing ratio for dyes with equal luminescence spectra but very different transients [13]. The doping of CdS/ZnS QDs with Mn ions leads to long-lived fluorescence lifetimes based on the dipole forbidden internal 3d-transition [14, 15]. In the present paper we demonstrate that in this way the fluorescence decay time of organic fluorophores can be shifted up to the ms time scale by coupling them to Mn-doped CdS/ZnS QDs.

2. Methods

In order to demonstrate the double energy transfer process among the three luminescence centres—first within the Mn-doped CdS/ZnS QDs, i.e. from the CdS/ZnS matrix to the Mn ions, and then second from the excited Mn ions to an organic dye—we conjugated the organic fluorophore ATTO633 to the surface of the Mn-doped CdS/ZnS QDs, see figure 1. For this purpose, firstly undoped and Mn-doped CdS/ZnS core-shell QDs were synthesized in the organic phase, as adopted from a previously reported method [16–19]. It must be pointed out that the Mn ions were incorporated into the ZnS shell and not the CdS core, followed by an additional ZnS shell which was grown on top of the doped shell. We thus refer to these NPs as CdS/Mn:ZnS/ZnS QDs. Transfer of the hydrophobic QDs to the aqueous phase was then achieved by overcoating the hydrophobic QDs in the organic phase with an amphiphilic polymer, followed by the evaporation of the organic phase and redispersion of the QDs in water, as reported in previous work [20–22]. The used amphiphilic polymer consisted of a polyisobutylene-alt-maleic anhydride hydrophilic backbone modified with dodecylamine hydrophobic side chains (PMA). This polymer wraps around the QDs with its hydrophobic side chains intercalating the hydrophobic surfactant molecules present on the QD surface after synthesis in organic solvent, while its hydrophilic backbone points towards the solution, thus providing colloidal stability. NH₂-modified ATTO590 (absorption maximum at 594 nm, emission maximum at 624 nm), NH₂-modified ATTO633 (absorption maximum at 629 nm, emission maximum at 657 nm), or NH₂-modified ATTO655 (absorption maximum at 663 nm, emission maximum at 684 nm), was directly incorporated into the polymer, and after the polymer coating of the QDs is thus present on the QD surface. In the present work, 2% of the maleic anhydride rings

in the polymer backbone were conjugated with ATTO dye, similar to previous reports [2, 20–23]. After the polymer coating procedure, several purification steps combining filtration and gel electrophoresis were carried out to remove the empty polymer micelles, which form in addition to the polymer-coated QDs as a by-product. For details, refer to the supporting information. Despite purification, some residual polymer micelles containing ATTO dye but with no QDs inside may remain.

Once the QDs had been purified and concentrated (via ultrafiltration) the following QD samples were prepared at the same QD concentration: undoped QDs (CdS/ZnS/ZnS); Mn-doped QDs (CdS/ZnS:Mn/ZnS); undoped QDs with ATTO633 on their surface (ATTO633-CdS/ZnS/ZnS), and Mn-doped QDs with ATTO633 on their surface (ATTO633-CdS/ZnS:Mn/ZnS). All QD samples were characterized by ultraviolet-visible (UV/Vis) absorption spectroscopy and fluorescence spectroscopy (see the supporting information for details). All measurements were performed in water. For spectrally resolved fluorescence measurements, the continuous wave photoluminescence (PL) spectra for the different samples were recorded with a Fluorolog-3 fluorescence spectrometer (model FL3-22, Horiba) under wavelength excitation at 350 nm. These steady-state fluorescence measurements were carried out by working with a sample volume of 30 μl in UV-compatible ultra-micro-cuvettes with a path-length of 1 cm. Time-resolved fluorescence measurements were made with a frequency triple-pulsed Nd:YAG laser operating at a wavelength of 355 nm with a fixed repetition rate of 10 Hz. The decay time of the exciting laser pulse was around 3 ns, which is the lower limit for lifetime determination. A sample volume of 100 μl was used in UV-compatible micro-cuvettes with a path-length of 1 cm. The excited area had a diameter of 1 mm resulting in an excitation density of around 1 J m^{-2} per pulse. The PL was collected perpendicular to the excitation and analysed with a 250 mm spectrograph using a 300-line-per-millimetre grating with a blaze wavelength of 500 nm. The resulting spectra were recorded with a gated iStar intensified charge-coupled device (ICCD), featuring a minimum gate width of 2 ns. For measuring long decay times, the gate width of the ICCD was gradually increased when the recorded intensity decreased to the background noise level. Due to this rise in exposure time for long periods after excitation it was possible to achieve a sensitivity of up to nine orders of magnitude. The decay curves were obtained by integrating the intensity of the particular PL band for the spectra measured at different times after the excitation pulse.

3. Results

In the first analysis, steady-state emission of the different QD samples was recorded. In figure 2, the normalized PL spectra are depicted for three different conjugates under continuous wavelength excitation at 350 nm. The solid red line shows the PL of undoped CdS/ZnS QDs with attached ATTO633 molecules (QD-ATTO633). The two featured bands can be

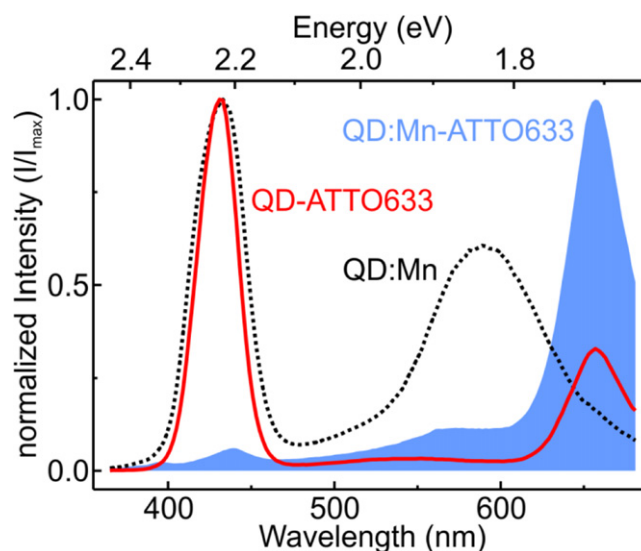


Figure 2. Normalized PL spectra are shown for three different QD conjugates under continuous wavelength excitation at 350 nm. The blue area shows the PL of the doped QDs with attached dye molecules (ATTO633-CdS/ZnS:Mn/ZnS), which is dominated by the dye band around 655 nm. The PL of undoped QDs with attached dye (ATTO633-CdS/ZnS/ZnS) is depicted by the solid red line and the PL of doped QDs without dye (CdS/ZnS:Mn/ZnS) is displayed by the dotted black line. All fluorescence spectra show a PL band around 430 nm caused by the QDs.

assigned to QD emission around 430 nm and the dye emission around 655 nm. From the corresponding QD absorption peak at around 392 nm (shown in the SI) the size of the CdS core of the QD was estimated to be 3.1 nm [24], neglecting the shift of the first exciton peak in the absorption spectrum, as well as the increase of the extinction coefficient of the QD upon the growth of a ZnS shell around the core. Corresponding transmission electron microscopy (TEM) results display a mean diameter of 4.5 ± 0.8 nm of the inorganic part of the CdS/ZnS/ZnS QDs (without the organic shell, which does not provide contrast), which is in reasonable agreement with the value determined from the UV/Vis absorption spectra (shown in the SI).

It is known from the literature that when Mn ions are incorporated into the ZnS shell, the quantum yield of Mn emission increases substantially in comparison with Mn dopants inside a CdS core or at the core-shell interface [25]. Moreover, the growth of several additional ZnS layers over CdS/Mn:ZnS (leading to CdS/Mn:ZnS/ZnS) was demonstrated to increase chemical stability, photostability and optical quality in terms of quantum yield [25, 26]. Note that in the present study, no structural analysis regarding the location of the Mn ions in the ZnS shell was performed, as a strict verification of doping would require [27–31]. However, due to synthesis protocol we can assume that the Mn ions are situated within the ZnS shell and not on the QD surface. The dashed black line in figure 2 shows the PL spectrum of the resulting CdS/Mn:ZnS/ZnS QDs. Here, the QD fluorescence at 430 nm is broader in comparison with the PL band of the undoped QDs. This fact indicates a slightly increased size distribution for the doped QDs, as the width of the PL band is

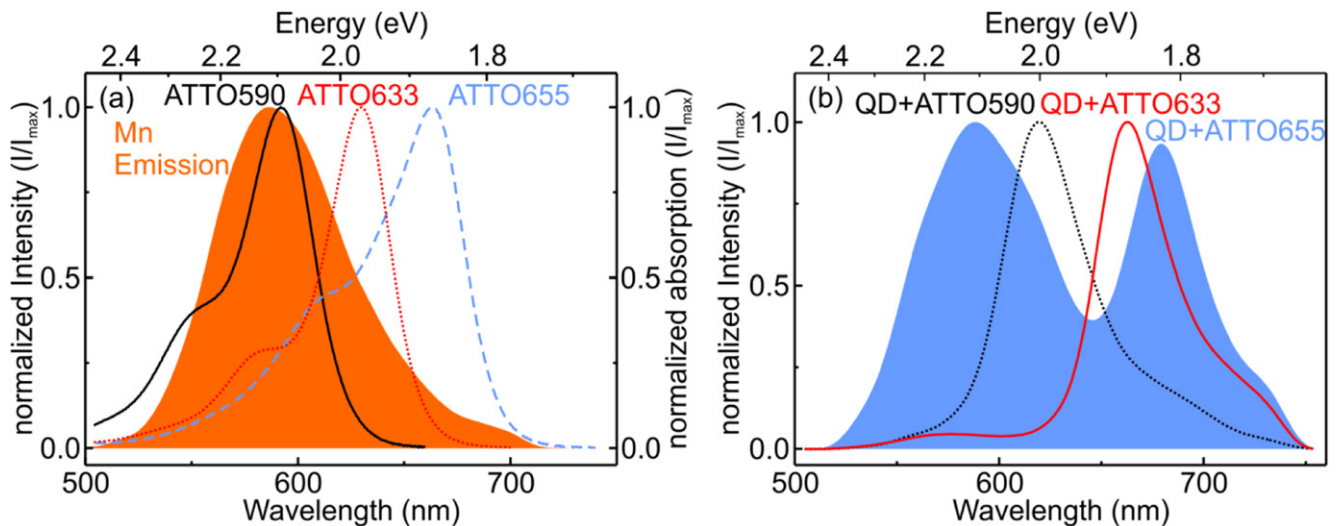


Figure 3. (a) The full (orange) area shows the normalized Mn emission (I/I_{max}) band of doped CdS/Mn:ZnS/ZnS QDs excited with 355 nm. The lines depict the normalized absorption bands for three different dye molecules, namely ATTO590, ATTO633 and ATTO655. (b) The normalized PL spectra for the Mn-doped QD dye conjugates with the three different dye molecules excited with 355 nm, i.e. ATTO590-CdS/Mn:ZnS/ZnS (black), ATTO633-CdS/Mn:ZnS/ZnS (red), and ATTO655-CdS/Mn:ZnS/ZnS (blue).

mainly determined by their size distribution [32]. The PL band around 590 nm can be assigned to the typical ${}^4T_1 \rightarrow {}^6A_1$ transition of the Mn ions on cation sites in ZnS [33]. The diameter of the inorganic part of the doped QDs as determined by TEM was 4.4 ± 0.7 nm (shown in the SI), and thus very similar to that of the undoped QDs.

The blue area in figure 2 shows the normalized PL spectrum of Mn-doped CdS/ZnS QDs with attached ATTO633 molecules. The spectrum is dominated by dye emission around 655 nm. Additionally, a Mn emission band around 590 nm can be observed, which only appears as a small shoulder in the low energetic region of the dye PL due to the relatively low intensity. At 430 nm, the PL band originating from the QD core is also visible. The low intensity of the QD fluorescence in comparison to the Mn PL and the ATTO633 bands indicates an effective energy transfer from the QD to the Mn states. The role of the Mn ions within the transfer process cannot be ascertained by continuous wave experiments. For a thorough investigation of the interaction between the Mn ions and the attached dye molecules, a study on Mn-doped QDs with different dye molecules was performed.

As the spectral overlap between the donor emission and the acceptor absorption is crucial for efficient energy transfer [34], a variation of this overlap was performed by using three different dye molecules with distinct absorption and emission spectra. In figure 3(a) the absorption spectra for the three different dye molecules, i.e. ATTO590, ATTO633 and ATTO655, are shown, which were attached to the CdS/Mn:ZnS/ZnS QDs. It is obvious that the characteristic absorption bands are very similar and differ only in the wavelength of the absorption maximum. Additionally, the normalized Mn emission of the doped QDs is depicted by the orange area. For the ATTO590 dye there is a very high spectral overlap between the Mn emission and the dye absorption, as the respective maxima lie at the same wavelength. Due to the

shifted absorption maximum of the ATTO633 dye, the spectral overlap is clearly reduced, which should lead to a less efficient energy transfer. For the ATTO655 dye this is even more valid.

In figure 3(b) the normalized emission spectra for the three Mn-doped QD dye conjugates with the different dye molecules at a 355 nm wavelength excitation are depicted (i.e. ATTO590-CdS/Mn:ZnS/ZnS, ATTO633-CdS/Mn:ZnS/ZnS, and ATTO655-CdS/Mn:ZnS/ZnS). The spectra were recorded from 10 to 20 μ s after the pulsed excitation. The dotted black line shows the emission of the doped ATTO590-CdS/Mn:ZnS/ZnS conjugate. Only the typical emission band originating from the dye molecules at around 620 nm is visible. As there is no emission band originating from the Mn ions, this implies a rather effective energy transfer from the Mn to the dye molecules. The spectrum of the ATTO633-CdS/Mn:ZnS/ZnS conjugate is depicted by the solid red line and is dominated by the dye emission as well. Nevertheless, a small band around 590 nm is visible, which can be assigned to the Mn transition. The emission spectrum of the ATTO655-CdS/Mn:ZnS/ZnS conjugate is given by the blue area in figure 3(b). Here, two PL bands of similar intensity are visible, which can be assigned to the Mn and dye emission, respectively. A comparison of these three spectra clearly shows a variation in the effectiveness of energy transfer for the different conjugates. For the highest spectral overlap, energy transfer leads to the disappearance of the Mn band in the ATTO590-CdS/Mn:ZnS/ZnS conjugate. In cases where there is a small overlap integral, the transfer is less effective leading to clearly visible Mn emission.

The rate of QD exciton to Mn state energy transfer was found by others to be strongly dependent on the doping location, i.e. the distance between the CdS core and the Mn ion in the ZnS shell [17]. We refer again to the schematic drawing of the Mn-doped QDs in figure 1. The CdS core is responsible for the typical QD emission band. The CdS core

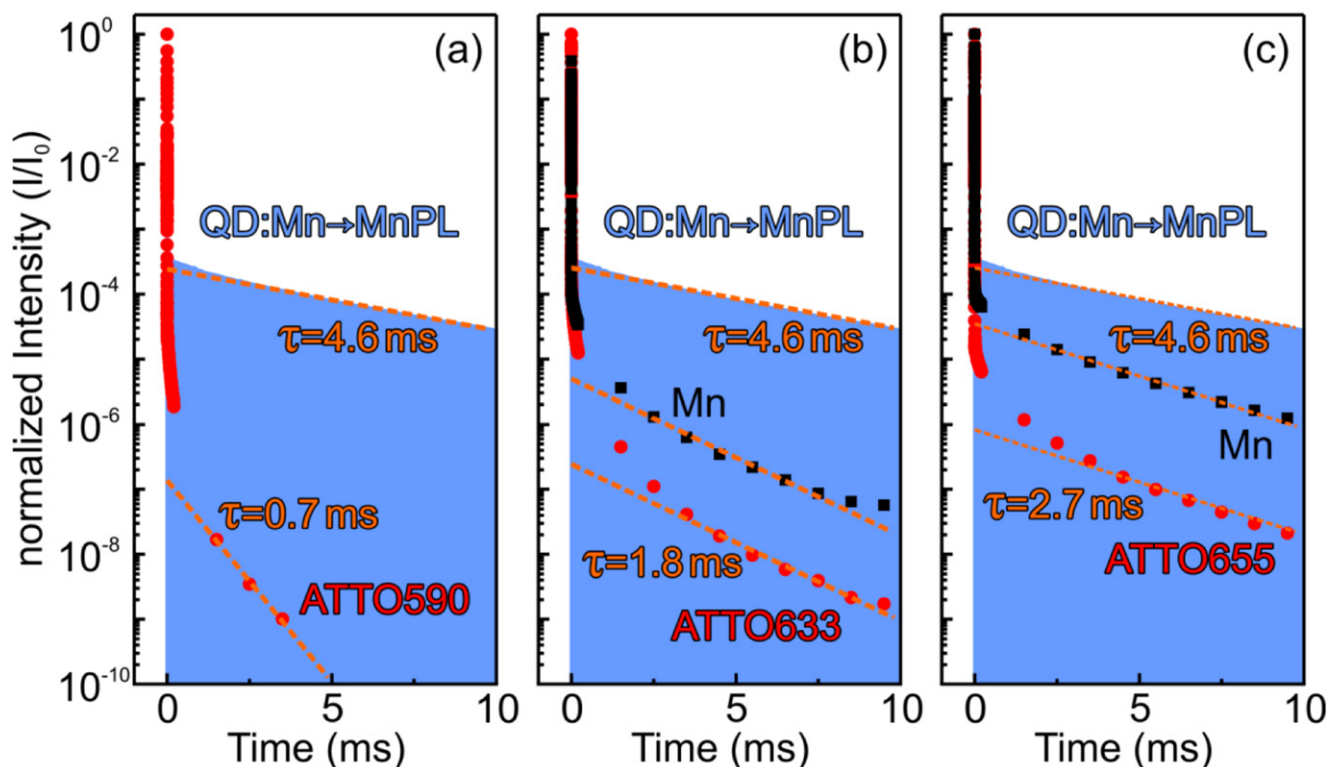


Figure 4. The normalized PL decay curves of Mn-doped QD conjugates with attached (a) ATTO590, (b) ATTO633, and (c) ATTO655 molecules are depicted. The full (blue) area in the graphs gives the decay of the Mn PL band at 585 nm for doped QDs without any attached dye molecules excited at 355 nm. The black squares show the Mn PL transient at 585 nm if the dyes are bound to the QD. The red points give the decay of the dyes at (a) 620 nm, (b) 655 nm and (c) 680 nm and the dotted lines represent a mono-exponential fit with the respective lifetimes given in the graph. For the ATTO590-CdS/Mn:ZnS/ZnS conjugate shown in (a), no Mn band was observable, and therefore only the dye PL decay is shown.

is overcoated by a ZnS shell, which is grown in a multi-step process as indicated by the dotted line. During this growth mechanism the Mn ions are incorporated within the ZnS shell [19]. After the additional ZnS shell, this CdS/Mn:ZnS/ZnS core-shell QD is then wrapped with an amphiphilic polymer onto which the dye molecules are attached. The excitation of the QD via impinging light is shown by the wavy line in figure 1, whereas the subsequent energy transfer is depicted by the green arrows. On the right-hand side of figure 1, the respective energy levels and the energy transfer are depicted schematically. It is clear that the excitation of the QD can undergo a direct energy transfer to the dye molecule or a stepwise transfer via the Mn ion. All three energy states corresponding to the three fluorescence emitters, namely that of the QD, the Mn ion and the dye molecule, can undergo a transition into the respective ground state by emitting a photon. The detection of the emitted PL, especially by time-resolved measurements, provides detailed information about the possible transfer processes.

In figure 4 the normalized PL decay curves are given for the different bands for the three conjugates—except for the ATTO590-CdS/Mn:ZnS/ZnS conjugate in (a), where the Mn PL band could not be observed. In all three graphs the decay of the Mn PL at 585 nm for the doped QDs without any attached dye molecules is given by the blue area. The Mn PL shows a fast decay for short times after excitation due to the

transfer of the excitation energy to the defect or trap states [35, 36]. After approximately one millisecond this transfer seems to be irrelevant to further decay characteristics, leading to a mono-exponential decay with a lifetime of about 4.6 ms, as indicated by the dotted line in figure 4. This value is significantly larger in comparison with the radiative lifetime of Mn states reported by others for pure bulk ZnS with very low Mn concentrations, which have been determined to be in the range between 1.8 ms and 2 ms [14, 37]. Higher Mn concentrations usually yield a faster non-exponential decay. From detailed concentration dependence analysis, an intrinsic lifetime of 3.3 ms has been revealed [38]. Longer lifetimes have also been reported for Mn PL in similar QD systems [12, 17, 39]. This can be explained by the influence of the reduced effective refractive index on the transition matrix element for QD materials with extensions much smaller than the emission wavelength [12].

For the conjugates with different dye molecules attached to the Mn-doped QDs we obtained smaller values for the decay times. This reduced lifetime of the Mn PL is proof of the non-radiative energy transfer from the Mn ions incorporated into the ZnS shell of the QDs, as simple reabsorption would not change the lifetime of the Mn donor states. It is obvious that the attached dye molecules operate as an energy acceptor for Mn excitation here. These dye molecules normally show a fast decay with a lifetime of several ns [40].

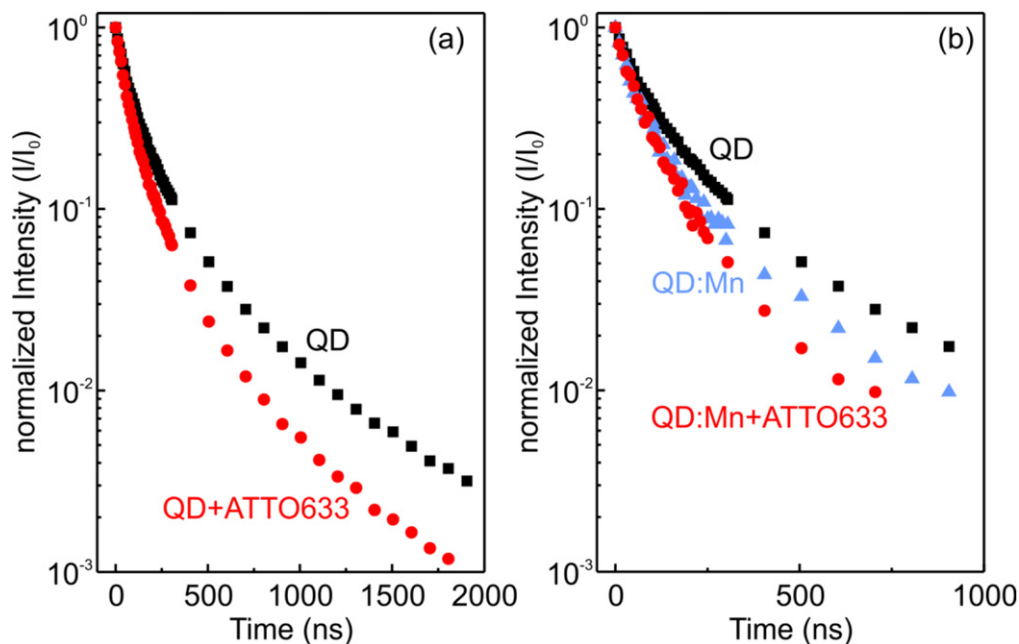


Figure 5. Decay curves of the QD PL around 430 nm for different QD conjugates excited at 355 nm. (a) Time behaviour of the QD PL band of CdS/ZnS/ZnS QDs with (red circles) and without (black squares) attached ATTO633 dye molecules. (b) Decay of the QD PL band for CdS/ZnS/ZnS (black squares) and CdS/Mn:ZnS/ZnS (blue triangles) QDs. The QD PL decay for ATTO633-CdS/Mn:ZnS/ZnS QDs (red circles) is also depicted.

Even the coupling to different QDs rarely extends their lifetime to the μs range [6, 13]. By attaching these molecules to Mn-doped QDs we obtained a dye PL lifetime of several ms. From the determined lifetimes the efficiency of the energy transfer (E) can be estimated by the following equation [41]:

$$E = 1 - \frac{\tau_{\text{DA}}}{\tau_{\text{D}}} \quad (1)$$

Here τ_{D} is the lifetime of the donor in the absence of an acceptor and τ_{DA} is the lifetime of the donor in the presence of an acceptor. For the ATTO590-CdS/ZnS:Mn/ZnS conjugate in figure 4(a) we can assume a Mn state lifetime of 0.7 ms, although the PL band is not visible due to the high dye intensity. With equation (1) we get a FRET efficiency of 0.85, 0.61 and 0.41 for the QD conjugates with ATTO590, ATTO633 and ATTO655 dyes respectively. As can be seen in figure 3 efficient energy transfer from the Mn to the dye states leads to a well-observable dye PL band. However, highly effective energy transfer is not always desirable as the energy transfer leads to a reduced lifetime of the Mn PL. This fact eventually limits the accessible lifetimes for the dyes after energy transfer.

For a detailed analysis of the possible transfer pathways, we selected the ATTO633-CdS/ZnS:Mn/ZnS conjugates. As can be seen in figure 1, three energy transitions of the conjugates are relevant, namely the QD excitons, the Mn internal transition and the dye transition. In the following, the time behaviour of the three respective luminescence bands is discussed individually. In figure 5 the transients are depicted. In figure 5(a) the QD PL is compared for CdS/ZnS/ZnS QDs with and without attached ATTO633 dye molecules. The decay is non-exponential in both systems with a PL

observable up to several ms. A significant change in the decay curve can be observed by attaching ATTO633 dye molecules to the CdS/ZnS/ZnS QDs. The QD PL decays faster due to radiationless energy transfer from the QD states to the dye states.

In figure 5(b), the PL decay of CdS/ZnS/ZnS QDs is compared to that of CdS/Mn:ZnS/ZnS QDs. In general, the QD PL is less intense for the doped QDs and can therefore only be observed in a limited intensity range of about two orders of magnitude. This reduced intensity is due to the effective energy transfer from the excitonic QD states to the Mn 3d-shell [20]. This is confirmed by the faster exciton decay of the Mn-doped QDs. For Mn-doped QDs with ATTO633 dye molecules the excitonic lifetime is reduced even further. Now both channels act as energy acceptors, and the energy transfers from the QDs to the Mn ions as well as directly to the dye states. The role of Mn ions as an energy donor has already been revealed in figure 4, where a faster Mn PL decay was observed for the QDs with attached dye molecules in comparison to QDs without.

In figure 6, the transients are depicted for the ATTO633 dye PL in a double logarithmic scale, which allows for a better separation of the different time regimes. The single dye molecules show a mono-exponential decay for several ns (blue triangles). The time behaviour is completely different when the molecules are bound to CdS/ZnS/ZnS QDs (red circles). The characteristic lifetime is now in the μs range. If dyes are attached to doped CdS/Mn:ZnS/ZnS QDs the decay characteristic changes again substantially (black squares). Up to a few μs the transients for dye molecules attached to doped and undoped QDs look very similar. The underlying characteristic time is caused by the energy transfer from the QD

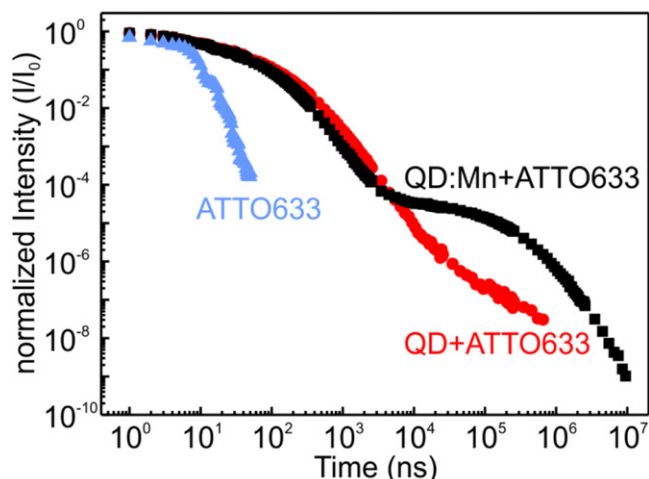


Figure 6. Decay curves of the ATTO633 dye PL at 655 nm in the different dye conjugates excited at 355 nm. The decay of free, i.e. unbound, dye molecules (blue triangles), ATTO633-CdS/ZnS/ZnS conjugates (black squares), and ATTO633-CdS/Mn:ZnS/ZnS conjugates (red circles) is shown. The data are plotted in a double logarithmic scale to point out the different time regimes.

excitons to the dye molecules, which is the dominant feeding mechanism in this time window. The small difference in this time window is due to the somewhat faster exciton decay in Mn-doped QDs, which is caused, as mentioned before, by the additional transfer to the Mn states. In the time regime of several μs up to ms, the distinction between doped and undoped QDs is most striking. Here the dye features a lifetime of several ms, which is identical to the lifetime of the Mn PL.

4. Conclusion

It has been demonstrated that the incorporation of Mn ions as dopants within the ZnS shell of CdS/ZnS core-shell QDs leads to an efficient energy transfer from the excitonic QD states to the Mn states. A multistep growth of the ZnS shell was carried out to control the location of the Mn ions. The effective incorporation of the Mn ions into the QD core-shell structure was confirmed by a clearly observable PL band around 580 nm, which is due to the typical Mn transition. This PL band showed a mono-exponential decay with a lifetime of about 4.6 ms. These Mn-doped CdS/Mn:ZnS/ZnS QDs were further functionalized with organic dye molecules leading to a third fluorescence emitter centre, and therefore to a third PL band. Continuous wave spectra indicated the complex interaction of the different energy states within the QD system. With a thorough investigation of the decay characteristics of the respective PL bands, it was possible to explore the non-radiative energy pathways. We thereby concluded that the QD states act as an energy donor for the Mn as well as for the dye states. Interestingly, the Mn states have a two-fold transfer characteristic, as they also work as an acceptor from the QD states and as a donor for the dye states. In particular, the feeding of the dye states from Mn excitation

led to a tremendous increase in the dye PL lifetime. By choosing a certain dye, and thereby a certain spectral overlap, it was possible to control the lifetime of the dye PL in the range of a few milliseconds.

The attachment of dye molecules to CdS/Mn:ZnS/ZnS QDs led to dye conjugates which could easily be distinguished by means of time-resolved PL measurements from single dye molecules and dye molecules attached to undoped QDs. Mn-doped CdS/Mn:ZnS/ZnS QDs as donors for fluorophores open up a new time regime and potentially allow for the use of dye molecules in complex temporal multiplexing applications. In earlier works [13] we were able to show that the use of undoped QDs leads to the unique and precise determination of the mixing ratio of single and attached dye molecules by time-resolved PL measurements with the same spectral response. Now, we have pointed out that the use of Mn-doped QDs may extend the possibilities of temporal multiplexing even further.

Acknowledgments

This work was supported by the Deutsche Forschungsgemeinschaft (DFG GRK 1782 to WJP and WH) and by the European Commission (grant FutureNanoNeeds to WJP). CCC acknowledges a postdoctoral fellowship from the Alexander von Humboldt foundation. NS acknowledges the Higher Education Commission (HEC) Pakistan and GC University Faisalabad (GCUF) Pakistan. We are grateful to M Schneider for his collaboration with the sample measurements.

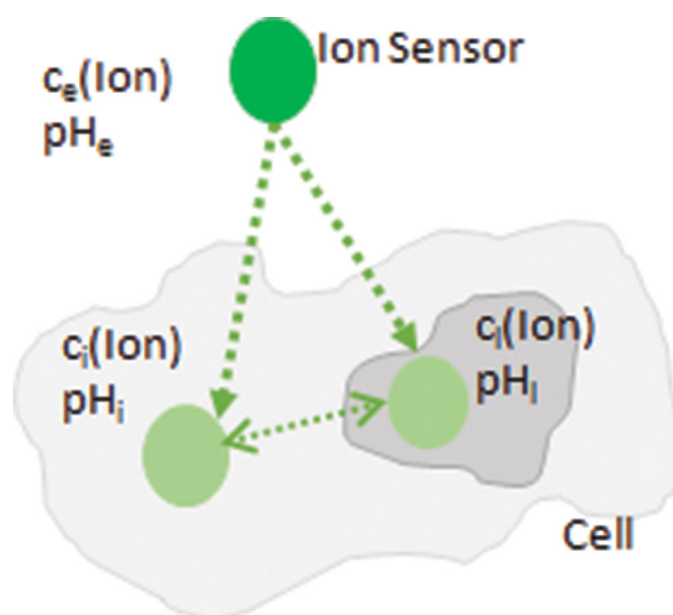
References

- [1] Hötzer B, Medintz I L and Hildebrandt N 2012 Fluorescence in nanobiotechnology: sophisticated fluorophores for novel applications *Small* **8** 2297–326
- [2] Wegner K D and Hildebrandt N 2015 Quantum dots: bright and versatile *in vitro* and *in vivo* fluorescence imaging biosensors *Chem. Soc. Rev.* **44** 4792–834
- [3] Jennings T L *et al* 2011 Reactive semiconductor nanocrystals for chemoselective biolabeling and multiplexed analysis *ACS Nano* **5** 5579–93
- [4] Jezek P, Mahdi F and Garlid K D 1990 Reconstitution of the beef-heart and rat-liver mitochondrial K^+/H^+ (Na^+/H^+) antiporter—quantitation of K^+ transport with the novel fluorescent-probe, Pbf1 *J. Biol. Chem.* **265** 10522–6
- [5] Graefe A, Stanca S E, Nietzsche S, Kubicova L, Beckert R, Biskup C and Mohr G J 2008 Development and critical evaluation of fluorescent chloride nanosensors *Anal. Chem.* **80** 6526–31
- [6] Abbasi A Z *et al* 2011 How colloidal nanoparticles could facilitate multiplexed measurements of different analytes with analyte-sensitive organic fluorophores *ACS Nano* **5** 21–5
- [7] Berezin M Y and Achilefu S 2010 Fluorescence lifetime measurements and biological imaging *Chem. Rev.* **110** 2641–84
- [8] Masters B R, So P T and Gratton E Multiphoton excitation fluorescence microscopy and spectroscopy of *in vivo* human skin *Biophys. J.* **72** 2405–12

- [9] Geißler D, Linden S, Liermann K, Wegner K D, Charbonnière L J and Hildebrandt N 2014 Lanthanides and quantum dots as Förster resonance energy transfer agents for diagnostics and cellular imaging *Inorg. Chem.* **53** 1824–38
- [10] Hildebrandt N, Wegner K D and Algar W R 2014 Luminescent terbium complexes: superior Förster resonance energy transfer donors for flexible and sensitive multiplexed biosensing *Coord. Chem. Rev.* **273** 125–38
- [11] Gill R, Willner I, Shweky I and Banin U 2005 Fluorescence resonance energy transfer in CdSe/ZnS-DNA conjugates: probing hybridization and DNA cleavage *J. Phys. Chem. B* **109** 23715–9
- [12] Medintz I L, Uyeda H T, Goldman E R and Mattoussi H 2005 Quantum dot bioconjugates for imaging, labelling and sensing *Nat. Mater.* **4** 435–46
- [13] Kaiser U, Aberasturi D J d, Malinowski R, Amin F, Parak W J and Heimbrod W 2014 Multiplexed measurements by time resolved spectroscopy using colloidal CdSe/ZnS quantum dots *Appl. Phys. Lett.* **104** 41901–4
- [14] Busse W, Gumlich H E, Meissner B and Theis D 1976 Time resolved spectroscopy of ZnS: Mn by dye laser technique *J. Lumin.* **12–13**, 693–700
- [15] de Mello Donegá C, Bol A A and Meijerink A 2002 Time-resolved luminescence of ZnS:Mn²⁺ nanocrystals *J. Lumin.* **96**, 87–93
- [16] Yu W W and Peng X 2002 Formation of high-quality CdS and other II-VI semiconductor nanocrystals in noncoordinating solvents: tunable reactivity of monomers *Angew. Chem. Int. Ed.* **41** 2368–71
- [17] Chen H Y, Maiti S and Son D H 2012 Doping location-dependent energy transfer dynamics in Mn-doped CdS/ZnS nanocrystals *ACS Nano* **6** 583–91
- [18] Chen O, Shelby D E, Yang Y, Zhuang J, Wang T, Niu C, Omenetto N and Cao Y C 2010 Excitation-intensity-dependent color-tunable dual emissions from manganese-doped CdS/ZnS core/shell nanocrystals *Angew. Chem. Int. Ed.* **49** 10132–5
- [19] Yang Y, Chen O, Angerhofer A and Cao Y C 2008 On doping CdS/ZnS core/shell nanocrystals with Mn *J. Am. Chem. Soc.* **130** 15649–61
- [20] Lin C-A J, Sperling R A, Li J K, Yang T-Y, Li P-Y, Zanella M, Chang W H and Parak W J 2008 Design of an amphiphilic polymer for nanoparticle coating and functionalization *Small* **4** 334–41
- [21] Zhang F, Lees E, Amin F, Rivera_Gil P, Yang F, Mulvaney P and Parak W J 2011 Polymer-coated nanoparticles: a universal tool for biolabelling experiments *Small* **7** 3113–27
- [22] Fernández-Argüelles M T et al 2007 Synthesis and characterization of polymer-coated quantum dots with integrated acceptor dyes as FRET-based nanoprobe *Nano Lett.* **7** 2613–7
- [23] Kaiser U, Aberasturi D J d, Vazquez-Gonzalez M, Carrillo-Carrion C, Niebling T, Parak W J and Heimbrod W 2015 Determining the exact number of dye molecules attached to colloidal CdSe/ZnS quantum dots in Förster resonant energy transfer assemblies *J. Appl. Phys.* **117** 024701
- [24] Yu W W, Qu L, Guo W and Peng X 2003 Experimental determination of the extinction coefficient of CdTe, CdSe, and CdS nanocrystals *Chem. Mater.* **15** 2854–60
- [25] Yang Y, Chen O, Angerhofer A and Cao Y C 2006 Radial-position-controlled doping in CdS/ZnS core/shell nanocrystals *J. Am. Chem. Soc.* **128** 12428–9
- [26] Labiadh H, Ben Chaabane T, Piatkowski D, Mackowski S, Lalevee J, Ghanbaja J, Aldeek F and Schneider R 2013 Aqueous route to color-tunable Mn-doped ZnS quantum dots *Mater. Chem. Phys.* **140** 674–82
- [27] Norris D J, Efros A L and Erwin S C 2008 Doped nanocrystals *Science* **319** 1776–9
- [28] Norris D J, Yao N, Charnock F T and Kennedy T A 2001 High-quality manganese-doped ZnSe nanocrystals *Nano Lett.* **1** 3–7
- [29] Zu L J, Norris D J, Kennedy T A, Erwin S C and Efros A L 2006 Impact of ripening on manganese-doped ZnSe nanocrystals *Nano Lett.* **6** 334–40
- [30] Erwin S C, Zu L J, Haftel M I, Efros A L, Kennedy T A and Norris D J 2005 Doping semiconductor nanocrystals *Nature* **436** 91–4
- [31] Shim M, Wang C, Norris D J and Guyot-Sionnest P 2001 Doping and charging in colloidal semiconductor nanocrystals *MRS Bull.* **26** 1005–8
- [32] Bawendi M G, Carroll P J, Wilson W L and Brus L E 1992 Luminescence properties of CdSe quantum crystallites—resonance between interior and surface Localized states *J. Chem. Phys.* **96** 946–54
- [33] Goede O and Heimbrod W 2001 Optical properties of (Zn,Mn) and (Cd,Mn) chalcogenide mixed crystals and superlattices *Phys. Status Solidi B* **146** 11–62
- [34] Dexter D L 1953 A Theory of sensitized luminescence in solids *J. Chem. Phys.* **21** 836–50
- [35] Förster T 1949 Experimentelle und theoretische untersuchung des zwischenmolekularen übergangs von elektronenanregungsenergie *J. Phys. Sci.* **4** 321–7
- [36] Kaiser U, Chen L, Geburt S, Ronning C and Heimbrod W 2011 Defect induced changes on the excitation transfer dynamics in ZnS/Mn nanowires *Nanoscale Res. Lett.* **6** 228–32
- [37] Gumlich H E 1981 Electro- and photoluminescence properties of Mn²⁺ in ZnS and ZnCdS *J. Lumin.* **23** 73–99
- [38] Goede O, Heimbrod W and Thong D D 1984 Non-exponential ZnS:Mn luminescence decay due to energy transfer *Phys. Status Solidi B* **126** K159–63
- [39] Cao S, Li C, Wang L, Shang M, Wei G, Zheng J and Yang W 2014 Long-lived and well-resolved Mn²⁺ ion emissions in CuInS-ZnS quantum dots *Sci. Rep.* **4** 7510
- [40] Resch-Genger U, Grabolle M, Cavaliere-Jaricot S, Nitschke R and Nann T 2008 Quantum dots versus organic dyes as fluorescent labels *Nat. Methods* **5** 763
- [41] van der Meer B W 2013 *FRET—Förster Resonance Energy Transfer* (Weinheim: Wiley) pp 23–62

Particle-Based Optical Sensing of Intracellular Ions at the Example of Calcium – What Are the Experimental Pitfalls?

Karsten Kantner, Sumaira Ashraf, Susana Carregal-Romero, Carolina Carrillo-Carrion, Mayeul Collot, Pablo del Pino, Wolfram Heimbrod, Dorleta Jimenez De Aberasturi, Uwe Kaiser, Lyubov I. Kazakova, Marco Lelle, Natalia Martinez de Baroja, Jose Maria Montenegro, Moritz Nazarenus, Beatriz Pelaz, Kalina Peneva, Pilar Rivera Gil, Nadeem Sabir, Lorenz Maximilian Schneider, Lyudmila I. Shabarchina, Gleb B. Sukhorukov, Margarita Vazquez, Fang Yang, and Wolfgang J. Parak*



From the Contents

1. Introduction897
2. Upon Cellular Internalization, Particle-Based Sensors are Typically Located Inside Intracellular Acidic Vesicles.....898
3. Many Ion-Sensitive Fluorophores Have Massive Crosstalk with pH899
4. Multiplexed Detection of Several Fluorophores Based on Different Fluorescence Lifetimes900
5. Discussion.....902

Colloidal particles with fluorescence read-out are commonly used as sensors for the quantitative determination of ions. Calcium, for example, is a biologically highly relevant ion in signaling, and thus knowledge of its spatio-temporal distribution inside cells would offer important experimental data. However, the use of particle-based intracellular sensors for ion detection is not straightforward. Important associated problems involve delivery and intracellular location of particle-based fluorophores, crosstalk of the fluorescence read-out with pH, and spectral overlap of the emission spectra of different fluorophores. These potential problems are outlined and discussed here with selected experimental examples. Potential solutions are discussed and form a guideline for particle-based intracellular imaging of ions.

1. Introduction

There is a large variety of ion-sensitive fluorophores available, which change their fluorescence intensity in the presence of the respective ion.^[1–7] With such fluorophores intracellular ion concentrations could, in principle, be determined, which would be an interesting tool for cell biology.^[8–16] Ions play an important role in biology, for example, in signaling. This comprises signal propagation via action potentials in neurons, for example, which is governed by local switching on and off of Na⁺ and K⁺ currents. Another important ion related to cellular signaling is Ca²⁺, which plays an important role in muscles. Having local ion-sensitive probes would allow the spatio-temporal observation of such signaling dynamics.

Most ion-sensitive fluorophores are based on organic molecules,^[1,2,5–7] but there are also intrinsically fluorescent (nano-)particles with sensitivity to certain ionic species.^[17–20] Ion-sensitive particles can be composed of a carrier particle functionalized with ion-sensitive organic fluorophores. The particle acts as a carrier for a read-out in the form of (organic) ion-sensitive fluorophores. This is possible by embedding the organic fluorophores in the volume of a porous particle matrix,^[21–23] by encapsulating them in a porous particle shell,^[24–26] or by linking them to the particle surface.^[27–29] Ideally, the carrier particle would not interfere with the photophysical properties of the attached fluorophore. However, in the case of metal particles, quenching effects of the fluorescence of organic fluorophores close to the particle surface are possible. Also in case of very high packing densities of the fluorophores on the particle surface, self-quenching effects may occur. In some scenarios as, for example, for fluorescence resonance energy transfer (FRET), interactions of the organic fluorophore with the particle carrier is wanted in order to tune the photophysical properties of the attached fluorophores, which will be described below. Alternatively, intrinsically ion-sensitive fluorescent particles such as quantum dots (QDs) can be sensitive to ions.^[102] In this case, the particle has a double function, acting as sensitive fluorophore and a carrier at the same time. In the following sections, all of these different geometries will be referred to simply as particles. These particles can range from the nanometer to the micrometer scale.^[30] Besides acting as carriers, charged particles can intentionally or unintentionally modify the ion response, as their typically charged surface forms a nano-environment in the proximity of the particle surface that is different from the bulk.^[27,31–34]

A particulate form of ion-sensitive fluorescence sensor offers several potential advantages. Concerning the signal-to-noise-ratio of the read-out, the emission intensity of ion-sensitive particles can be very high (in the case of intrinsically fluorescent particles such as QDs, this is due to their high absorption cross-section;^[35,36] in the case of organic fluorophores, it is due to the linkage of several fluorophores per particle).^[37–39] Next, the interaction with their environment, such as with cells, is predominantly governed by the physico-chemical properties of the particle surface. As particles sensitive to different ions can have the same physico-chemical properties, they also will have the same interaction with cells. In contrast, as organic fluorophores sensitive to different ions typically



Wolfgang Parak studied physics at the Technische Universität München, and made his PhD thesis in the group of Prof. Hermann Gaub at the Ludwig Maximilians Universität München, Germany. After his postdoctoral studies in the group of Prof. Paul Alivisatos at the University of California, Berkeley, USA, he returned to the Ludwig Maximilians Universität as Assistant and later Associate Professor. Since 2007, Wolfgang Parak has been a Full Professor at the Philipps Universität Marburg, Germany, and since 2013 also group leader at CIC Biomagune in Spain.



Karsten Kantner studied physics in Marburg and is currently working on his PhD thesis in the group of Prof. Parak at the Philipps University of Marburg.

K. Kantner, Dr. S. Ashraf, Dr. S. Carregal-Romero, Dr. C. Carrillo-Carrion, Prof. W. Heimbrod, Dr. D. J. De Aberasturi, U. Kaiser, Dr. J. M. Montenegro,^[+] M. Nazareus, Dr. B. Pelaz, Dr. P. Rivera Gil, N. Sabir, L. M. Schneider, M. Vazquez, F. Yang, Prof. W. J. Parak
Fachbereich Physik, Philipps-Universität Marburg
Marburg, Germany

E-mail: wolfgang.parak@physik.uni-marburg.de

Dr. S. Carregal-Romero, Dr. P. del Pino, Dr. D. J. de Aberasturi,
Dr. N. M. de Baroja, Prof. W. J. Parak
CIC BiomaGUNE
San Sebastian, Spain

Dr. M. Collot
Ecole Normale Supérieure, CNRS
Paris, France

Dr. L. I. Kazakova, Dr. L. I. Shabarchina
Institute of Theoretical and Experimental Biophysics
Russian Academy of Science
Pushchino, Russian Federation

Dr. M. Lelle, Dr. K. Peneva
Max Planck Institute for Polymer Research
Mainz, Germany

Prof. G. B. Sukhorukov
School of Engineering and Materials Science
Queen Mary University of London
London, UK

M. Vazquez
Inorganic Chemistry Department
Faculty of Pharmacy
University of Santiago de Compostela
Santiago de Compostela, Spain

^[+]Present Address: Central Research Services, University of Malaga,
Bulevar Louis Pasteur 33, 29071 Málaga, Spain

DOI: 10.1002/sml.201402110



have very different molecular structures and thus different physico-chemical properties (their polarity can range from hydrophilic to hydrophobic, for example), they will interact differently with cells. The pathway of cellular uptake of fluorescent particles can therefore be quite different from plain organic fluorophores. Playing with the size of the particle that acts as the carrier (nano- or microparticles), the location of the sensor inside the cells can be designed and thus information about the ion concentrations in different cellular regions can be obtained. While nanoparticles are preferentially located in endolysosomal compartments, microparticles can also be found in phagolysosomal vesicles, which allows the design of ion-sensitive particles depending on the location of the ion of interest. Due to potentially different intracellular locations and also because of the protection by the particle, particulate fluorophores may be less degraded by intracellular enzymes, and also cause less toxic intracellular effects (in particular when their sensing part is directly located on the particle surface). Concerning multiplexed sensing, the possibility of working with detection schemes involving temporal or spatial discrimination can circumvent the problem of spectral overlap and, thus, different ion-sensitive fluorophores can be detected in parallel.^[40,41] Naturally, besides these advantages there are also problems associated with particle-based intracellular ion-sensing, which will be highlighted in the following sections based on experimental examples. While the given analysis holds true in a general way for small biologically relevant ions such as Na^+ , K^+ , Cl^- , H^+ , the statements above are illustrated by selected experimental data. For reasons of homogeneity, the experimental data are presented for the case of Ca^{2+} -sensing, though results would be similar for other ions. The technical details for the experiments can be found in the Supporting Information.

2. Upon Cellular Internalization, Particle-Based Sensors are Typically Located Inside Intracellular Acidic Vesicles

The classical entry of particles into cells is via endocytosis. While endocytosis can involve a lot of different pathways,^[42–45] it results in a localization of the particles in acidic intracellular vesicles (endosomes, lysosomes).^[25,46–49] In such a scenario, the particles would sense the ion concentrations inside these vesicles, but not in the cellular cytosol.^[8,50] For many applications, sensing of ion concentrations in the cytosol would be favorable. Administration of particles by microinjection or electroporation allows the placing of particles in the cytosol, though these techniques are clearly invasive and would have severe limitations for in vivo applications. However, there is also clear evidence that certain particle geometry scenarios exist in which particles can be delivered to the cytosol upon spontaneous cellular uptake.^[51,52] In the case of delivery to the cytosol, the particles can be either first endocytosed and then released from the intracellular vesicles (“endosomal escape”),^[53–55] or they can directly traverse the cell membrane (i.e., by transient poration) and thus bypass endocytotic uptake.^[56] The details of such mechanisms are still under scientific discussion. For

fast uptake into cells and delivery through the cell membrane to the cytosol, a common functionalization of the particle surface involves specific peptide sequences, e.g., cell-penetrating peptides (CPPs),^[57–59] which usually are derived from viruses. The data shown in **Figure 1** demonstrate an example, in which polyethylene glycol (PEG)-modified particles bearing CPPs at the termini of the PEG molecules were internalized in vitro by HeLa cells to a higher extent than similar particles without CPP functionalization. Quantification of particle internalization can be done via different techniques, such as transmission electron microscopy (TEM),^[60–62] fluorescence microscopy,^[63–65] flow cytometry,^[47,50] and inductively coupled plasma mass spectrometry (ICP-MS).^[66,67] As flow cytometry and ICP-MS do not possess direct lateral resolution at a sub-cellular level, these techniques do not allow one to distinguish between internalized particles which are free in the cytosol from those which are localized inside intracellular vesicles. Even worse, these methods do not allow intracellular particles to be distinguished from particles just sticking to the outer cell membrane. However, this limitation has been overcome using protocols for removing particles attached to the surface based on iodide etching^[68] or, in the case of flow cytometry, by using the local pH around the particles as a discriminator between internalized (acidic pH) and extracellular (neutral pH) particles.^[69] In contrast, fluorescence microscopy, when applied together with appropriate immunostaining methods, and in particular TEM, due to its high spatial resolution, can demonstrate particle internalization, and can in principle also indicate whether internalized particles are inside intracellular vesicles or not.^[47,49,52] However, in many cases, uptake studies are based on fluorescence microscopy images without staining of intravesicular membranes (cf. Figure 1), with the consequence that, from such images, no conclusion about the intracellular localization of the particles can be drawn. In fact, it is important to be highly critical about the possible delivery of particles to the cytosol. Just the presence of CPPs on the particle surface does not automatically mean their delivery to the cytosol. This is illustrated in the example shown in Figure 1, which is based on two CPPs that both are rich in NH_2 groups. In these data, one can see a clear indication of enhanced cellular uptake (cf. the ICP-MS data), but neither a reliable quantification nor the intracellular location of the particles can be derived. Even if the same CPPs have been demonstrated in the literature for one particle system resulting in delivery to the cytosol, without experimental verification it must not be assumed that the same CPPs will also work for other systems in the same manner. Depending on the respective particle geometry (surface chemistry, density of CPPs, size of particles, distance of CPPs to the particle core, etc.), the effects of attached CPPs, as well as the physico-chemical properties of the particles themselves may be quite different. In the case of the example presented in Figure 1, one has to take into account that PEG molecules are partly coiled and, in this way, the CPPs at the terminal ends do not always point towards the solution, but may be buried in the PEG shell instead. Also, the density of the CPPs may play a role. Thus, without experimental proof concerning the characterization of the used particle system as well as the chosen cell system, one should not assume the presence of particles in the cytosol.

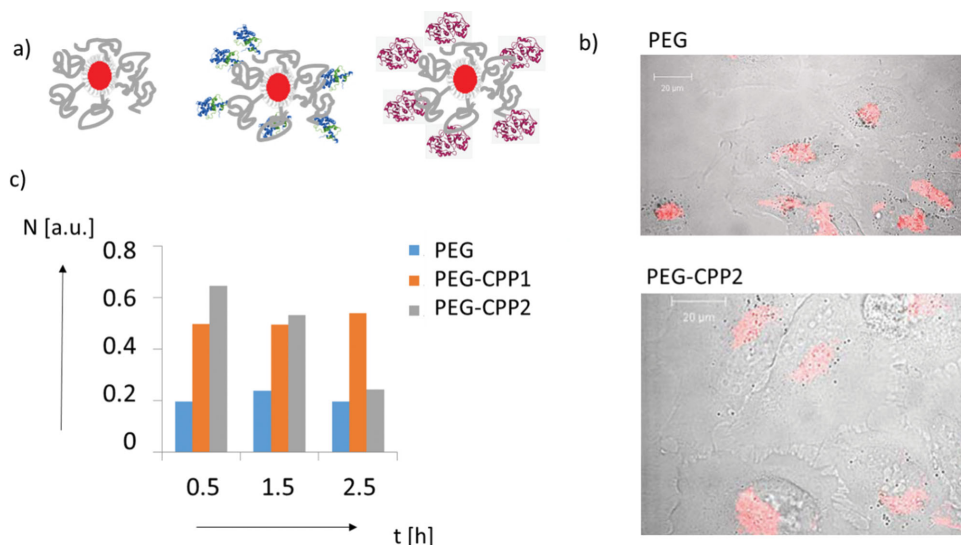


Figure 1. HeLa cells were incubated with polymer-coated Au nanoparticles (core diameter $d_c \approx 4.6$ nm) with the red fluorophore Cresyl violet (CV) integrated in their polymer shell.^[70] The surface of these nanoparticles was modified with PEG of molecular weight $M_w = 3000$ Da.^[71] For some particles, the terminal end of each PEG molecule was conjugated with cell-penetrating peptides (CPPs) rich in NH_2 groups. Two different CPPs were used as random examples. a) Sketch of the three different particles, with PEG, PEG-CPP1, and PEG-CPP2 surfaces. b) Overlay of the bright-field and red fluorescence images of HeLa cells after 6 h of incubation with the particles. The scale bars correspond to 20 μm . c) The amount of internalized particles N (as quantified by the atomic gold content inside cells) was determined with ICP-MS after $t = 0.5, 1.5,$ and 2.5 h of incubation. The decrease in N for PEG-CPP2 was most likely due to the death of some cells. In both cases, the presence of CPPs enhanced uptake of particles by cells. The presented data here do not allow for any conclusion about the intracellular location of the internalized particles. Note that the fluorescence images shown in (b) are overexposed, and thus no accurate and precise quantitative data about differences in uptake between the different particles can be derived. This “homogeneous” distribution of fluorescence along the cell must in particular not be mistaken as proof for delivery to the cytosol. The granular structure of the intracellular vesicles in which the particles are embedded can be seen in cases where appropriate particle concentrations and imaging parameters are used.^[46,72,73]

There is no easy solution to the “endosomal escape dilemma”. It is most important to be aware of this potential problem. Most uptake studies, without a proper colocalization study, are not able to distinguish between particles free in the cytosol and particles embedded in intracellular vesicles. As mentioned above, the standard route of particle internalization by cells is endocytosis.^[62] Thus, unless proven differently,^[51,53] particles should be assumed to be in acidic intracellular vesicles, and thus the read-out of such ion-sensitive particles would determine the ion concentrations inside the endosomes/lysosomes,^[8,74] and not the ion concentrations in the cellular cytosol. In this way, particle-based ion-sensitive particles are ideal for sensing inside endosomes/lysosomes, and one smart strategy would be to look for potential applications in this direction, e.g., sensing related to lysosomal storage diseases, instead of targeting the cytosol. Otherwise, in cases where applications definitely require sensing in other intracellular compartments, sensing methodologies need to be accompanied by profound localization studies providing information about the particle localization.

3. Many Ion-Sensitive Fluorophores Have Massive Crosstalk with pH

As pointed out previously, unless special surface coatings and very small particles are used, internalized particles are typically located in acidic intracellular vesicles, i.e., in an environment with low pH. Unfortunately, many ion-sensitive fluorophores have significant crosstalk with pH, as shown in

the examples given in **Figure 2**. Thus, without knowledge of the local pH value of the particle environment, the concentration of the respective ions cannot be determined. Besides pH, many ion-sensitive fluorophores also have crosstalk with other ions. For example, potassium-sensitive fluorophores have crosstalk with sodium, and vice versa.^[41]

Crosstalk with pH is a severe problem for intracellular (in vitro) ion sensing. On their standard internalization pathway from the typical slightly alkaline extracellular medium, particles are located in subsequently more and more acidic intracellular vesicles. In this way, the internalization of particles involves massive changes in pH.^[8,24] Thus, in the case of a particulate ion-sensitive fluorophore which not only responds to its target ion but also to pH, it is not straightforward to interpret changes in fluorescence intensity, as they may reflect changes in target ion concentration or in pH. This is demonstrated in **Figure 3**, where particles, here micrometer-sized multilayer capsules with integrated calcium-sensitive fluorophores (Calcium Green-1 linked to dextran), were added to cells and their fluorescence was recorded for extracellular as well as for internalized particles. For the calcium-sensitive fluorophore, it is not clear whether the change in fluorescence emission upon cellular internalization, leading to localization in the lysosome,^[49] is due to changes in Ca^{2+} or in pH. Thus, with this particle-based calcium sensor, it is not possible in a straightforward way to determine lysosomal calcium concentrations.

Again, there is no easy solution concerning avoiding crosstalk of ion-sensitive fluorophores with pH. Being aware of the

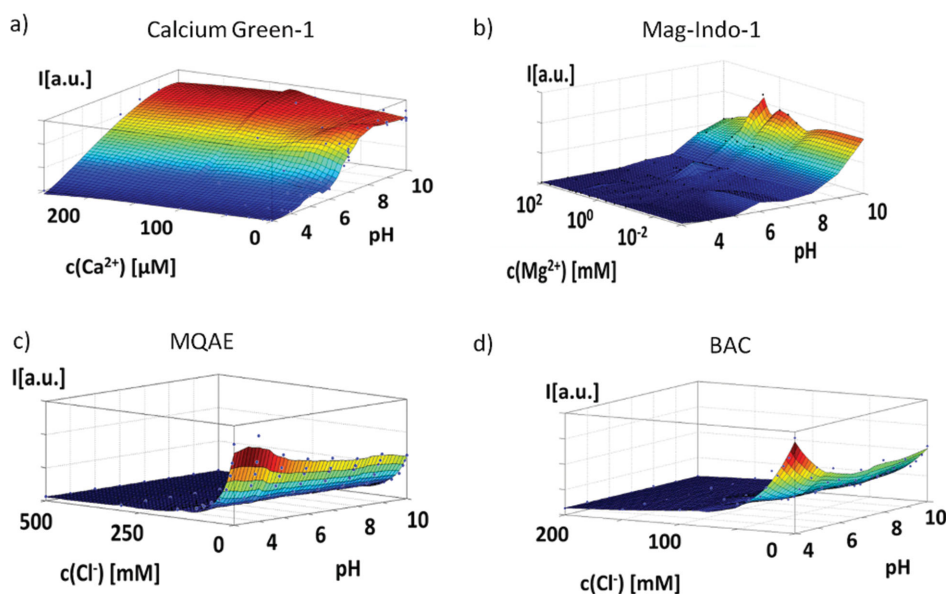


Figure 2. Different sensitive fluorophores were added to solutions in which the concentration c of one ionic specie as well as pH were varied, and their fluorescence intensity I was measured. a) N -[2-[2-[2-bis(carboxymethyl)amino]-5-[[2',7'-dichloro-3',6'-dihydroxy-3-oxospiro[isobenzofuran-1(3H),9'-[9H]xanthene)-5-yl]carbonyl]amino]phenoxy]ethoxy]phenyl]- N -(carboxymethyl) (Calcium-Green-1) specific for calcium.^[75] b) 1H-Indole-6-carboxylic acid, 2-[3-[2-[(acetyloxy)methoxy]-2-oxoethoxy]-4-[bis[2-[(acetyloxy)methoxy]-2-oxoethyl]amino]phenyl], (acetyloxy)methyl ester (Mag-Indo-1) specific for magnesium.^[76] c) N -(Ethoxycarbonylmethyl)-6-methoxyquinolinium bromide (MQAE) specific for chloride.^[77] d) 10,10'-Bis[3-carboxypropyl]-9,9'-acridiniumdinitrate (BAC) specific for chloride.^[78] In all cases the emission intensity I of the fluorophore does not only respond to changes in the concentration of the target ions, but also to changes in pH.

problem is clearly only the first step. Naturally one may think of developing ion-sensitive fluorophores which do not respond to pH. Alternatively, in case one needs to rely on existing particle-based fluorophores that are affected by crosstalk with pH, one can think of a multiplexed read-out of several fluorophores, as will be discussed below. Here, the advantage of the “particle” character comes into play: As two particle-based fluorophores with the same surface chemistry/dimensions will have the same uptake pathway and intracellular location, several particle-based fluorophores selective to different ions could be applied and read-out at the same time. In case two Ca^{2+} -sensitive fluorophores show different crosstalk to pH, a 2D calibration curve could be obtained. By reading out the values of different Ca^{2+} -sensitive fluorophores in parallel, the Ca^{2+} concentration could be determined even without knowledge of the local pH. In a similar way, a Ca^{2+} -sensitive fluorophore could be combined with a pH-sensitive fluorophore. Again, a 2D calibration curve correlating the read-out of both fluorophores would allow determination of both the pH and the Ca^{2+} concentration. In this way, however, two different fluorophores need to be read-out simultaneously which, due to spectral overlap of fluorescence emission, can be challenging, as will be explained in detail in the following section.

4. Multiplexed Detection of Several Fluorophores Based on Different Fluorescence Lifetimes

For many applications it would be desirable to determine the intracellular concentration of several ions in parallel.

This is the case if there is, for example, crosstalk between different fluorophores, and calibration curves correlating the read-out of different fluorophores are required (see above). Such a case is shown in **Figure 4**, where the read-out of a Ca^{2+} -sensitive fluorophore depends on both the Ca^{2+} concentration and also the pH. In this way, it would be desirable to combine the Ca^{2+} -sensitive fluorophore (which has crosstalk with pH) with a pH-sensitive fluorophore. However, the emission spectra of many ion-sensitive fluorophores unfortunately overlap, and thus the number of fluorophores that can be spectrally resolved and independently detected in parallel is limited.^[40,80,81] The fluorescence spectrum of the Ca^{2+} -sensitive fluorophore shown in Figure 4 is relatively broad, and thus it would be complicated to find a pH-sensitive fluorophore emitting in a very different spectral range.

One solution to circumvent this problem is to use multiplexed detection techniques which are not based on spectral resolution. Besides distinguishing different fluorophores from separate emission peaks (i.e., spectral resolution), other ways of discrimination are possible. If the fluorophore-carrying particles are big enough to be optically resolved (i.e., sized above the optical resolution limit due to refraction), individual particles can be laterally resolved and identified by respective barcodes (i.e., lateral resolution).^[40,41,82–84] While this is not possible for smaller particles, they still can be resolved by different fluorescence lifetimes (i.e. temporal resolution).^[40] If two different fluorophores possess different lifetimes, their emission can be distinguished with time-resolved fluorescence spectroscopy. This also offers the advantage that no absolute intensity information is required, which depends on the number of particles inside each cell. This principle

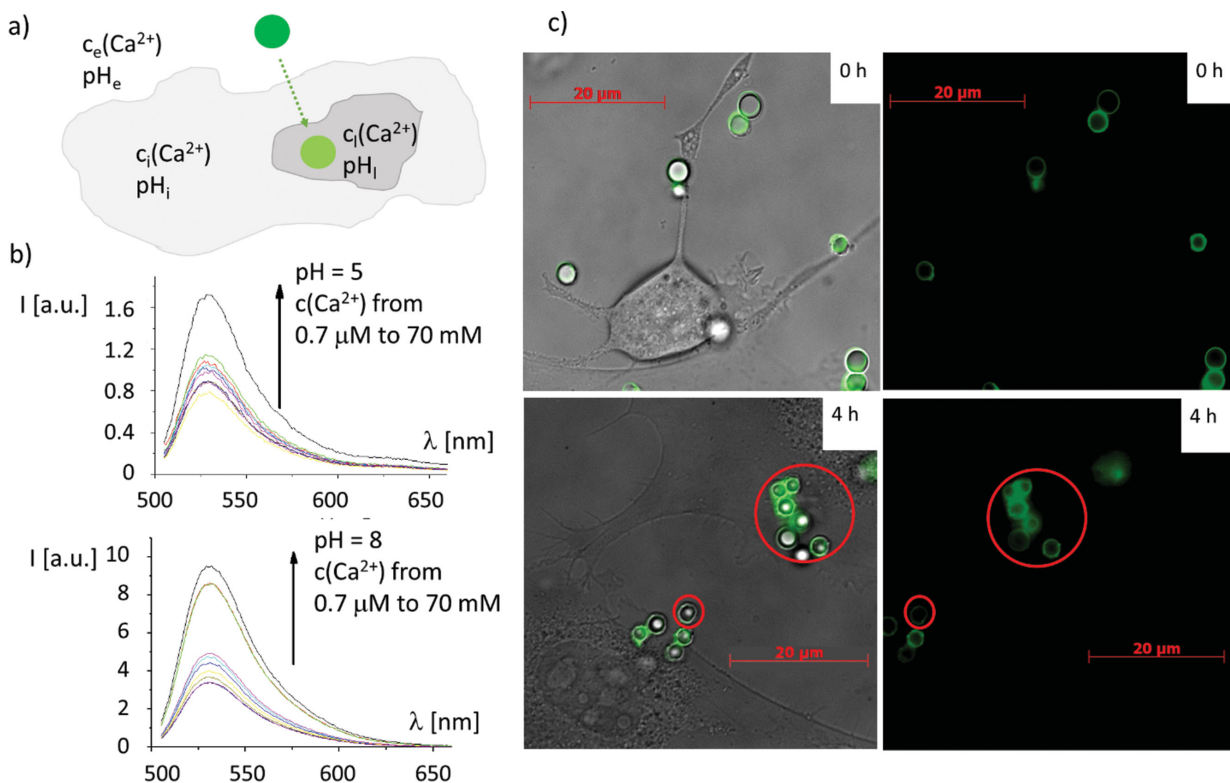


Figure 3. Micrometer-sized particles as synthesized by layer-by-layer assembly were loaded with the Ca^{2+} -sensitive fluorophore Calcium Green-1 linked to dextran.^[26,79] a) One has to differentiate between different local concentrations: extracellular calcium and pH, $c_e(\text{Ca}^{2+})$ and pH_e , intracellular calcium and pH in the cytosol, $c_i(\text{Ca}^{2+})$ and pH_i , and calcium and pH inside lysosomes, $c_l(\text{Ca}^{2+})$ and pH_l . Upon internalization the particles undergo several acidification steps in their local environment, from the extracellular space to their final localization inside lysosomes.^[49] b) Fluorescence emission spectra $I(\lambda)$ of Calcium Green-1 loaded particles depend on calcium, but also on pH. Changes in pH infer crosstalk with the Ca^{2+} -sensitive read-out. c) Ca^{2+} -sensitive particles were added to cells and microscopy images were recorded. Fluorescence images, together with an overlay with bright-field images, are shown. The scale bars correspond to 20 μm . After 4 h of incubation, some particles were internalized (the ones in the big red circle), whereas other particles were located outside cells (the one in the small red circle). However, due to crosstalk, changes in emission intensity between extracellular particles and particles inside the lysosome cannot be unequivocally correlated with changes in calcium concentration. Reduction in fluorescence can be caused by lowering of the calcium concentration, but also by lowering in pH. Therefore, if the local pH is unknown, the calcium concentration cannot be determined.

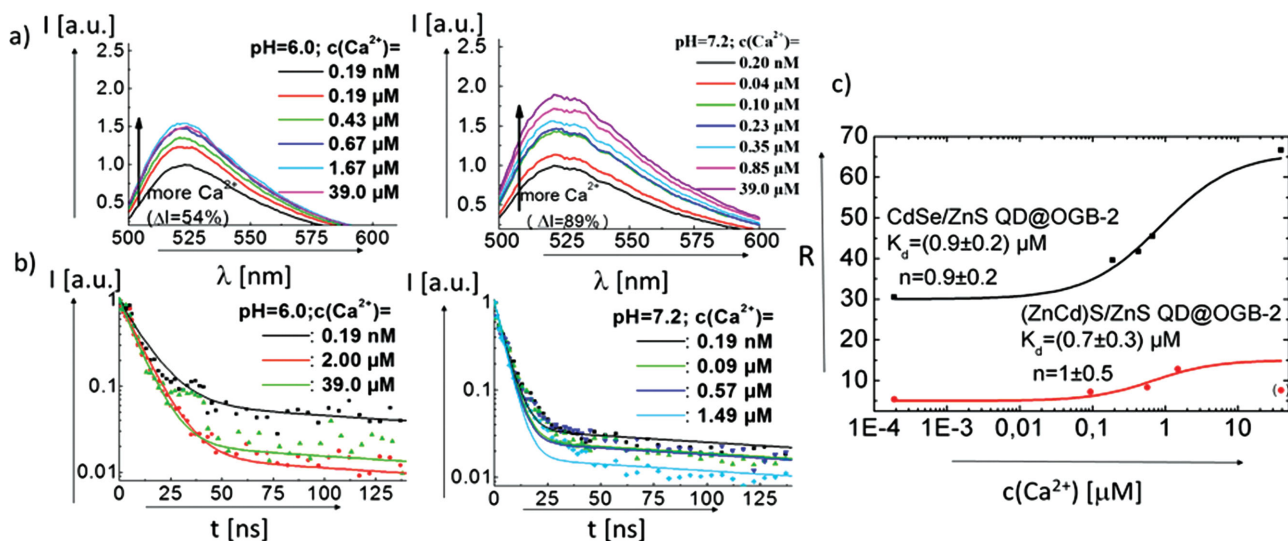


Figure 4. a) The fluorescence emission of OGB-2 depends on the Ca^{2+} concentration as well as on pH (recorded at 350 nm excitation wavelength). b) OGB-2 had been linked closely to the surface of $(\text{Zn}_x\text{Cd}_{1-x})\text{S}/\text{ZnS}$ QDs and time resolved fluorescence (at the OGB-2 emission wavelength) was recorded. Decay times depend on Ca^{2+} and pH. c) From the different decay times, a resulting response curve $R(c(\text{Ca}^{2+}))$ can be derived, which is shown here for OGB-2 coupled to $(\text{Zn}_x\text{Cd}_{1-x})\text{S}/\text{ZnS}$ and to CdSe/ZnS QDs at pH 7.2. From these curves, dissociation constants K_d can be obtained (for details, refer to the Supporting Information).

has already been applied for ion-sensitive fluorophores.^[85–87] While many organic fluorophores have similar lifetimes of a few nanoseconds, fluorescent nanoparticles such as QDs can have much longer photoluminescence lifetimes which, by using doping, can reach even milliseconds.^[88] If fluorophores are coupled closely to the surface of QDs, and the emission spectrum of the QDs overlaps with the excitation spectrum of the fluorophores, FRET occurs.^[89–92] Upon FRET from the QD to the fluorophores, the effective fluorescence lifetime of the fluorophores is increased towards the fluorescence lifetime of the QDs.^[93,94] In this way, the detection of ions could be carried out upon linkage of ion-sensitive fluorophores to the surface of QDs. The optical changes induced by ion complexation produce changes in the FRET process and, consequently, in the fluorophore lifetime that can be determined in time-resolved fluorescence measurements.^[95] The principle of time-resolved fluorescence measurements and ion-concentration determination via fluorescence lifetimes is illustrated in Figure 4, with the example of the Ca^{2+} -sensitive fluorophore Oregon Green Bapta-2 (OGB-2),^[96,97] which was coupled to the surface of $(\text{Zn}_x\text{Cd}_{1-x})\text{S}/\text{ZnS}$ and CdSe/ZnS (Lumidot 480 bought from Sigma Aldrich) QDs.^[98,99] The fluorescence spectra of OGB-2 depend on the calcium concentration but, as mentioned above, like many organic fluorophores, also on pH. The Ca^{2+} - and pH-dependence can also be seen in time resolved fluorescence, also when OGB-2 is coupled to the surface of QDs and excited via FRET. The time resolved fluorescence curves can be fitted with a simple kinetic model, which provides the relevant lifetimes.^[93] While the lifetimes themselves depend on the calcium concentration, they can be combined to a resulting response curve R , which is derived from all fit parameters. Assuming a linear increase of the FRET rate as calcium binds to OGB-2, the dissociation constants of Ca^{2+} binding to OGB-2 can be determined from this Ca^{2+} -dependent response curve (cf. Figure 4). In this way, instead of quantifying Ca^{2+} via intensity changes at a certain emission wavelength, it can be carried out via changes in fluorescence lifetime. This offers the possibility for temporally resolved multiplexed measurements of multiple ion concentrations in parallel.^[40]

5. Discussion

The examples shown in this review indicate that particle-based intracellular ion-sensing is by far not trivial and involves several pitfalls. From the point of view of the sensor itself, one should be aware of the fact that the presence of the particles can change the fluorescence response, as particles impose a different nano-environment, which changes ion concentrations as compared to the bulk.^[27,31,32] Another important drawback in the development of particle-based ion sensors originates from the few commercially available ion-sensitive fluorophores with enough specificity. To get a wide range of selective ion-sensitive fluorophores towards different target cations and anions of interest is a big challenge that needs to be addressed in order to advance fluorescence-based intracellular ion sensing. There are also several important points to take into account when ion-sensitive

particles are used for sensing ion concentration in cells: First, the location of the particle sensors needs to be experimentally determined and, unless experimentally proven otherwise, they should be assumed to be inside highly acidic intracellular vesicles and not free in the cytosol or other cellular organelles. Thus, in the most straightforward way, applications which involve irregularities in ion concentrations inside endosomes/lysosomes could be investigated, such as lysosomal storage diseases. Localization of the sensor particles in endosomes/lysosomes involves massive changes in the pH surrounding the particles upon their internalization by cells. Transitions occur from the slightly alkaline/neutral extracellular medium to the acidic environment of endosomes/lysosomes. Due to crosstalk of many ion-sensitive fluorophores with pH, this affects the ion-sensitive fluorescence read-out. Thus, for most intracellular ion-sensing experiments, knowledge of the local pH around the particle sensors would be needed, which could be achieved by additionally using pH-sensitive sensor particles. The effect of pH might also impose limits on sensors which involve enzymes as recognition elements, such as urease,^[100] glucose oxidase, or lactate oxidase to convert the analyte (urea, glucose, or lactate) into H^+ ,^[101] which then is measured as a pH-dependent fluorescence signal. Therefore, in biological media such as the interior of cells, these sensors might give signal changes which would be problematic to interpret. Multiplexed sensing of several ions (or other relevant molecules) in parallel would offer a solution, not only to crosstalk with pH but also in the case of interference with other molecules. Thus, a reasonable strategy would involve determining the fluorescence read-out of different ion-sensitive fluorophores (or pH) in parallel. However, spectral overlap of different fluorophores sensitive to different ions/molecules imposes a severe limit, and hampers detection of several fluorophores in parallel. One solution is to resolve different fluorophores not spectrally, but in different modes. Discrimination can, for example, be achieved via determination of fluorescence lifetimes.

Supporting Information

Supporting Information is available from the Wiley Online Library or from the author.

Acknowledgements

The authors are grateful to Dr. Joana Rejman for helpful technical discussions. This work was supported by DFG GRK 1782 (grants to WJP and WH) and in part by Ministry of Education and Science of the Russian Federation, contracts 02.740.11.5226, 14.740.11.1363 and Russian Foundation for Basic Research 13–04–01507 A. SA, BP, and CCC are grateful to the Alexander von Humboldt Foundation for postdoctoral fellowships. NS is grateful to DAAD and HEC for a PhD fellowship.

- [1] R. D. Carpenter, A. S. Verkman, *Org Lett* **2010**, *12*(6), 1160–1163.
- [2] X. Xie, Y. Qin, *Sens. Actuat. B* **2011**, *156*(1), 213–217.
- [3] M. J. Ruedas-Rama, A. Orte, E. A. H. Hall, J. M. Alvarez-Pez, E. M. Talavera, *Analyst* **2012**, *137*(6), 1500–1508.
- [4] N. Wanichacheva, K. Setthakarn, N. Prapawattanapol, O. Hanmeng, V. S. Lee, K. Grudpan, *J. Luminescence* **2012**, *132*(1), 35–40.
- [5] W. Jiang, Q. Q. Fu, H. Y. Fan, W. Wang, *Chem. Commun.* **2008**, (2), 259–261.
- [6] V. V. Martin, A. Rothe, Z. Diwu, K. R. Gee, *Bioorg. Medicinal Chem. Lett.* **2004**, *14*(21), 5313–5316.
- [7] P. Nandhikonda, M. P. Begaye, M. D. Heagy, *Tetrahedron Lett.* **2009**, *50*(21), 2459–2461.
- [8] P. Rivera Gil, M. Nazarenus, S. Ashraf, W. J. Parak, *Small* **2012**, *8*(6), 943–948.
- [9] T. Mistri, M. Dolai, D. Chakraborty, A. R. Khuda-Bukhsh, K. K. Das, M. Ali, *Org. Biomolec. Chem.* **2012**, *10*(12), 2380–2384.
- [10] E. Arunkumar, A. Ajayaghosh, J. Daub, *J. Am. Chem. Soc.* **2005**, *127*(9), 3156–3164.
- [11] L. Zeng, E. W. Miller, A. Pralle, E. Y. Isacoff, C. J. Chang, *J. Am. Chem. Soc.* **2006**, *128*(1), 10–11.
- [12] L. Xue, C. Liu, H. Jiang, *Chem. Commun.* **2009**, (9), 1061–1063.
- [13] X. J. Peng, J. J. Du, J. L. Fan, J. Y. Wang, Y. K. Wu, J. Z. Zhao, S. G. Sun, T. Xu, *J. Am. Chem. Soc.* **2007**, *129*(6), 1500.
- [14] D. W. Domaille, E. L. Que, C. J. Chang, *Nat. Chem. Biol.* **2008**, *4*(3), 168–175.
- [15] X. A. Zhang, D. Hayes, S. J. Smith, S. Friedle, S. J. Lippard, *J. Am. Chem. Soc.* **2008**, *130*(47), 15788–15789.
- [16] K. Komatsu, Y. Urano, H. Kojima, T. Nagano, *J. Am. Chem. Soc.* **2007**, *129*(44), 13447–13454.
- [17] Y. F. Chen, Z. Rosenzweig, *Analyt. Chem.* **2002**, *74*(19), 5132–5138.
- [18] W. J. Jin, M. T. Fernandez-Argüelles, J. M. Costa-Fernandez, R. Pereiro, A. Sanz-Medel, *Chem. Commun.* **2005**, *2005*, 883–885.
- [19] M. T. Fernandez-Argüelles, W. J. Jin, J. M. Costa-Fernandez, R. Pereiro, A. Sanz-Medel, *Analyt. Chim. Acta* **2005**, *549*, 20–25.
- [20] A. S. Susha, A. Munoz Javier, W. J. Parak, A. L. Rogach, *Colloids Surf. A* **2006**, *281*, 40–43.
- [21] H. A. Clark, S. L. R. Barker, M. Brasuel, M. T. Miller, E. Monson, S. Parus, Z. Y. Shi, A. Song, B. Thorsrud, R. Kopelman, A. Ade, W. Meixner, B. Athey, M. Hoyer, D. Hill, R. Lightle, M. A. Philbert, *Sens. Actuat. B* **1998**, *51*(1–3), 12–16.
- [22] H. A. Clark, M. Hoyer, S. Parus, M. A. Philbert, R. Kopelman, *Microchimica Acta* **1999**, *131*(1–2), 121–128.
- [23] M. Brasuel, R. Kopelman, T. J. Miller, R. Tjalkens, M. A. Philbert, *Analyt. Chem.* **2001**, *73*(10), 2221–2228.
- [24] O. Kreft, A. Muñoz Javier, G. B. Sukhorukov, W. J. Parak, *Journal Of Materials Chemistry* **2007**, *17*, 4471–4476.
- [25] U. Reibetanz, D. Halozan, M. Brumen, E. Donath, *Biomacromolecules* **2007**, *8*, 1928–1933.
- [26] L. L. del Mercato, A. Z. Abbasi, W. J. Parak, *Small* **2011**, *7*, 351–363.
- [27] F. Zhang, Z. Ali, F. Amin, A. Feltz, M. Oheim, W. J. Parak, *ChemPhysChem* **2010**, *11*, 730–735.
- [28] J. Isaad, A. El Achari, *Tetrahedron* **2013**, *69*(24), 4866–4874.
- [29] M. J. Ruedas-Rama, E. A. H. Hall, *Analyt. Chem.* **2008**, *80*(21), 8260–8268.
- [30] S. Carregal-Romero, J.-M. Montenegro, W. J. Parak, P. Rivera-Gil, *Frontiers Pharmacol.* **2012**, *3*, 70.
- [31] A. Riedinger, F. Zhang, F. Dommershausen, C. Röcker, S. Brandholt, G. U. Nienhaus, U. Koert, W. J. Parak, *Small* **2010**, *6*(22), 2590–2597.
- [32] F. Zhang, E. Lees, F. Amin, P. Rivera-Gil, F. Yang, P. Mulvaney, W. J. Parak, *Small* **2011**, *7*, 3113–3127.
- [33] C. Carrillo-Carrion, M. Nazarenus, S. Sánchez Paradinas, S. Carregal-Romero, M. J. Almendral, M. Fuentes, B. Pelaz, P. del Pino, I. Hussain, M. J. D. Clift, B. Rothen-Rutishauser, X.-J. Liang, W. J. Parak, *Curr. Op. Chem. Engineer.* **2014**, *4*, 88–96.
- [34] C. Pfeiffer, C. Rehbock, D. Hühn, C. Carrillo-Carrion, D. J. d. Aberasturi, V. Merk, S. Barcikowski, W. J. Parak, *J. R. Soc., Interface* **2014**, *11*, 20130931.
- [35] C. A. Leatherdale, W.-K. Woo, F. V. Mikulec, M. G. Bawendi, *J. Phys. Chem. B* **2002**, *106*(31), 7619–7622.
- [36] S. Pu, M. Yang, C. Hsu, C. Lai, C. Hsieh, S. Lin, Y. Cheng, P. Chou, *Small* **2006**, *2*(11), 1308–1313.
- [37] A. Huber, T. Behnke, C. Würth, C. Jaeger, U. Resch-Genger, *Analyt. Chem.* **2012**, *84*(8), 3654.
- [38] D. G. Mullen, M. Fang, A. Desai, J. R. Baker, B. G. Orr, M. M. Banaszak Holl, *ACS Nano* **2010**, *4*(2), 657–670.
- [39] D. G. Mullen, A. M. Desai, J. N. Waddell, X. M. Cheng, C. V. Kelly, D. Q. McNerny, I. J. Majoros, J. R. Baker, L. M. Sander, B. G. Orr, M. M. B. Holl, *Bioconjug. Chem.* **2008**, *19*(9), 1748–1752.
- [40] A. Z. Abbasi, F. Amin, T. Niebling, S. Friede, M. Ochs, S. Carregal-Romero, J. M. M. Martos, P. Rivera-Gil, W. Heimbrot, W. J. Parak, *ACS Nano* **2011**, *5*, 21–25.
- [41] L. L. del Mercato, A. Z. Abbasi, M. Ochs, W. J. Parak, *ACS Nano* **2011**, *5*(12), 9668–9674.
- [42] L. Shang, K. Nienhaus, G. U. Nienhaus, *J. Nanobiotechnol.* **2014**, *12*, 5.
- [43] S. Xu, B. Z. Olenyuk, C. T. Okamoto, S. F. Hamm-Alvarez, *Adv. Drug Deliv. Rev.* **2013**, *65*(1), 121–138.
- [44] T. G. Iversen, T. Skotland, K. Sandvig, *Nano Today* **2011**, *6*(2), 176–185.
- [45] G. Sahay, D. Y. Alakhova, A. V. Kabanov, *J. Controlled Release* **2010**, *145*(3), 182–195.
- [46] W. J. Parak, R. Boudreau, M. L. Gros, D. Gerion, D. Zanchet, C. M. Micheel, S. C. Williams, A. P. Alivisatos, C. A. Larabell, *Adv. Mater.* **2002**, *14*(12), 882–885.
- [47] C. Schweiger, R. Hartmann, F. Zhang, W. J. Parak, T. Kissel, P. Rivera Gil, *J. Nanobiotechnol.* **2012**, *10*(1), 28.
- [48] S. De Koker, B. G. De Geest, C. Cuvelier, L. Ferdinande, W. Deckers, W. E. Hennink, S. De Smedt, N. Mertens, *Adv. Funct. Mater.* **2007**, *17*(18), 3754–3763.
- [49] L. Kastl, D. Sasse, V. Wulf, R. Hartmann, J. Mircheski, C. Ranke, S. Carregal-Romero, J. A. Martínez-López, R. Fernández-Chacón, W. J. Parak, H.-P. Elsaesser, P. Rivera Gil, *ACS Nano* **2013**, *7*(8), 6605–6618.
- [50] M. Semmling, O. Kreft, A. Muñoz Javier, G. B. Sukhorukov, J. Käs, W. J. Parak, *Small* **2008**, *4*(10), 1763–1768.
- [51] P. Nativo, I. A. Prior, M. Brust, *ACS Nano* **2008**, *2*(8), 1639–1644.
- [52] C. Brandenberger, C. Mühlfeld, Z. Ali, A.-G. Lenz, O. Schmid, W. J. Parak, P. Gehr, B. Rothen-Rutishauser, *Small* **2010**, *6*, 1669–1678.
- [53] K. Boeneman, J. B. Delehanty, J. B. Blanco-Canosa, K. Susumu, M. H. Stewart, E. Oh, A. L. Huston, G. Dawson, S. Ingale, R. Walters, M. Domowicz, J. R. Deschamps, W. R. Algar, S. DiMaggio, J. Manono, C. M. Spillmann, D. Thompson, T. L. Jennings, P. E. Dawson, I. L. Medintz, *ACS Nano* **2013**, *7*, 3778–3796.
- [54] J. B. Delehanty, C. E. Bradburne, K. Boeneman, K. Susumu, D. Farrell, B. C. Mei, J. B. Blanco-Canosa, G. Dawson, P. E. Dawson, H. Mattoussi, I. L. Medintz, *Integrative Biology* **2010**, *2*(5–6), 265–277.
- [55] H. Mattoussi, G. Palui, H. B. Na, *Adv. Drug Deliv. Rev.* **2012**, *64*(2), 138–166.
- [56] A. Verma, O. Uzun, Y. H. Hu, Y. Hu, H. S. Han, N. Watson, S. L. Chen, D. J. Irvine, F. Stellacci, *Nat. Mater.* **2008**, *7*(7), 588–595.

- [57] H. W. Child, P. A. Del Pino, J. M. De La Fuente, A. S. Hursthouse, D. Stirling, M. Mullen, G. M. McPhee, C. Nixon, V. Jayawarna, C. C. Berry, *ACS Nano* **2011**, 5(10), 7910–7919.
- [58] T. Dejjardin, J. de la Fuente, P. Del Pino, E. P. Furlani, M. Mullin, C. A. Smith, C. C. Berry, *Nanomedicine* **2011**, 6(10), 1719–1731.
- [59] J. M. de la Fuente, C. C. Berry, *Bioconjug. Chem.* **2005**, 16(5), 1176–1180.
- [60] B. D. Chithrani, A. A. Ghazan, C. W. Chan, *Nano Lett.* **2006**, 6(4), 662–668.
- [61] D. B. Peckys, N. de Jonge, *Nano Lett.* **2011**, 11(4), 1733–1738.
- [62] M. Nazareus, Q. Zhang, M. G. Soliman, P. del Pino, B. Pelaz, S. Carregal_Romero, J. Rejman, B. Rothen-Ruthishauser, M. J. D. Clift, R. Zellner, G. U. Nienhaus, J. B. Delehanty, I. L. Medinez, W. J. Parak, *Beilstein J Nanotechnol.* **2014**, DOI: 10.3762/bjnano.5.161.
- [63] D. Hühn, K. Kantner, C. Geidel, S. Brandholt, I. De Cock, S. J. H. Soenen, P. Rivera Gil, J.-M. Montenegro, K. Braeckmans, K. Müllen, G. U. Nienhaus, M. Klapper, W. J. Parak, *ACS Nano* **2013**, 7(4), 3253–3263.
- [64] A. Muñoz Javier, O. Kreft, A. Piera Alberola, C. Kirchner, B. Zebli, A. S. Susha, E. Horn, S. Kempter, A. G. Skirtach, A. L. Rogach, J. Rädler, G. B. Sukhorukov, M. Benoit, W. J. Parak, *Small* **2006**, 2(3), 394–400.
- [65] M. Mahmoudi, A. M. Abdelmonem, S. Behzadi, J. H. Clement, S. Dutz, M. R. Ejtehadi, R. Hartmann, K. Kantner, U. Linne, P. Maffre, S. Metzler, M. K. Moghadam, C. Pfeiffer, M. Rezaei, P. Ruiz-Lozano, V. Serpooshan, M. A. Shokrgozar, G. U. Nienhaus, W. J. Parak, *ACS Nano* **2013**, 7(8), 6555–6562.
- [66] A. M. Alkilany, P. K. Nagaria, C. R. Hexel, T. J. Shaw, C. J. Murphy, M. D. Wyatt, *Small* **2009**, 5(6), 701–708.
- [67] P.-H. Yang, X. Sun, J.-F. Chiu, H. Sun, Q.-Y. He, *Bioconjug. Chem.* **2005**, 16(3), 494–496.
- [68] E. C. Cho, J. W. Xie, P. A. Wurm, Y. Xia, *Nano Lett.* **2009**, 9, 1080.
- [69] M. Semmling, O. Kreft, A. M. Javier, G. B. Sukhorukov, J. Käs, W. J. Parak, *Small* **2008**, 4(10) 1763.
- [70] C.-A. J. Lin, R. A. Sperling, J. K. Li, T.-Y. Yang, P.-Y. Li, M. Zanella, W. H. Chang, W. J. Parak, *Small* **2008**, 4(3), 334–341.
- [71] R. A. Sperling, T. Pellegrino, J. K. Li, W. H. Chang, W. J. Parak, *Adv. Funct. Mater.* **2006**, 16(7), 943–948.
- [72] M. Dahan, T. Laurence, F. Pinaud, D. S. Chemla, A. P. Alivisatos, M. Sauer, S. Weiss, *Optics Lett.* **2001**, 26(11), 825–827.
- [73] P. Rivera_Gil, S. D. Koker, B. G. De_Geest, W. J. Parak, *Nano Lett.* **2009**, 9(12), 4398–4402.
- [74] P. Rivera_Gil, C. V. Vazquez, V. Giannini, M. P. Callao, W. J. Parak, M. A. C. Duarte, R. A. Alvarez-Puebla, *Angew. Chem.* **2013**, 52, 13694–13698.
- [75] M. Eberhard, P. Erne, *Biochem. Biophys. Res. Commun.* **1991**, 180(1), 209–215.
- [76] G. A. Rutter, N. J. Osbaldeston, J. G. McCormack, R. M. Denton, *Biochem. J.* **1990**, 271(3), 627–634.
- [77] A. S. Verkman, M. C. Sellers, A. C. Chao, T. Leung, R. Ketcham, *Analyt. Biochem.* **1989**, 178(2), 355–361.
- [78] N. D. Sonawane, J. R. Thiagarajah, A. S. Verkman, *J. Biological Chem.* **2002**, 277(7), 5506–5513.
- [79] N. Antipina Maria, B. Sukhorukov Gleb, *Adv. Drug Deliv. Rev.* **2011**, 63(9), 716–729.
- [80] H. Arya, Z. Kaul, R. Wadhwa, K. Taira, T. Hirano, S. C. Kaul, *Biochem. Biophys. Res. Commun.* **2005**, 329(4), 1173–1177.
- [81] P. K. Chattopadhyay, D. A. Price, T. F. Harper, M. R. Betts, J. Yu, E. Gostick, S. P. Perfetto, P. Goepfert, R. A. Koup, S. C. De Rosa, M. P. Bruchez, M. Roederer, *Nat. Med.* **2006**, 12(8), 972.
- [82] H. Xu, M. Y. Sha, E. Y. Wong, J. Uphoff, Y. Xu, J. A. Treadway, A. Truong, E. O'Brien, S. Asquith, M. Stubbins, N. K. Spurr, E. H. Lai, W. Mahoney, *Nucleic Acids Res.* **2003**, 31(8), e42.
- [83] X. Gao, S. Nie, *Anal. Chem.* **2004**, 76(8), 2406–2410.
- [84] J. A. Lee, S. Mardiyani, A. Hung, A. Rhee, J. Klostranec, Y. Mu, D. Li, W. C. W. Chan, *Adv. Mater.* **2007**, 19(20), 3113.
- [85] U. Lieberwirth, J. Arden-Jacob, K. H. Drexhage, D. P. Herten, R. Müller, M. Neumann, A. Schulz, S. Siebert, G. Sagner, S. Klingel, M. Sauer, J. Wolfrum, *Analyt. Chem.* **1998**, 70, 4771–4779.
- [86] S. H. Minhindukulasuriya, T. K. Morcone, L. B. McGown, *Electrophoresis* **2003**, 24, 20–25.
- [87] K. Hoffmann, T. Behnke, D. Drescher, J. Kneip, U. Resch-Genger, *ACS Nano* **2013**, 7, 6674–6684.
- [88] C. Gan, Y. Zhang, D. Battaglia, X. Peng, M. Xiao, *Appl. Phys. Lett.* **2008**, 92(2411111).
- [89] T. Förster, *Annalen der Physik* **1948**, 437(1–2), 55–75.
- [90] I. L. Medintz, A. R. Clapp, H. Mattoussi, E. R. Goldman, B. Fisher, J. M. Mauro, *Nat. Mater.* **2003**, 2, 630–638.
- [91] R. Freeman, L. Bahshi, T. FINDER, R. Gill, I. Willner, *Chem. Commun.* **2009**, (7), 764–766.
- [92] A. V. Yakovlev, F. Zhang, A. Zulqurnain, A. Azhar-Zahoor, C. Luccardini, S. Gaillard, J. M. Mallet, P. Tauc, J. C. Brochon, W. J. Parak, A. Feltz, M. Oheim, *Langmuir* **2009**, 25(5), 3232–3239.
- [93] T. Niebling, F. Zhang, Z. Ali, W. J. Parak, W. Heimbrot, *J. Appl. Phys.* **2009**, 106, 104701.
- [94] J. S. Kang, g. Piszczek, J. R. Lakowicz, *J. Fluorescence* **2002**, 12, 97–103.
- [95] U. Kaiser, D. J. d. Aberasturi, R. Malinowski, F. Amin, W. J. Parak, W. Heimbrot, *Appl. Phys. Lett.* **2014**, 104, 041901.
- [96] A. V. Agronskaia, L. Tertoolen, H. C. Gerritsen, *J. Biomed. Optics* **2004**, 9, 1230–1237.
- [97] R. Y. Tsien, *Biochemistry* **1980**, 19, 2396–2404.
- [98] W. K. Bae, M. K. Nam, K. Char, S. Lee, *Chem. Mater.* **2008**, 20, 5307–5313.
- [99] B. O. Dabbousi, J. Rodriguez-Viejo, F. V. Mikulec, J. R. Heine, H. Mattoussi, R. Ober, K. F. Jensen, M. G. Bawendi, *J. Phys. Chem. B* **1997**, 101(46), 9463–9475.
- [100] L. I. Kazakova, L. I. Shabarchina, G. B. Sukhorukov, *Phys. Chem. Chem. Phys.* **2011**, 13(23), 11110.
- [101] O. Y. Kochetkova, L. I. Kazakova, D. A. Moshkov, M. G. Vinokurov, L. I. Shabarchina, *Russian J. Bioorg. Chem.* **2013**, 39(5), 504–509.
- [102] A. S. Susha, A. M. Javier, W. J. Parak, A. L. Rogach, *Colloids Surf. A* **2006**, 281, 40.

Received: July 17, 2014
Revised: September 24, 2014
Published online: December 15, 2014

Quantum-Dot-Based Photoelectrochemical Sensors for Chemical and Biological Detection

Zhao Yue,[†] Fred Lisdat,[‡] Wolfgang J. Parak,[‡] Stephen G. Hickey,[§] Liping Tu,[†] Nadeem Sabir,[‡] Dirk Dorfs,[#] and Nadja C. Bigall^{‡,#,*}

[†]Department of Electronics, Nankai University, Tianjin 300071, P.R. China

[‡]Fachbereich Physik und WZMW, Philipps Universität Marburg, Marburg, Germany

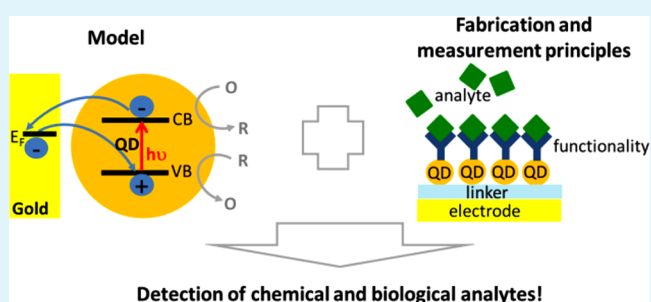
[§]Physikalische Chemie/Elektrochemie, Technische Universität Dresden, 01069 Dresden, Germany

[‡]Biosystems Technology, Technical University of Applied Sciences, Wildau, Germany

[#]Physical Chemistry and Electrochemistry, Leibniz University of Hannover, 30167 Hannover, Germany

ABSTRACT: Quantum-dot-based photoelectrochemical sensors are powerful alternatives for the detection of chemicals and biochemical molecules compared to other sensor types, which is the primary reason as to why they have become a hot topic in nanotechnology-related analytical methods. These sensors basically consist of QDs immobilized by a linking molecule (linker) to an electrode, so that upon their illumination, a photocurrent is generated which depends on the type and concentration of the respective analyte in the immediate environment of the electrode. The present review provides an overview of recent developments in the fabrication methods and sensing concepts concerning direct and indirect interactions of the analyte with quantum dot modified electrodes. Furthermore, it describes in detail the broad range of different sensing applications of such quantum-dot-based photoelectrochemical sensors for inorganic and organic (small and macro-) molecules that have arisen in recent years. Finally, a number of aspects concerning current challenges on the way to achieving real-life applications of QD-based photochemical sensing are addressed.

KEYWORDS: photoelectrochemistry, quantum dots, nanoparticles, photocurrent, sensors



1. INTRODUCTION

Quantum dot (QD)-based sensors for chemical and biological detection are presently a technological hot topic^{1–8} because of the special optical and electronic properties of the component QDs^{9–15} plus the possibility to relatively easily functionalize them with a wide variety of biological as well as for other important applications relevant molecules.^{10,16–18} In principle, there are several ways that one may take advantage of the optical and electronic properties of QDs to design analytical methods for the detection of chemicals and biomolecules. This review focuses on sensors based on an electronic output, which consist of QDs immobilized on a conductive electrode. These systems can generate photocurrents which are sensitive to the chemical environment of the surrounding solution (see Figure 1). Although optical transducers based on fluorescence, fluorescence resonance energy transfer (FRET), chemiluminescence resonance energy transfer (CRET), and other mechanisms are already widespread,^{1–4,19–38} the area of QD-based photoelectrochemical sensors has recently evolved into a rather new and important branch of biosensing, as many of their properties are advantageous when compared to the other sensor types. For example, even though they are still model systems, they are easy to operate, because they yield an

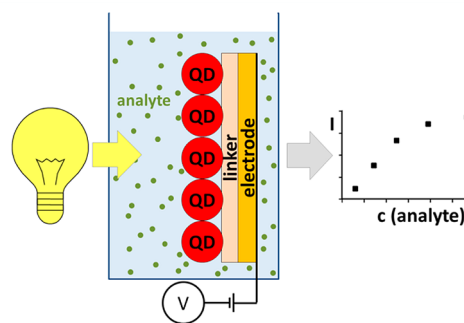


Figure 1. Schematic representation of a QD-based photoelectrochemical sensor. QDs are immobilized by a linker to an electrode, which is placed in a solution. Upon illumination of this electrode, a photocurrent is generated depending on the type and concentration of the analyte in the surrounding solution.

Special Issue: Forum on Biomedical Applications of Colloidal Photoluminescent Quantum Dots

Received: November 27, 2012

Accepted: March 14, 2013

Published: April 3, 2013

electronic output without the necessity to purchase expensive optical equipment. In addition to the potential applied, the impinging light can provide a means for controlling the desired reaction.

Furthermore, QD-based photoelectrochemical sensors have the following advantages: (1) As QDs serve as “pumps” for the charge carrier transfer between the conductive electrode and the redox agent (oxidant and reductant) through tunneling processes, one can achieve photoelectrochemical sensors with a fast response and high sensitivity. Through further coupling with biocatalytic reactions, this leads to the possibility to detect certain substances that cannot be detected using common optical property based analytical methods. (2) Only small dark-currents are observed in QD-based systems, because the immobilization layer, which links the nanoparticles to the electrode surface and thus, attenuates alternate electron transfer reactions. Under illumination this situation changes significantly and redox reactions can occur, thus the QDs play a key role as photoactivators of the sensor. Due to the broad absorption spectra of the QDs their photoelectrochemical sensor systems can be excited by a common white light source. This enables the design of simple, cheap, and portable sensor systems. (3) QD-based photoelectrochemical sensors can easily be extended to light-addressable sensors by the spatially resolved illumination of a selected area of the electrode provided that a spatially resolved immobilization of the recognition elements can be performed. As an extension of this strategy it should be possible to obtain spatially resolved coding or multichannel detection.³⁹ Compared to the traditional Si-based light addressable sensors,⁴⁰ QD-based light addressable sensors can potentially possess a higher lateral resolution, because the photoexcited electron–hole pairs should diffuse less within the semiconductor layer.^{41–43} (4) The use of QDs opens the possibility to efficiently chemically couple additional moieties to the QDs, e.g., biomolecules.

As may be gleaned from the above, the great potential of QD-based photoelectrochemical sensors is clear. Because many recent reviews have already focused on QD-based optical sensors,^{3,15} in this review, we focus our attention on the photoelectrochemical applications of QDs for chemical and biological detection. Once the functional principle and some advantages of these systems have been laid out, we describe several fabrication routes developed within recent years. In the sections that follow, the state-of-the-art in the detection of chemicals and biomolecules is described and the broad range of molecules already detectable by QD-based photoelectrochemical sensors is presented. Finally, an overview to conclude the actual observations is given and future perspectives are discussed.

1.1. Functional Principle. As a general rule, this type of photoelectrochemical sensor consists of QDs immobilized onto an electrode, which in most cases is achieved via an organic linker layer. Subsequent to the excitation of the QDs and under the application of an appropriate potential, electrons can tunnel from the electrode to the valence band of the QDs, and electrons present in the conduction band of the QDs can tunnel to oxidant molecules (electron acceptors) in the surrounding solution. Hence, in such a case, the cathodic photocurrent generated monotonically increases with increasing concentration of the oxidant present in solution. By contrast, if reducing molecules (electron donors) exist in solution, tunneling of electrons from the solution phase to the

valence band of the QDs and of electrons from the conduction band to the electrode occurs. It can therefore be seen that both the direction and the amplitude of the resulting photocurrent are determined by the concentration of molecules (to be detected) and by the bias potential applied to the electrode. A commonly employed schematic depicting the detection principle is shown in Figure 2. As previously mentioned,

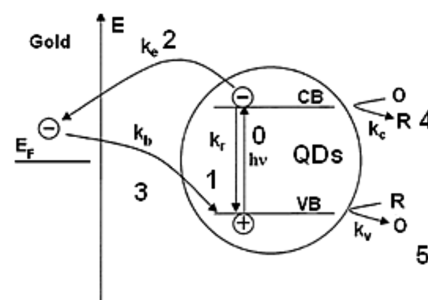


Figure 2. Energy diagram of photoinduced charge carrier transfer in a QD-based photoelectrochemical system corresponding to the models presented within refs 44–47. k_r is the rate of the relaxation pathway, k_c and k_b are the electron transfer rates from the conduction band to the electrode and from the electrode to the valence band, respectively. k_c and k_v are the transfer rate from the conduction band to a molecule in solution (O) being reduced to R, and the transfer rate from a molecule (R) in solution being oxidized (to O) to the valence band, respectively.

upon illumination, electrons in the QDs are excited, which subsequently have the possibility to either tunnel to the gold electrode (with a transfer rate k_c (2), or to solution and reduce oxidants (transfer rate k_c (4). Generated excited state holes can be filled by electrons tunneling from the electrode to the QDs (rate k_b (3) or tunneling from reductants in solution to the QDs (rate k_v (5). Hence, several electron transfer processes (2–5) are competing with the excitation process (0) and the recombination process (1), altogether yielding a net photocurrent. The amplitude, shape, and direction of this photocurrent will be controlled by the kinetics of each individual step.

The rates k_c and k_b , which are tunneling rates between the QDs and the electrode, strongly depend on the energy barrier height (determined by the linker material), on the barrier distance (determined by the thickness of the linker material), as well as on the difference between the Fermi level of the gold electrode and the energetic bands of the QDs.⁴⁸ Hence, k_c and k_b are influenced by the chemical composition and thickness of the linker, the applied potential, the size or material composition of the QDs and the surface modification protocol used for creating the interface with the solution. k_v is the electron tunneling rate from the reductants in solution to the photoinduced holes in the valence band of the QDs. k_c is the transfer rate of photoinduced electrons from the conduction band of the QDs tunneling to the electron acceptors O in solution. Consequently, k_v and k_c are influenced by the concentration of donors and acceptors in solution and by the surface properties of the modified QDs.

From a comparison between the theoretical models,^{46,49} simulations,^{46,47} and experimental results,⁴¹ it can clearly be seen that the energetic position of the conduction band and the valence band of the QDs (determined by the size and composition of the QDs), the distance between the gold electrode surface and the QDs (i.e., the thickness and conductive properties of the immobilization layer), the position

of the Fermi level in the gold electrode (i.e., the bias potential), and the concentration of the redox agent in solution will all influence the output characteristics of the photocurrent. Therefore, one has to take particular account of all these parameters when designing an appropriate QD-based photoelectrochemical sensor. When all other parameters remain constant, the amplitude of the photocurrent will follow the charge transfer rates as determined by the redox agent concentration (k_v or k_c) at the respective bias potential. Hence, it is reasonable that QD-based photoelectrochemical detection of different molecules is quantifiable by measuring the amplitude of the photocurrent.

All theoretical studies describe the same basic concept, with the exception of the description of the role surface states in the QDs, which are commonly referred to as "traps".^{44–47,50–53} Traps are energetic states that usually appear because of the break in symmetry at the surface of QDs and which result in artifacts such as vacancies, defects etc., which can be located within the band gap of the QDs.^{54–56} Once such states exist, excited electrons (or holes) may occupy them (meaning they are "trapped") and, if many such states are present and/or trapping events occur with a high probability, significant depopulation of the conduction band (or the holes in the valence band) can result. For applications in which QDs are used as fluorescent dyes, usually efforts are undertaken to minimize the amount of surface traps that occur because such states result in a reduction of the photoluminescence quantum yield. However, in the field of QD-based photoelectrochemical sensors, the role of trap states is hotly debated and often controversial. In recent publications, two different kinds of models regarding the role of trap states can be found with the frequently discussed controversial question being whether the direction of the photocurrent follows the applied bias potential or not. Using time-resolved photoelectrochemical measurements, several research groups independently obtained similar charge transfer models for QD-based photoelectrochemical setups with gold and ITO electrodes.^{44,45,50–53,57–62} According to their observations, for QDs of different materials and different charge carrier trapping properties, different models are required to be developed. For CdS QDs, it has been demonstrated that hole traps play the main role in the photocurrent generation. Here, the direction of the photocurrent did not follow the bias potential, even though the amplitude and shape profiles did. In a separate study obtained for PbS QDs, for the same bias voltage range, different directions in the photocurrent were observed. In a further work, published by Nakanishi et al., multilayers of QDs on gold electrodes were characterized by Fourier transform infrared reflection absorption spectroscopy (FT-IRRAS)^{63,64} where a similar behavior was observed, namely that only positive photocurrents resulted for both positive and negative bias potentials at the electrode. The corresponding model, in which charge carrier trapping plays an important role for the resulting photocurrent, takes into account the more complex situation where traps are present. This model is an extension of that presented in Figure 2, which results from the combined studies within several other research groups.^{2,41,65–72} In their observations, the direction of the photocurrent was clearly reversible and determined by the bias potential applied. Here, a bias potential more negative than the Fermi level resulted in a negative photocurrent, and a bias potential more positive than the Fermi level in a positive photocurrent. Also, for photoelectrodes with CdSe or CdSe/ZnS core/shell QDs, it

was observed that the amplitude of the photocurrent followed the absorption spectra of the QDs, and that the direction of the photocurrent followed the direction of the bias potential.^{69,73} This is highly indicative that in these cases, the photocurrents arose from electron hole pairs undisturbed by trap states.

One possible explanation for the many and varied observational discrepancies that one finds in the literature may be due to the use of QD materials of different quality especially with respect to the amount of trap states present. Interestingly, many of the older publications report on the importance of trap states, while more recent publications report more on the minor role of trap states, and is a change that may be considered to coincide with the development of improved QD synthesis routes which produce materials with higher photoluminescence quantum yields resulting from the presence of fewer defect states. The quality of the QDs and the type of surfactant molecules present at the QD surface crucially influence the occurrence (in terms of number and energetic level) of traps. The presence of a surface state can reduce the transfer rate to the electrode or to the redox molecule (depending on the type of trap state) and hence make the photocurrent become unidirectional, whereas the amplitude of the photocurrent will be influenced by the light intensity.

Despite the reported differences in the experimental results concerning the role of the trap states as described above, the possibility of photoelectrochemical detection of substances in solution is not prevented: it does not matter whether positive or negative potentials are applied or if the direction of the photocurrent is reversible or not under different bias voltages, the main observation remains, namely that the amplitude of the photocurrent depends on the concentration of the donor/acceptor compounds. However, there are some inherent disadvantages when surface states play the main role in a photoelectrochemical detection system. The first is that in the case where one type of QD is used, the system can only be used to either oxidize molecules or to reduce them. For example, Katz et al.⁶⁵ reported the simultaneous photoelectrochemical detection of both the oxidized and reduced states of cytochrome c employing only one type of QD by a simple variation of the bias potential. If surface states had played the main role in the charge carrier separation step, the photocurrent would not have been reversible. In that case, only the oxidized or the reduced cytochrome c species would have been detectable. Second, if the photocurrent is dominated by trap states that are not size-dependent, multichannel detection or coding parallel analysis based on the size-dependent properties of the QDs in a photoelectrochemical sensor system cannot be achieved. Therefore, for such kinds of applications, it is strongly recommended to avoid the occurrence of surface states when designing and fabricating QD-based photoelectrochemical sensors. However, these trap related issues are solvable through the use of well passivated state of the art QDs (e.g., core shell or core multi-shell QDs) and are expected to further diminish in their importance, especially when one views the rapid progress made within the colloid chemical synthesis of QDs over the past decades.

1.2. Advantages. As described in the previous section, QDs act as a mediator in the electron transfer between molecules and a conductive electrode, with the photocurrent scaling as a function of the analyte concentration. As a consequence, some biomolecules such as nicotinamide adenine dinucleotide (NADH) or even proteins become detectable.^{1,66} Besides the above-described advantages of using light as a

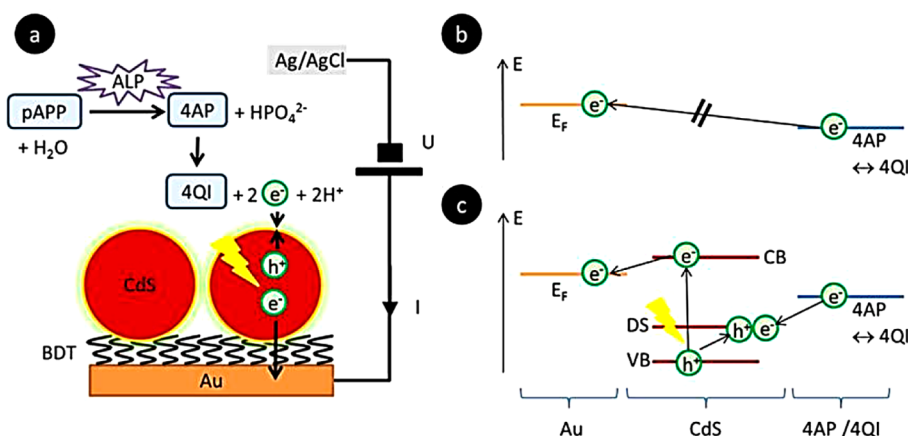


Figure 3. (a) Detection scheme for indirect detection of *p*-aminophenyl phosphate by QDs immobilized on a gold electrode. The energy schemes show that (b) in the absence of light, no current is detected, whereas (c) under illumination, charge transfer can happen, which leads to the generation of a photocurrent. Reprinted with permission from ref 76. Copyright 2011 BioMed Central.

sensorial read-out tool, in some cases QD-based photoelectrochemical sensor systems can provide higher sensitivities and lower detection limits than metal nanoparticle or QD-based optical sensors or even conventional electrochemical sensors.^{74,75}

a. Low Limit of Detection. Most of the reported sensing schemes based on QDs work in a similar concentration range to that of alternative systems that use optical or electrochemical transduction principles. However, some studies have devoted much effort to showing the potential of using photoelectrochemical detection with respect to their very low detection limits.

In a report published by Yildiz et al.,⁷⁴ electrochemical and photoelectrochemical detection of tyrosinase (an indicative marker for melanoma cancer cells) activity were realized by using Pt nanoparticles and CdS QDs as electrocatalytic labels and photoelectrochemical reporter units, respectively. The limit of detection (LOD) of tyrosinase was tested and compared with other analytical techniques such as QD-based optical sensors, ion-sensitive field-effect transistor (FET) devices and quartz crystal microbalance (QCM). While the Pt nanoparticle based electrochemical method was shown to be the least sensitive method among the three electronic sensors for analyzing tyrosinase, the photoelectrochemical detection of tyrosinase activity was demonstrated to possess the highest sensitivity and showed the lowest detection limit. Golub et al.⁷⁵ have exploited a common aptasensor configuration for the electrochemical and photoelectrochemical detection of cocaine. Here the gold electrode was functionalized with one aptamer subunit, while another aptamer subunit was linked either to a Pt nanoparticle, a Au nanoparticle or a CdS quantum dot. In the presence of cocaine, the close proximity of the electrode to the respective nanoparticle was detectable either via the reduction of H_2O_2 (in case of Pt nanoparticles), via the changes in photocurrent in the presence of triethanol amine (in case of CdS QDs) or via the changes in the reflectance spectra caused by the changes in the surface plasmon resonances (in case of Au nanoparticles). For the CdS-based detection of cocaine, the photocurrent was generated by the ejection of the conduction band electrons into the electrode, and the filling of the valence-band holes by a charge transfer from a sacrificial electron donor in the vicinity. The intensities of the photocurrents were controlled by the amount of supramolecular cocaine-aptamer complexes attached to the electrode. All three configurations

revealed a common advantage over the available aptasensors due to a reduced background signal. Also in this investigation the photoelectrochemical method provided the lowest LOD of cocaine corresponding to 1×10^{-6} M compared to 1×10^{-5} M (electrochemical detection with Pt nanoparticles). The two articles described above display the first proof that for certain arrangements and good-quality quantum dots, the limit of detection can be significantly lower for QD-based photoelectrochemical sensors than for different optical or electrochemical QD-based sensor systems.

b. Low Working Potential. Khalid et al.⁷⁶ designed a photoelectrochemical sensor for the indirect detection of *p*-aminophenyl phosphate (*p*APP) that can operate at rather low potential (see Figure 3). The sensor was based on the electrochemical conversion of 4-aminophenol at a QD modified electrode under illumination. First, in an enzymatic reaction, *p*APP was degraded to 4-aminophenol. Upon illumination of the QDs, electron hole pairs were generated, so that the photoexcited holes from the valence band of the QDs lead to oxidation of the 4-aminophenol, while the photoexcited electrons were transferred to the Au electrode. An oxidation photocurrent which was dependent on the presence of 4-aminophenol could thus be detected. In the absence of QDs, oxidation of 4-aminophenol by the gold electrode did not take place if the applied bias potential was not sufficiently high. However, with a QD interlayer, detection could already be achieved at low working potentials. This observation supports the general assumption that with the correct arrangement within the QD-based photoelectrochemical sensors, the working potential and hence the energy consumption can be reduced significantly in certain cases. Another example in this direction is the oxidation of NADH at potentials around 0 V vs Ag/AgCl.³⁵

2. FABRICATION METHODS

As previously mentioned a QD-based photoelectrochemical sensor usually consists of an electrode (gold, TiO_2 , indium tin oxide (ITO), fluorine doped tin oxide (FTO), carbon, etc.) onto which the QDs are immobilized. Optically transparent electrodes have the advantage that the illumination can be applied from the back side which reduces any unwanted photochemical or photophysical interactions with the solution.

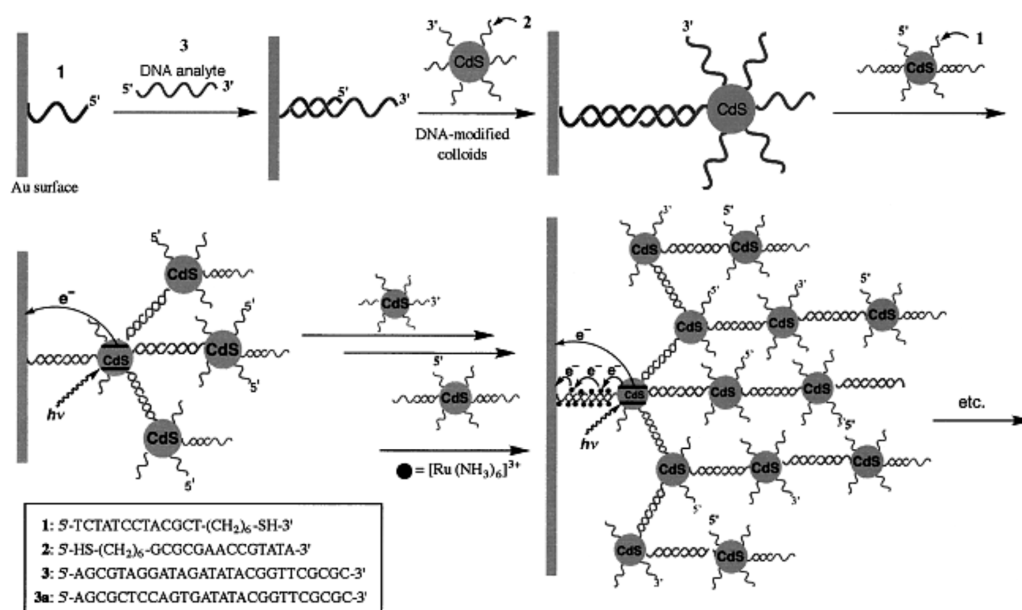


Figure 4. Organization of oligonucleotide/DNA-cross-linked arrays of CdS nanoparticles and photoelectrochemical response of the nanoarchitectures. Reprinted with permission from ref 73. Copyright 2001 Wiley–VCH Verlag GmbH.

However, usually these types of electrodes are relatively rough, which can be disadvantageous for certain applications.

QD-based photoelectrochemical sensors are normally fabricated in three steps: synthesis and modification of the QDs, immobilization of a linker molecule layer and deposition of the QDs onto the electrode. The present review does not address the synthesis of QDs and their surface modification. Instead, it is specifically about the immobilization of the QDs on the electrodes, which is a very important parameter in the fabrication of high-end photoelectrochemical sensors, and which will be discussed in more detail in the following subsection.

2.1. Assembly Methods of QDs onto Electrodes. To immobilize the QDs on a conductive electrode, chemical assembly methods onto a variety of different insulating or conducting materials can generally be employed. For the connection of QDs to gold electrodes, linker molecules with two thiol groups such as alkanedithiols,^{63,64} 1,4-dithiane,^{45,66} 1,4-benzene-dithiol,^{41,69} 1,6-hexanedithiol,⁴⁵ stilbenedithiol,⁷² etc., have been demonstrated to be advantageous because thiol groups bind strongly to both the QDs and the gold surface. For linking QDs to TiO₂ or indium tin oxide (ITO) electrodes, silane molecules with an additional functional group such as (3-aminopropyl)trimethoxysilane or (3-mercaptopropyl)trimethoxysilane are commonly used.^{53,77}

Several research groups have already attempted to provide a common model to explain the QD/self-assembled monolayer (SAM)/electrode structure in a number of different ways and with different analytical tools.^{41,44–47,49–53,57–62,64,68,78–87} The general photoelectrochemical knowledge gained through understanding this kind of system has broader implications since similar structures can be found in use for applications such as solar cells with high photon conversion efficiencies. Hence, many solar energy research-based groups have also intensively studied such QD/SAM/electrode systems, which has led to an improvement in our understanding of QD-based photoelectrochemical sensors.^{88–90}

Because of its capacity as an in-series component the type of linker molecule used is of utmost importance. This can be seen for example from the works of Bakkers et al.⁵⁰ and Yue et al.,⁴¹ which describe how, in absence of thiol molecules the QDs are not tightly bound to the electrodes, and that the length of the SAM molecules significantly affects the charge transfer rate. The presence of too great a distance within these mostly insulating materials strongly reduces or even prevents the photocurrent, since the distance-dependent tunneling processes are attenuated. Furthermore it should be mentioned that good passivation resulting from a high-quality SAM is frequently not achieved. For example, short chained dithiol molecules have been observed to not form SAMs, and the binding of both thiol functional groups to the gold electrode also needs to be prevented.⁷² For these reasons, it is clear that the composition and thickness of the linking material as well as the quality of the SAM formed is highly important for the quality of any resulting sensor system.⁹¹

Furthermore, densely packed layers of QDs on the electrode will provide a better performance than if the QDs are individually distributed. Therefore, a variety of nanoparticle assembly techniques has been developed such as the previously described assembly mediated by functional molecules, embedding the QDs in polyelectrolyte multilayers (so-called layer-by-layer systems), or directed assembly⁹² e.g. by means of block-copolymers.^{93–95} To achieve optimum tuning of the layer properties, the nanoparticle assemblies have been studied intensely by different measurement techniques such as cyclic voltammetry,⁴¹ scanning tunneling microscopy,⁷⁹ X-ray photon spectroscopy,⁶³ atomic force microscopy,⁹⁶ quartz crystal microbalance,⁹⁷ and surface plasmon resonance.⁷⁵

Apart from monolayers of QDs on electrodes, the performance of multilayered systems has been frequently studied in QD-based photoelectrochemical sensing systems. Generally it has been found that multilayered deposition of QDs produce larger and more stable photocurrent amplitudes which scale with the number of layers.^{63,64,73,75,98} Chemical linkers were employed so that layers of metal NPs or carbon nanotubes

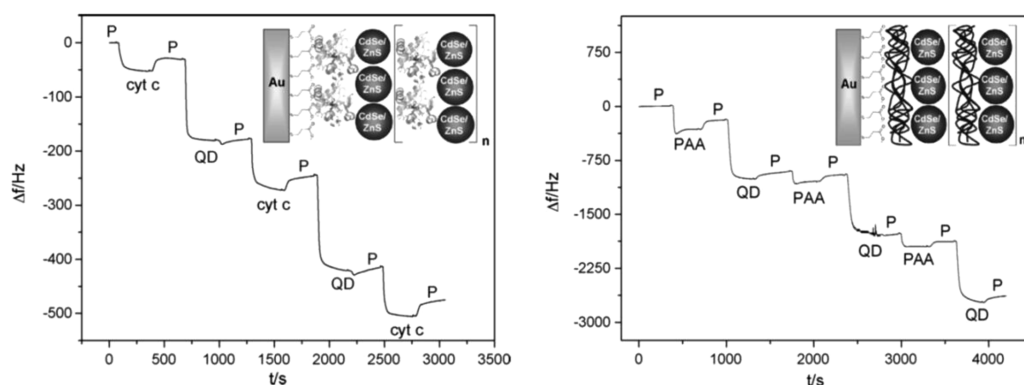


Figure 5. Multilayer formation with (left) cytochrome c and (right) PAA both exhibiting a positive surface charge and mercaptopropionic acid-modified CdSe/ZnS QDs exhibiting a negative surface charge. The assembly processes were followed by quartz crystal microbalance measurements in a flow cell. The insets display the respective setup scheme. Adapted with permission from ref 102. Copyright 2012 Elsevier.

could be included between the QDs and the electrodes, which was observed to enhance the charge carrier transfer and hence improve the photocurrent.^{99,100} Golub et al.¹³ and Willner et al.^{73,75} successfully employed duplex DNA chains as linking material to construct mono- and multilayers of QDs. Because the conductivity of the stacked systems in dsDNA is limited, intercalators were added to the DNA, which lead to a significantly improved conductivity. Alternatively, redox active shuttle molecules or substances that interact electrostatically with DNA can also be used. The immobilization and enhancement process is shown in the diagram in Figure 4.

In addition to the assembly methods based on covalent linking, electrochemical deposition techniques,^{22,101} physical methods (such as spin coating),⁴¹ and electrostatic adsorption (such as layer-by-layer assembly of positively charged polyelectrolytes and negatively charged QDs^{41,47}) have been widely studied. Polyelectrolyte assisted layer-by-layer methods were found to be an interesting approach for a number of reasons. First, the polyelectrolyte plays the role of a linker and at the same time provides advantageous conditions for interparticle electron transfer. Second, a polyelectrolyte assisted layer-by-layer method opens the possibility to further integrate additional species. For example, metal ions can be included which have been shown to result in a higher photocurrent stability.⁴⁷ Other approaches are to embed charged proteins, which can be tailored to yield defined reactions with certain analyte molecules¹⁰² or even to include different types of functional nanoparticles.

Göbel et al.¹⁰² have made a comparative study between the photocurrents of two different QD multilayer systems, whereby one system was constructed by electrostatic adsorption of the redox protein cytochrome c and the other by a positively charged polyelectrolyte (poly(allylamine hydrochloride), PAA) (see Figure 5). Although both photocurrents were observed to follow the number of deposited QD layers, the Au/(cytochrome c/QDs)_n system showed only a slight enhancement of the photocurrents since the cytochrome c cannot facilitate the electron transfer between the QD layers. However, the Au/(PAA/QDs)_n system provided a proportional increase in the photocurrent with the number of deposited layers, which was explained by the fact that PAA ensures short distances between the QDs and thus allows a rather undisturbed interparticle electron transfer. This example also shows that the choice of materials employed for the construction of the

QD multilayers by electrostatic adsorption plays a very important role in yielding a high photocurrent output.

2.2. Improving the Charge Carrier Separation. In order for the sensors to obtain higher photocurrents and sensitivities, improving the separation efficiency of the photogenerated electron and hole pairs from the QDs is crucial. In the following paragraph, approaches to achieve this are discussed.

As explained in section 1.1, charge carrier transfer competes with the recombination process and since the recombination process is very fast, it is likely that photoinduced electrons and holes cannot be efficiently separated, which limits the photocurrent. As mentioned above, electron or hole donors such as ascorbic acid can be introduced to the system in order to improve the electron hole separation. In ref 71, methylene blue is described as being able to improve the charge carrier separation. Methylene blue is also an effective organic electron transfer mediator used for sensors and biosensors. The application of methylene blue not only enabled the measurement of higher photocurrent values, but photocurrents at lower QD concentrations were also observed. Of course, such reactions interfere with a direct analyte conversion at the QDs, but they are valuable for the detection of QD labels bound to the surface by a biospecific recognition event.

To improve the separation efficiency and therefore the photocurrent, composite QD assemblies and hybrid nanostructures have recently been used and studied. Metals such as gold nanoparticles and semiconductor nanomaterials (nanoparticles, nanowires, carbon nanotubes, TiO₂, SnO₂, etc.) have all been used to increase the separation efficiency of photoinduced electron hole pairs. Two different kinds of hybrid nanosystems in particular have been tested: the first type are nano-heterostructures arising from special types of synthesis,⁷² e.g., dimeric nanoobjects of which at least one domain consists of a semiconducting material. The second type of hybrid nanosystem arises from assembly methods of separate semiconductor QDs together with nanoparticles from different materials e.g. metals.^{100,103,104} The combination of two different nanomaterials in a nanoheterostructure by synthetic methods (such as the synthesis of CdS-SnO₂ nanoheterodimers) can result in an increase in the probability of charge carrier separation in the system, and hence in improved photoelectrochemical properties. Here, the conduction band electrons in the CdS-particles were transferred to the conduction band of the SnO₂, resulting in a delocalization of the electron and the hole (see diagram in Figure 6). Examples

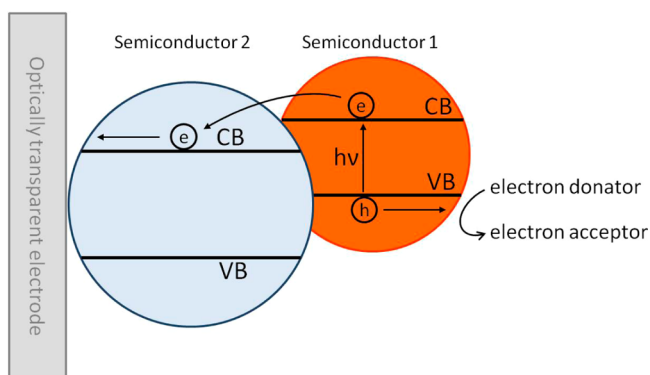


Figure 6. Schematic drawing of the suppression of charge carrier recombination in a semiconductor nanoheterostructure with properly aligned band gaps. In the excited state, electrons are transferred from the conduction band of semiconductor 1 to the conduction band of semiconductor 2. Because of the spatial separation of the electrons and holes, direct recombination is suppressed. The electron is then transferred to the electrode, and the hole (which remains in semiconductor 1) is filled by an electron donor from the solution.¹⁰⁸

of nanoheterostructures for the charge-carrier separation are nanoobjects composed from CdS and Au,⁸¹ CdS and carbon nanotubes¹⁰⁵ or graphene,¹⁰⁶ CdSe and C60 molecules,¹⁰⁷ as well as the afore-mentioned system from CdS and SnO₂.¹⁰⁸

Similarly, metal nanoparticles, semiconductor nanomaterials and organic molecules can be deposited on top of QDs or between the QDs and the electrodes in order to generate photocatalytic activity, which is attributed to the effective separation of the excited electrons and holes which have been formed in the semiconductor domain of the hybrid system. Examples of such systems are: CdS QDs on TiO₂ nanocrystallites¹⁰⁹ or CdS on TiO₂ electrodes,¹¹⁰ CdS QDs and Au NPs on electrodes,^{100,111} CdS/ZnO hierarchical nanospheres,¹¹² and QDs in combination with bipyridinium or cyclodextrin.^{91,113,114} Also, CdS/carbon nanotube composites have been used in order to increase the charge carrier separation rate (see Figure 7).^{99,105,115} In the approach of

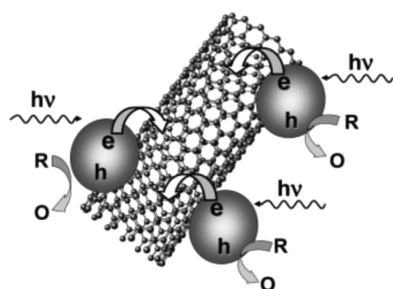


Figure 7. Charge-transfer interaction between photoexcited CdS nanoparticles and single-wall carbon nanotubes. Reprinted with permission from ref 105. Copyright 2005 Wiley–VCH Verlag GmbH.

Robel et al. where CdS–carbon nanotube nanocomposite suspensions were used, an effective electron transfer from the excited CdS QDs to the single-walled carbon nanotubes¹⁰⁵ was confirmed by transient absorption spectroscopy, which indicated an efficient electron separation efficiency. A different approach involves chemically assisted assembly methods to include carbon nanotubes between the QDs and the electrode.^{99,115} This can be obtained for example by exploiting thiol or amino groups. The efficiency of such a system can be

seen from the work of Sheeney-Haj-Ichia et al.⁹⁹ in which high photocurrents are reported. Here, furthermore, it was suggested that the length of the carbon nanotubes played a major role for the amplitude of the photocurrents, and it was presumed that the defects in the carbon nanotubes affected the extent of charge carrier separation. However, recent results have revealed that CdS/graphene hybrid nanostructure can exhibit even better charge separation properties than single-walled carbon nanotube/QDs systems.^{116,117} In a previous article of Sheeney-Haj-Ichia et al.,¹⁰⁰ Au NPs were employed to enhance photoinduced charge separation. In either case, whether the Au NPs were inserted between the QDs and the electrode, or whether the Au NPs were immobilized on top of the QD layer, enhanced photocurrents (compared to a simple CdS–QD only interface) were observed, which was attributed to an increase in the charge carrier separation in the Au/CdS hybrid system. However, the efficiency differed with respect to the position occupied by the Au NPs within the assembly. In this study, the insertion of Au NPs between the electrode and the QDs led to better photoelectrochemical properties than other Au–CdS arrangements.

From the aforementioned studies, it can be seen that carbon nanotubes, Au NPs, TiO₂ NPs, etc., can be used both in nanoheterostructures, hybrid or combined systems to improve the charge carrier separation and hence increase the photocurrent. The difference between these two types of setup is that the nanoheterostructures provide better charge separation because of the tight connection of the two material domains within one particle, but on the other hand hybrid structures resulting from the assembly of different individual nanocomponents are much easier to achieve. It should be pointed out that although a variety of different nanomaterials can enhance the charge carrier separation efficiency; the location of these nanomaterials inside the QD-based photoelectrochemical system is crucial, especially in the case of hybrid nanoassemblies. A change in their position will lead to a change in the separation efficiency.

2.3. Reducing the Drift. Unstable photocurrent output (drift) is one shortcoming of QD-based photoelectrochemical sensors.^{41,110,118} There are two main causes for the drift of the photocurrent output. The first is a poor connection between the QDs and the electrode, whereas the second is charging and discharging (also called photocorrosion) of the excited QDs. In the following paragraphs, these two causes of unstable photocurrents will be discussed in more detail.

a. Improving the Connection between the QDs and the Electrode. Unstable photocurrents can occur when QDs are disassembled from the electrode during the measurement, which results for instance when the link between the QDs and the gold electrode is not strong enough. This observation was confirmed during scanning tunneling microscopy measurements, as described by Ogawa et al.⁷⁸ To prevent the disassembly of the QDs during the photocurrent measurements, different electrodes, self-assembly materials, and SAM methods have been studied in order to improve the link between electrode and QDs. Khalid et al.⁷² compared the photocurrent stabilities from three different types of electrodes (Au@glass, mica and SiO₂) and for different SAM materials annealed at different temperatures. In this case, Au@SiO₂ provided the lowest drift, and stilbene dithiol SAMs heated at 300 K provided much better SAM results (highest order and lowest drift, most probably due to the strongest linking of the

QDs to the surface) than, for example, nonannealed stilbene dithiol SAMs.

Electrochemical assembly of a *p*-aminothiophenol-capped CdS QD monolayer on *p*-aminothiophenol-functionalized gold surfaces was described by Granot et al.⁹⁷ Using this method, the QDs were covalently bound to form a densely packed monolayer on the surface. Here, the cross-linker molecules additionally provided an improved photoelectrochemical performance, since the electron transport of the conduction band electrons by the aromatic cross-linker facilitated charge carrier separation, which lead to the generation of a higher photocurrent.

In addition to covalent and electrostatic binding of the QDs to the electrodes, assembly methods employing hydrogen bonding such as through complementary barbiturate-triaminodiazine¹¹⁹ or specific guanine-cytosine (G-C) and adenine-thymine (A-T) interactions¹²⁰ have also been successfully introduced. This type of binding exhibits a high stability in aqueous buffer solutions. For example, the G-C and A-T bridging units immobilized the QDs on the electrode, and furthermore provided an efficient interface for the electron transfer. The work on hydrogen bond mediated assembly methods with QD layers on gold based on nucleic base pairing has been further extended by the research group of Itamar Willner.^{121–123} Tel-Vered et al.¹²¹ have shown the CdS programmed assembly of CdS QDs by means of DNA. This enabled control over the exact composition and orientation of the resulting nanostructure and hence over the tunneling distances, which lead to control over the intensities and directions of the resulting photocurrents.

Because of the limited electronic coupling of the DNA-bound QDs to electrodes and a rather low coverage of the electrode surface with semiconductor nanoparticles (the absence of a densely packed interface), the photocurrent between the DNA-immobilized QDs and the electrode is only moderate. Freeman et al.¹²² and Gill et al.¹²³ described the intercalation of doxorubicin or methylene blue into duplex DNA chains that enhanced the charge transport through the DNA bridges. Here, the resulting DNA linker structure acted as a conductive pathway for the charge transport, which lead to higher photocurrents and to the possibility of switching the photocurrent direction by means of the potential applied on the electrode (see Figure 8).

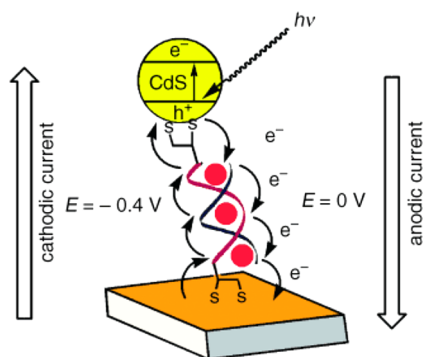


Figure 8. CdS nanoparticles immobilized on a gold electrode by a double-stranded DNA linker molecule. Depending on the redox state of an intercalating molecule, either anodic or cathodic photocurrents are detected. Reprinted with permission from ref 123. Copyright 2005 Wiley-VCH Verlag GmbH.

A different approach for significantly reducing the initial current drift and increasing the signal-to-noise ratio involved the addition of a polymer film on the top of the assembled QDs.⁴¹ Again in this case the reduced drift was attributed to the fact that the polymer film prevents loss of the underlying QDs from the Au electrode. However, the changed chemical environment (due to the presence of the polymer) can also change the probability to populate surface states, or can reduce particle-particle communication. A similar observation was described by Pardo-Yissar et al.,¹²⁴ namely, that the presence of a capping on the QD layer leads to a more stable readout than the absence of such a capping.

b. Reducing the Charging and Discharging of the QDs. Another reason for the occurrence of drift is that the QDs can act as capacitors. According to the model described above, the photocurrent occurs because of charging (reduction by the electrode) and discharging (oxidation by the electrode) of QDs. When no electron donors or acceptors are in solution, the QDs will be continuously oxidized or reduced by the electrode, respectively. Because there are only a limited number of atoms in the QDs, and since the number of photoinduced electron-hole pairs is limited, the photocurrent changes over time.

To solve this problem, normally, we add different electron donors and hole donors to the solution such as triethanolamine,⁷³ Na₂S,⁸⁶ and Na₂SO₃⁵² at pH 12, in order to warrant that the QDs stay in an electroneutral state and therefore reduce the output drift. Also, ascorbic acid can be added to overcome the charging and discharging problem of the QDs.¹¹⁸ In that case, the ascorbic acid acts as an efficient and nontoxic electron donor for scavenging photogenerated holes under mild conditions and therefore inhibits the photocorrosion of the QDs. A different approach involves the use of redox pairs such as Fe²⁺ and Fe³⁺, which are included in the QD layers (e.g., by the layer-by-layer method). These ions can play the role of electron donors and hole donors to avoid the QDs being totally oxidized or reduced.⁴⁷ It has to be mentioned here, that for analytical applications the presence of such substances is often not beneficial because they can interfere with the signal generation process. However, when the presence of QDs on the surface has to be analyzed, this effect can be advantageously applied.

Tanne et al.¹²⁵ have shown that the photocurrent is strongly influenced by the oxygen concentration. Oxygen plays the role of an electron acceptor. This is particularly visible under negative polarization and is influenced by the pH of the solution. The effect can be used for direct sensing, however, when other processes are studied, the removal of oxygen from the solution may be crucial for yielding a defined readout without interference by varying oxygen levels.

3. DETECTION OF CHEMICALS

QD-based photoelectrochemical systems have been widely used and studied in fabricating different kinds of sensors and new solar cells.⁸⁸ As the present review focuses mostly on the QD-based photoelectrochemical applications for chemical and biological detection, in this section, possible applications for such electrode systems are presented and discussed. QD-based photoelectrochemical sensors can be designed in basically two ways, namely either for direct or indirect measurement of the molecular concentrations.

There are two types of direct measurement setups. In the first, QDs are immobilized on the electrode and subsequently, appropriately modified. A potential is applied to the electrode,

so that electron transfer between the charge carriers of the excited state QDs and the corresponding and specific redox molecules can take place. The resulting photocurrent intensity corresponds to the concentration of substances to be detected.^{66,76,126} Another direct measurement method is based on the principle that the analyte molecules can influence the binding properties of the QD layer on the electrode, which means that more or less QDs are immobilized on the electrode. This is related, for example, to the detection of binding reactions for which one partner is labeled with QDs. After the assembly, the photocurrent will follow the concentration of the molecules to be detected.^{43,75} However, in certain cases, direct electron transfer between the QDs and molecules does not occur. Therefore, detection is realized by indirect measurements. For example, in many cases reaction byproducts can act as electron-acceptor or donor units which activate the photoelectrochemical operation of the QDs.¹²⁴ Another possibility resulting in an indirect measurement is the use of photoelectrochemical signal chains. In this way, a redox agent can act as a shuttle molecule between the QDs and the molecules or the catalyst, and thus enable the detection.^{65,69}

In this section, sensors for a variety of such detectable molecules are presented employing either direct or indirect methods. One such molecular sensor is an ultrasensitive cysteine sensor constructed by Long et al.⁷⁰ In this setup, a Nafion film which was both chemically and photochemically inert was employed as the matrix to confine a stable spatial distribution of methyl viologen coated QDs by electrostatic interaction, which enabled the specific detection of cysteine. Methyl viologen was used to enhance the electron extraction from the excited QDs. The Nafion/CdS coated ITO electrode system was shown to be effective in the detection of cysteine with a fast response and high sensitivity: the cysteine lead to the highest response compared to all other amino acids investigated or to the blank solution, and the intensity of the signal was linear with respect to the cysteine concentration.

Another QD-based photoelectrochemical sensor, sensitive to metal ions such as Cu^{2+} , was reported by Wang et al.¹²⁷ where thioglycolic-acid-capped CdS QDs immobilized on an ITO electrode were used in order to develop a highly sensitive and selective photoelectrochemical sensor for Cu^{2+} ions. In the presence of Cu^{2+} ions in a triethanolamine solution, Cu_xS was presumably formed on the surface of the CdS QDs. This material transformation coincided with the generation of a lower energy level providing an effective pathway for the recombination of electron hole pairs in the QDs. Because of these electron–hole recombination centers (Cu^+ or Cu_xS), the electron transfer process from the QDs to the electrode was diminished, so that a decrease in the photocurrent was observed. Hence, the intensity decrease of the photocurrent was proportional to the Cu^{2+} concentration. On the basis of the same interaction principle, a new ITO/ZnO/CdS photoelectrochemical sensor for Cu^{2+} detection that displayed an even better performance was developed by Shen et al.¹¹² Hierarchical nanospheres consisting of a large ZnO domain and smaller CdS domains were attached to an ITO electrode for the selective sensing of Cu^{2+} ions. Here, the light scattering of the ZnO spheres and the heterointerface between the CdS domains and the ZnO provided an enhanced light absorption and charge separation, hence resulting in an improvement in the photocurrent intensity.

Further examples of photoelectrochemical sensors for small molecules are oxygen detection based on illuminated CdSe/

ZnS quantum dots¹²⁵ or hydrogen peroxide detection. Because CdS and CdSe/ZnS QDs do not provide a suitable interface for hydrogen peroxide conversion, an alternative method was introduced by Khalid et al. who employed CdS-FePt nanoheterodimers to build H_2O_2 photoelectrochemical sensors working without the need for an enzyme.⁷² CdS-FePt nanoheterodimers were linked to a gold electrode via a SAM of dithiol molecules yielding a FePt-CdS/SAM/Au structure. The CdS domain, which was in good electrical contact with the gold electrode, allowed for photocurrent generation. The FePt domain acted as a catalytic site for the reduction of H_2O_2 . The H_2O_2 sensitivity of the FePt-CdS/SAM/Au electrode was observed to be higher than in the case when FePt NPs were coimmobilized with CdS QDs on gold (FePt/CdS/SAM/Au). This result furthermore opened a new way for applications of nanoheterodimers using photoelectrochemical detection.

4. BIOMOLECULAR DETECTION

4.1. Enzyme-Based Sensors. The first enzyme-based, indirect photoelectrochemical sensor described in this review is sensitive to acetylcholine via changes in the photocurrent which are dependent on the amount of acetylcholine present.¹²⁴ The sensor system described by Pardo-Yissar et al. is composed of acetylcholine esterase functionalized CdS QDs which are covalently linked to a gold electrode. The addition of acetylthiocholine to the system results in the acetylcholine esterase catalyzing the hydrolysis of acetylthiocholine to thiocholine and acetate. Thiocholine, as an electron donor, can be oxidized by the valence-band holes from the QDs, and the conduction-band electrons from the QDs can be transferred to the electrode, which results in the generation of a photocurrent, the amplitude of which is thus dependent on the amount of acetylthiocholine present in the system (or the presence of enzyme inhibitors).

Glucose can best be detected by photoelectrochemical QD sensors if combined with suitable enzymes in indirect measurements.^{67,125,126,128} Schubert and co-workers⁶⁷ reported the direct sensitive detection of nicotinamide adenine dinucleotide (NADH) in the range of 20 μM to 2 mM at a rather low bias potential by using a photoelectrode system consisting of CdSe/ZnS QDs attached to gold. The indirect detection of glucose by signal chains became possible, since the glucose signal could be converted to NADH by electron transfer via the enzyme glucose dehydrogenase, and subsequently NADH was detected by an electron transfer to the illuminated QDs resulting in a photocurrent. Similarly, indirect detection of glucose was achieved by Tanne et al. by creating a signal chain from glucose via glucose oxidase and molecular oxygen via CdSe/ZnS QDs toward the electrode.¹²⁵ On the basis of the influence that the oxygen concentration has on the photocurrent, the enzymatic activity of glucose oxidase catalyzing the oxidation of glucose by the reduction of O_2 was evaluated. During illumination, the photocurrent was reduced as a result of the oxygen consumption. The sensing properties of this type of electrode were strongly influenced by the amount the enzyme on top of the QD layer, which was found to be easily adjustable using the layer-by-layer technique. Interestingly, a similar system—based on the oxygen sensitivity of the CdSe/ZnS electrode—could also be developed for the detection of sarcosin using sarcosin oxidase as biocatalyst.¹²⁹ The aforementioned glucose sensors are based on signal chains of glucose–glucose dehydrogenase–NADH–QDs or glucose–glucose oxidase–oxygen–QDs. However, the enzyme can also be

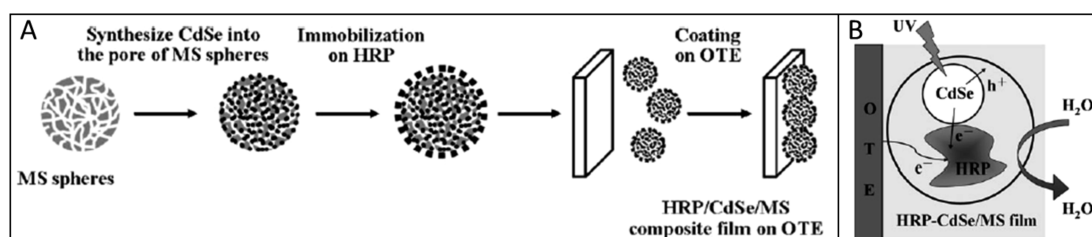


Figure 9. (A) Schematic diagram of the fabrication procedure of the horseradish peroxidase–QD–mesoporous silica/electrode composite film on an optically transparent electrode (OTE) and (B) charge transport scheme of the resulting system. Reproduced with permission from ref 133. Copyright 2010 Springer-Verlag.

coupled to an electrode by means of a shuttle molecule, which facilitates a mediated electron transfer from the biocatalyst. An example of this kind of detection principle can be found in a work by Zheng et al.¹²⁸ In this approach, a photoelectrochemical electrode was constructed by alternately depositing water-soluble CdSe–CdS QDs and a mixture of [Co(phen)₃]^{2+/3+} and poly(ethyleneimine) on a TiO₂ electrode. An enhanced photocurrent and hence sensitivity was observed, which was attributed to the [Co(phen)₃]²⁺ ions, capturing holes from the QDs and therefore suppressing electron–hole recombination. In this setup, the electrode was able to transfer charge carriers from the reduced enzyme, so that the obtained photocurrent depended on the concentration of glucose.

Zhao et al.^{130,131} introduced 4-chloro-1-naphthol to an ITO/TiO₂/CdS/horseradish peroxidase photoelectrochemical biosensing system yielding high H₂O₂ sensitivity. The biocatalytic reaction yielded an insoluble product on the surface of the electrode, by which the photocurrent could be influenced. As a result, a so-called biocatalytic precipitation amplified photoelectrical detection of H₂O₂ was achieved. The resulting detection limit of 5.0×10^{-10} M from this indirect technique was much lower than that of previously reported direct photoelectrical sensors for H₂O₂ using TiO₂ nanotubes/horseradish peroxidase electrodes with a detection limit of 1.8×10^{-7} M,¹³² but the sensor does not allow online measurements.

4.2. Sensors Based on Direct QD–Protein Interaction.

QDs modified with a variety of different surface modifications and immobilized on a gold electrode have been employed to detect the small redox protein cytochrome c.^{65,66,69} In a first example, CdSe/ZnS core/shell QDs were immobilized on a gold electrode by Stoll and co-workers⁶⁶ using dithiane as a linker molecule. Upon exchanging the original layer of hydrophobic surfactant molecules from the QD surface with a hydrophilic one (mercaptopyropionic acid or mercaptosuccinic acid), oxidized cytochrome c could be detected under illumination at a negative bias potential. Katz et al. employed mercaptopyridine to modify the surface of CdS QDs, which were introduced in a QD-based photoelectrochemical sensor for the direct detection of cytochrome c.⁶⁵ Cathodic or anodic photocurrents were observed in the presence of oxidized or reduced cytochrome c, respectively. These results demonstrate control over the direction of the photocurrent generated by CdS QDs by means of the cytochrome c added in different oxidation states. Hence, it should be pointed out again, that the direction of the photocurrent is a very important element when designing biosensors, since it can provide useful information concerning the oxidation state of the biomolecules to be detected. Furthermore, other biomolecules could be detected

by the indirect measurement of cytochrome c (as was shown by Katz et al.).⁶⁵ For example, by activating a secondary cytochrome c mediated biocatalytic process, lactate and NO₃⁻ were measured indirectly. In the presence of oxidized cytochrome c, the oxidation of lactate by lactate dehydrogenase was activated photoelectrocatalytically while generating an anodic photocurrent. Upon photoexcitation of the QDs, conduction band electrons were injected into the electrode, and at the same time cytochrome c was oxidized by holes from the valence band. The resulting oxidized cytochrome c mediated the lactate dehydrogenase oxidation. Similarly, the use of cytochrome c in its reduced form enabled the bioelectrocatalytic reduction of NO₃⁻ to NO₂⁻ by nitrate reductase, while generating a cathodic photocurrent. In a further set of experiments by Stoll et al., QDs with different surface modifications (mercaptopyropionic acid, mercaptosuccinic acid and mercaptopyridine) were compared by measuring the photocurrent arising from the direct electron transfer of the redox protein cytochrome c.⁶⁹ For both oxidation states of cytochrome c, the use of 4-mercaptopyridine yielded the highest photocurrent and best electrode performance with respect to the facilitated protein electrode interaction. Therefore, 4-mercaptopyridine modified QDs were further investigated in a signal chain sensitive for superoxide radicals. The generation of superoxide radicals in solution was detected following the cytochrome c reoxidation at the illuminated electrode. Thus, the photocurrent correlated to the superoxide concentration in solution.

Another protein for which direct interaction with the QDs has been reported is horseradish peroxidase. Under illumination, the enzyme oxidized by H₂O₂ can be reduced back by excited state electrons from the conduction band of the QDs. Hence, the cathodic photocurrent is sensitive to the H₂O₂ concentration. Yang and co-workers¹³³ described the preparation of CdSe QDs inside mesoporous silica spheres, with subsequent preparation of a horseradish peroxidase–QD–mesoporous silica/electrode (see Figure 9). The CdSe/mesoporous silica composite was shown to exhibit an efficient charge carrier separation with recombination being minimized. A further example for horseradish peroxidase-based hydrogen peroxide sensing exploited TiO₂ nanotubes (see ref 132).

Other sensor systems were constructed for the detection of formaldehyde^{134,135} and glutamate¹²⁶ with the respective dehydrogenase. For these systems, however, more mechanistic studies appear to be necessary in order to verify their potential dependence and analyze the possibility of direct analyte reactions.

4.3. Sensors for Binding Reactions. QD-based photoelectrochemical sensors can also be modified with antibodies for biochemical analysis of, for example, immunoglobulin. G.

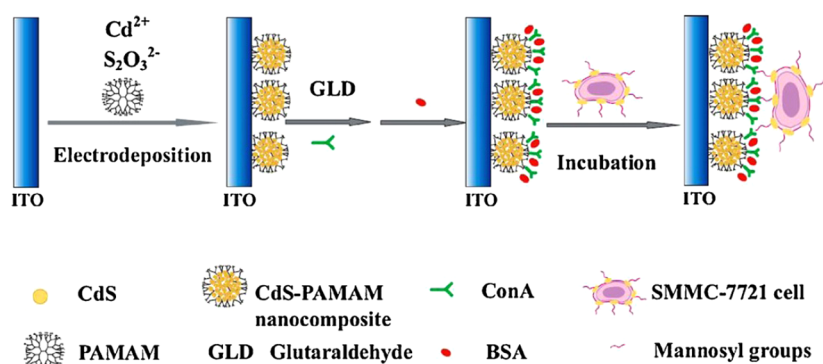


Figure 10. Detection of human hepatoma carcinoma cells by QD-based photoelectrochemical methods. Reproduced with permission from ref 22. Copyright 2010 Elsevier B.V.

Wang et al. have developed such a photoelectrochemical immunosensor¹¹⁸ by preparing a multilayer film via layer-by-layer assembly of a polyelectrolyte and QDs onto an ITO electrode and by attaching goat antimouse immunoglobulin G to the QDs. The immunoglobulin G concentration was measured through the decrease in the photocurrent intensity, which is due to the increase in steric hindrances upon immunocomplex formation. A detection limit of 8.0 pg/mL at 0 V (vs. Ag/AgCl) was achieved. A similar method was used to detect α -fetoprotein antigen by Wang and co-workers.¹¹⁰ The photoelectrochemical immunosensor was developed by alternately dipping the TiO₂ modified ITO electrode into a [Cd(NH₃)₄]²⁺ and S²⁻ solution repeatedly and coating with chitosan and α -fetoprotein antibodies. Linear responses to α -fetoprotein in the range of 50 pg/mL to 50 ng/mL as well as a relatively low detection limit of 40 pg/mL were achieved. The photoelectrochemical results for the detection of α -fetoprotein showed acceptable accuracy in five human sera, such that this methodology was found to be potentially attractive for clinical immunoassays. Another interesting system to be described is a photoelectrochemical thrombin sensor which includes layers of graphene to enhance the charge separation and increase the photocurrent. Zhang et al. developed a sensing strategy for the highly sensitive and specific detection of thrombin based on the use of a specific aptamer and a layer-by-layer assembly of poly(acrylic acid) functionalized graphene combined with positively charged CdSe QD (ITO/graphene/CdSe QDs).¹¹⁷ This system exhibited a detection limit of 4.5×10^{-13} M and significantly higher photocurrents than in the absence of graphene. This photoelectrochemical sensor exhibited stable photocurrents even in the presence of a 10-fold excess of foreign proteins, such as immunoglobulin G, bovine serum albumin and lysozyme. One of the most promising applications for biosensing is cancer diagnosis via the detection of tumor markers. For example, tyrosinase (an indicative marker for melanoma cancer cells) activity was successfully detected with a QD-based photoelectrochemical setup by Yildiz et al. (as already mentioned above).⁷⁴

In the QD-based sensors described so far, the amount of QDs mounted onto the electrode is constant during the operation of the sensor and the detected (photo)current is varied via the reactions induced in the presence of an analyte which somehow affects the electron transfer from or toward the QD (e.g., via the generation of oxidizable/reducible species). However, the following sensor systems are different, since here the detectable molecules will influence the immobilization process of the QDs on the electrode and hence lead to a

variation in the amount of QDs at the electrode interface which in turn will vary the amplitude of the detected photocurrent. For example, as described in refs 73 and 121–123, DNA was employed to immobilize QDs on electrodes. Mismatch of the DNA will influence the consistency of the QD film attached to the surface and, by measurement of the photocurrent change, the DNA mismatch can be detected. DNA does not only function as a bridging unit for QDs, but in addition the duplex DNA can act as a matrix for the incorporation of an intercalator molecule, such as methylene blue, facilitating the charge transport through the DNA bridges. The intercalation of molecular units was observed to be perturbed by single-base mismatches. Hence, this kind of photocurrent-generating system can be employed as a tool for base mismatch detection in DNA, opening interesting and important future applications in DNA detection.^{73,123} A powerful DNA mismatch concept was adopted by Baş et al.⁴³ Here, target ssDNA competed with QD-ssDNA conjugates. By monitoring the decrease in the photocurrent generated from the QD-ssDNA conjugate, quantitative determination of the target ssDNA was enabled.

Besides the detection of certain biomolecules, first results on the specific detection of certain cell types with QD-based photoelectrochemical methods have already been obtained. For example, a photoelectrochemical sensor for specific cell detection (Ramos cells) was developed by Zhang et al.¹³⁶ employing a layer-by-layer assembly of a positively charged polyelectrolyte and negatively charged QDs on ITO. The resulting electrodes were tested as sensors for the Ramos cells through the recognition of DNA aptamers which were covalently attached to the electrode. Even though the linear performance of this setup was observed only within 1 order of magnitude in cell concentrations (from 160 to 1600 cells/mL) with a detection limit of 84 cells/mL, this result displays a proof of principle for this kind of specific cell detection via QD-based photoelectrochemical devices. A different cell type that could be specifically detected is SMMC-7721 human hepatoma carcinoma cells.²² The photoelectrochemical cell-sensor was fabricated by Qian et al. via the electrodeposition of poly(amidoamine) and QDs onto ITO and subsequent attachment of a layer of concanavalin A (see Figure 10). The concanavalin A specifically recognized mannosyl groups from the cell surface with the photocurrent intensity decreasing upon the cells binding to the photosensitive film. The cell concentration was detectable from 5.0×10^3 to 1×10^7 cells mL⁻¹.

Looking at all these different mechanisms as outlined in this section, it becomes obvious that the field of techniques available

Table 1. Overview of the Sensor Systems Discussed in This Review for Quantum-Dot-Based Photoelectrochemical Detection of Chemicals and Biomolecules^a

type of analyte	type of QDs	detection mechanism	authors
Cu ²⁺	thioglycolic-acid-capped CdS QDs	direct	Wang et al. ¹²⁷
	ZnO nanospheres with CdS QDs	direct	Shen et al. ¹¹²
O ₂	CdSe/ZnS core shell QDs	direct	Tanne et al. ¹²⁵
H ₂ O ₂	CdS-FePt heterodimer	indirect	Khalid et al. ⁷²
	CdS QDs	indirect	Zhao et al. ^{130,131}
	CdSe QDs inside mesoporous silica spheres	indirect	Yang et al. ¹³³
superoxide radicals	4-mercaptopyridine-functionalized CdSe/ZnS	indirect	Stoll et al. ⁶⁹
nitrate	mercaptopyridine-functionalized CdS QDs	indirect	Katz et al. ⁶⁵
cysteine	methyl-viologen-coated CdS QDs	direct	Long et al. ⁷⁰
acetylthiocholine (+esterase inhibitors)	acetylcholine-esterase-functionalized CdS QDs	indirect	Pardo-Yissar et al. ¹²⁴
glucose	CdSe/ZnS core shell QDs	indirect	Schubert et al.; ⁶⁷ Tanne et al., ¹²⁵ Zheng et al. ¹²⁸
sarcosine	CdSe/ZnS core shell QDs	indirect	Riedel et al. ¹²⁹
<i>p</i> -aminophenyl phosphate	CdS QDs	indirect	Khalid et al. ⁷⁶
lactate	mercaptopyridine-functionalized CdS QDs	indirect	Katz et al. ⁶⁵
cocaine	aptamer-functionalized CdS QDs	direct	Golub et al. ⁷⁵
tyrosinase	CdS QDs modified with tyrosine methyl ester	indirect	Yildiz et al. ⁷⁴
cytochrome c	mercaptopropionic-acid-functionalized CdSe/ZnS core shell QDs	direct	Stoll et al. ⁶⁶
	mercaptopyridine-functionalized CdS QDs	direct	Katz et al. ⁶⁵
DNA mismatch	CdS QDs	direct	Willner et al.; ⁷³ Tel-Vered et al.; ¹²¹ Freeman et al.; ¹²² Gill et al.; ¹²³ Bas et al. ⁴³
α -fetoprotein antigen	CdS QDs	indirect	Wang et al. ¹¹⁰
thrombin	graphene/CdSe QDs layer by layer structure	indirect	Zhang et al. ¹¹⁷
immunoglobulin G	CdS QDs	indirect	Wang et al. ¹¹⁸
Ramos cells	CdSe QDs	direct	Zhang et al. ¹³⁶
SMMC-7721 human hepatoma carcinoma cells	CdS/poly(amidoamine) nanocomposite	direct	Qian et al. ²²

^aThe order of appearance is sorted by the type of analyte starting from ions and small molecules, via biomolecules, to cells.

in the detection of biomolecules is quite broad. Apart from many different direct measurements already conducted, a variety of indirect measurements e.g. of reaction byproducts or by utilizing the assistance of intercalating molecules have already been employed as strategies to circumvent the sometimes difficult to apply direct measurement techniques. In total, this has already resulted in a variety of biomolecules which can presently be detected using quantum-dot-based photoelectrochemical sensors (see Table 1), which as a research field is continuously being extended.

5. CONCLUSIONS

Concepts, fabrication methods, improvements, and applications of QD-based photoelectrochemical sensors have been described with the main focus being on biochemical detection. It can be seen that because of the light-directed read-out and the broad range of functionalization possibilities, QD-based photoelectrochemical sensors have great potential and a promising future for applications such as biosensing. The variety of molecules presently detectable can be seen from Table 1, which summarizes the systems described in this article. However, since QD-based photoelectrochemical sensors are still in their infancy, some challenges still remain among which are: (1) the variety of sensing concepts and applications in the detection of different molecules will have to be further expanded by designing more specific QD/biomolecule hybrid systems or special nanoheterostructure building blocks. (2) QD-based photoelectrical sensors need to be further developed in order to achieve multichannel detection sensors with an aim to finding

applications, e.g., in drug screening or medical analysis. (3) As with developments in the fabrication of QD-based solar cells, methodologies should be sought such that QD-based photoelectrochemical devices that have a similar structure may be fabricated in the same way. This will be beneficial for commercial production and practical use. (4) So far, most QD-based photoelectrochemical sensors are based on the most commonly studied QD systems, which are unfortunately predominantly based on Cd or Pb compounds, both of which are accompanied by toxicity issues. To avoid this, particularly in medical diagnosis, more work will have to be done, in order to expand the already large array of materials, to include less toxic QD materials, examples of which are fluorescent metal nanoparticles, carbon dots, InP, or Zn-based materials. (5) Electrode developments for analytical purposes have to show the applicability of this new type of sensor in real samples. This is related to signal height and stability but also to interference-free measurements. Much progress has already been achieved in the pursuit of these developments, and there is presently no reason to expect that future developments will not aid in the delivery of the advances required to compete with or even surpass the performances of the present generation of sensor devices.

■ AUTHOR INFORMATION

Corresponding Author

*E-mail: nadja.bigall@pci.uni-hannover.de. Phone: +49 511 762-16068.

Author Contributions

The manuscript was written through contributions of all authors. All authors have given approval to the final version of the manuscript.

Notes

The authors declare no competing financial interest.

ACKNOWLEDGMENTS

Z.Y. is grateful for financial support from the National Natural Science Foundation of China (61001056), Natural Science Foundation of Tianjin, China (10JCZDJC15300). Parts of this work were supported by DFG (GRK 1782).

REFERENCES

- (1) Luo, X.; Morrin, A.; Killard, A. J.; Smyth, M. R. *Electroanalysis* **2006**, *18*, 319–326.
- (2) Gill, R.; Zayats, M.; Willner, I. *Angew. Chem., Int. Ed.* **2008**, *47*, 7602–7625.
- (3) Algar, W. R.; Tavares, A. J.; Krull, U. J. *Anal. Chim. Acta* **2010**, *673*, 1–25.
- (4) Freeman, R.; Willner, B.; Willner, I. *J. Phys. Chem. Lett.* **2011**, *2*, 2667–2677.
- (5) Lei, J.; Ju, H. *Chem. Soc. Rev.* **2012**, *41*, 2122–2134.
- (6) Amelia, M.; Lincheneau, C.; Silvi, S.; Credi, A. *Chem. Soc. Rev.* **2012**, *41*, 5728–5743.
- (7) Deng, S.; Ju, H. *Analyst* **2013**, *138*, 43–61.
- (8) Lu, Z. S.; Li, C. M. *Curr. Med. Chem.* **2011**, *18*, 3516–3528.
- (9) Smith, A. M.; Duan, H.; Mohs, A. M.; Nie, S. *Adv. Drug Delivery Rev.* **2008**, *60*, 1226–1240.
- (10) Parak, W. J.; Pellegrino, T.; Plank, C. *Nanotechnology* **2005**, *16*, R9–R25.
- (11) Dabbousi, B. O.; Rodriguez-Viejo, J.; Mikulec, F. V.; Heine, J. R.; Mattoussi, H.; Ober, R.; Jensen, K. F.; Bawendi, M. G. *J. Phys. Chem. B* **1997**, *101*, 9463–9475.
- (12) Hines, M. A.; Guyot-Sionnest, P. *J. Phys. Chem.* **1996**, *100*, 468–471.
- (13) Peng, X.; Schlamp, M. C.; Kadavanich, A. V.; Alivisatos, A. P. *J. Am. Chem. Soc.* **1997**, *119*, 7019–7029.
- (14) Gao, X.; Yang, L.; Petros, J. A.; Marshall, F. F.; Simons, J. W.; Nie, S. *Curr. Opin. Biotechnol.* **2005**, *16*, 63–72.
- (15) Medintz, I. L.; Uyeda, H. T.; Goldman, E. R.; Mattoussi, H. *Nat. Mater.* **2005**, *4*, 435–446.
- (16) Parak, W. J.; Gerion, D.; Pellegrino, T.; Zanchet, D.; Micheel, C.; Williams, S. C.; Boudreau, R.; Le Gros, M. A.; Larabell, C. A.; Alivisatos, A. P. *Nanotechnology* **2003**, *14*, 15–27.
- (17) Rodríguez-Hernández, J.; Chécot, F.; Gnanou, Y.; Lecommandoux, S. *Prog. Polym. Sci.* **2005**, *30*, 691–724.
- (18) Grodzinski, P.; Silver, M.; Molnar, L. K. *Expert Rev. Mol. Diagn.* **2006**, *6*, 307–318.
- (19) Lin, C.-A. J.; Liedl, T.; Sperling, R. A.; Fernández-Arguelles, M. T.; Costa-Fernández, J. M.; Pereiro, R.; Sanz-Medel, A.; Chang, W. H.; Parak, W. J. *J. Mater. Chem.* **2007**, *17*, 1343–1346.
- (20) Ma, X.; Tan, H.; Kipp, T.; Mews, A. *Nano Lett.* **2010**, *10*, 4166–4174.
- (21) Zhang, F.; Ali, Z.; Amin, F.; Riedinger, A.; Parak, W. *Anal. Bioanal. Chem.* **2010**, *397*, 935–942.
- (22) Qian, Z.; Bai, H.-J.; Wang, G.-L.; Xu, J.-J.; Chen, H.-Y. *Biosens. Bioelectron.* **2010**, *25*, 2045–2050.
- (23) Zayats, M.; Willner, I. In *Biosensing for the 21st Century*; Renneberg, R., Lisdat, F., Eds.; Springer: Berlin, 2008; Vol. 109, pp 255–283.
- (24) Golub, E.; Niazov, A.; Freeman, R.; Zatsepin, M.; Willner, I. *J. Phys. Chem. C* **2012**, *116*, 13827–13834.
- (25) Wang, J.; Liu, G.; Merkoçi, A. *J. Am. Chem. Soc.* **2003**, *125*, 3214–3215.
- (26) de la Escosura-Muñiz, A.; Ambrosi, A.; Merkoçi, A. *Tr. Anal. Chem.* **2008**, *27*, 568–584.
- (27) Wang, J.; Liu, G.; Wu, H.; Lin, Y. *Small* **2008**, *4*, 82–86.
- (28) Cui, R.; Pan, H.-C.; Zhu, J.-J.; Chen, H.-Y. *Anal. Chem.* **2007**, *79*, 8494–8501.
- (29) Willner, I.; Zayats, M. *Angew. Chem., Int. Ed.* **2007**, *46*, 6408–6418.
- (30) Katz, E.; Willner, I.; Wang, J. *Electroanalysis* **2004**, *16*, 19–44.
- (31) Chikkaveeraiah, B. V.; Bhirde, A. A.; Morgan, N. Y.; Eden, H. S.; Chen, X. *ACS Nano* **2012**, *6*, 6546–6561.
- (32) Fang, X.; Han, M.; Lu, G.; Tu, W.; Dai, Z. *Sens. Actuators, B* **2012**, *168*, 271–276.
- (33) Jiang, H.; Wang, X. *Anal. Chem.* **2012**, *84*, 6986–6993.
- (34) Peng, S.; Zhang, X. *Microchim. Acta* **2012**, *178*, 323–330.
- (35) Wang, H.; Chen, Q.; Tan, Z.; Yin, X.; Wang, L. *Electrochim. Acta* **2012**, *72*, 28–31.
- (36) Wang, J.; Han, H.; Jiang, X.; Huang, L.; Chen, L.; Li, N. *Anal. Chem.* **2012**, *84*, 4893–4899.
- (37) Jie, G.; Liu, B.; Pan, H.; Zhu, J.-J.; Chen, H.-Y. *Anal. Chem.* **2007**, *79*, 5574–5581.
- (38) Sun, L.; Bao, L.; Hyun, B.-R.; Bartnik, A. C.; Zhong, Y.-W.; Reed, J. C.; Pang, D.-W.; Abruña, H. C. D.; Malliaras, G. G.; Wise, F. W. *Nano Lett.* **2008**, *9*, 789–793.
- (39) Parak, W. J.; Hofmann, U. G.; Gaub, H. E.; Owicki, J. C. *Sens. Actuators, A* **1997**, *63*, 47–57.
- (40) Owicki, J. C.; Wallace Parce, J. *Biosens. Bioelectron.* **1992**, *7*, 255–272.
- (41) Yue, Z.; Khalid, W.; Zanella, M.; Abbasi, A.-Z.; Pfreundt, A.; Rivera Gil, P.; Schubert, K.; Lisdat, F.; Parak, W. J. *Analyt. Bioanal. Chem.* **2010**, *396*, 1095–1103.
- (42) Xiao, F.; Lai, Y.; Zhang, N.; Bai, J.; Xian, Y.; Jin, L. *Chin. J. Chem.* **2012**, *30*, 1168–1176.
- (43) Baş, D.; Boyacı, İ. *Analyt. Bioanal. Chem.* **2011**, *400*, 703–707.
- (44) Bakkers, E.; Reitsma, E.; Kelly, J. J.; Vanmaekelbergh, D. *J. Phys. Chem. B* **1999**, *103*, 2781–2788.
- (45) Bakkers, E.; Roest, A. L.; Marsman, A. W.; Jennekens, L. W.; de Jong-van Steensel, L. I.; Kelly, J. J.; Vanmaekelbergh, D. *J. Phys. Chem. B* **2000**, *104*, 7266–7272.
- (46) Hojeij, M.; Eugster, N.; Su, B.; Girault, H. H. *Langmuir* **2006**, *22*, 10652–10658.
- (47) Hojeij, M.; Su, B.; Tan, S.; Mériquet, G.; Girault, H. H. *ACS Nano* **2008**, *2*, 984–992.
- (48) Polymeropoulos, E. E. *J. Appl. Phys.* **1977**, *48*, 2404–2407.
- (49) Su, B.; Fermin, D. J.; Abid, J.-P.; Eugster, N.; Girault, H. H. *J. Electroanal. Chem.* **2005**, *583*, 241–247.
- (50) Bakkers, E.; Marsman, A. W.; Jennekens, L. W.; Vanmaekelbergh, D. *Angew. Chem., Int. Ed.* **2000**, *39*, 2297–2299.
- (51) Bakkers, E.; Kelly, J. J.; Vanmaekelbergh, D. *J. Electroanal. Chem.* **2000**, *482*, 48–55.
- (52) Hickey, S. G.; Riley, D. J. *J. Phys. Chem. B* **1999**, *103*, 4599–4602.
- (53) Hickey, S. G.; Riley, D. J. *Electrochim. Acta* **2000**, *45*, 3277–3282.
- (54) Kuçur, E.; Bücking, W.; Nann, T. *Microchim. Acta* **2008**, *160*, 299–308.
- (55) Eychmüller, A.; Hasselbarth, A.; Katsikas, L.; Weller, H. *Berichte Der Bunsen-Gesellschaft-Physical Chemistry Chemical Physics* **1991**, *95*, 79–84.
- (56) Chestnoy, N.; Harris, T. D.; Hull, R.; Brus, L. E. *J. Phys. Chem.* **1986**, *90*, 3393–3399.
- (57) Drouard, S.; Hickey, S. G.; Riley, D. J. *Chem. Commun.* **1999**, 67–68.
- (58) Hickey, S. G.; Riley, D. J.; Tull, E. J. *J. Phys. Chem. B* **2000**, *104*, 7623–7626.
- (59) Riley, D. J.; Tull, E. J. *J. Electroanal. Chem.* **2001**, *504*, 45–51.
- (60) Peter, L. M.; Riley, D. J.; Tull, E. J.; Wijayantha, K. G. U. *Chem. Commun.* **2002**, 1030–1031.
- (61) Riley, D. J.; Waggett, J. P.; Wijayantha, K. G. U. *J. Mater. Chem.* **2004**, *14*, 704–708.
- (62) Doherty, R. P.; Hickey, S. G.; Riley, D. J.; Tull, E. J. *J. Electroanal. Chem.* **2004**, *569*, 271–274.

- (63) Nakanishi, T.; Ohtani, B.; Uosaki, K. *J. Phys. Chem. B* **1998**, *102*, 1571–1577.
- (64) Nakanishi, T.; Ohtani, B.; Shimazu, K.; Uosaki, K. *Chem. Phys. Lett.* **1997**, *278*, 233–237.
- (65) Katz, E.; Zayats, M.; Willner, I.; Lisdat, F. *Chem. Commun.* **2006**, 1395–1397.
- (66) Stoll, C.; Kudera, S.; Parak, W. J.; Lisdat, F. *Small* **2006**, *2*, 741–743.
- (67) Schubert, K.; Khalid, W.; Yue, Z.; Parak, W. J.; Lisdat, F. *Langmuir* **2010**, *26*, 1395–1400.
- (68) Yue, Z.; Zhang, W.; Wang, C.; Liu, G.; Niu, W. *Mater. Lett.* **2012**, *74*, 180–182.
- (69) Stoll, C.; Gehring, C.; Schubert, K.; Zanella, M.; Parak, W. J.; Lisdat, F. *Biosens. Bioelectron.* **2008**, *24*, 260–265.
- (70) Long, Y.-T.; Kong, C.; Li, D.-W.; Li, Y.; Chowdhury, S.; Tian, H. *Small* **2011**, *7*, 1624–1628.
- (71) Baş, D.; Boyacı, İ. H. *Electroanalysis* **2009**, *21*, 1829–1834.
- (72) Khalid, W.; El Helou, M.; Murböck, T.; Yue, Z.; Montenegro, J.-M.; Schubert, K.; Göbel, G.; Lisdat, F.; Witte, G.; Parak, W. J. *ACS Nano* **2011**, *5*, 9870–9876.
- (73) Willner, I.; Patolsky, F.; Wasserman, J. *Angew. Chem., Int. Ed.* **2001**, *40*, 1861–1864.
- (74) Yildiz, H. B.; Freeman, R.; Gill, R.; Willner, I. *Anal. Chem.* **2008**, *80*, 2811–2816.
- (75) Golub, E.; Pelossof, G.; Freeman, R.; Zhang, H.; Willner, I. *Anal. Chem.* **2009**, *81*, 9291–9298.
- (76) Khalid, W.; Göbel, G.; Hühn, D.; Montenegro, J. M.; Rivera-Gil, P.; Lisdat, F.; Parak, W. J. *J. Nanobiotechnol.* **2011**, *9*, 46.
- (77) Poppe, J.; Gabriel, S.; Liebscher, L.; Hickey, S. G.; Eychmüller, A. *J. Mater. Chem. C* **2013**, *1*, 1515–1524.
- (78) Ogawa, S.; Fan, F.-R. F.; Bard, A. J. *J. Phys. Chem.* **1995**, *99*, 11182–11189.
- (79) Ogawa, S.; Hu, K.; Fan, F.-R. F.; Bard, A. J. *J. Phys. Chem. B* **1997**, *101*, 5707–5711.
- (80) Hu, K.; Brust, M.; Bard, A. J. *Chem. Mater.* **1998**, *10*, 1160–1165.
- (81) Kamat, P. V. *J. Phys. Chem. B* **2002**, *106*, 7729–7744.
- (82) Kamat, P. V.; Shanghavi, B. *J. Phys. Chem. B* **1997**, *101*, 7675–7679.
- (83) Sant, P. A.; Kamat, P. V. *Phys. Chem. Chem. Phys.* **2002**, *4*, 198–203.
- (84) Sharma, S. N.; Pillai, Z. S.; Kamat, P. V. *J. Phys. Chem. B* **2003**, *107*, 10088–10093.
- (85) Baker, D. R.; Kamat, P. V. *Adv. Funct. Mater.* **2009**, *19*, 805–811.
- (86) Miyake, M.; Torimoto, T.; Nishizawa, M.; Sakata, T.; Mori, H.; Yoneyama, H. *Langmuir* **1999**, *15*, 2714–2718.
- (87) Nakanishi, T.; Ohtani, B.; Uosaki, K. *Jpn. J. Appl. Phys.* **1997**, *36*, 4053–4056.
- (88) Kamat, P. V. *J. Phys. Chem. C* **2008**, *112*, 18737–18753.
- (89) Tang, J.; Sargent, E. H. *Adv. Mater.* **2011**, *23*, 12–29.
- (90) Sargent, E. H. *Nat. Photonics* **2012**, *6*, 133–135.
- (91) Sheeney-Haj-Ichia, L.; Wasserman, J.; Willner, I. *Adv. Mater.* **2002**, *14*, 1323–1326.
- (92) Mann, S. *Nat. Mater.* **2009**, *8*, 781–792.
- (93) Gowd, E. B.; Nandan, B.; Bigall, N. C.; Eychmüller, A.; Formanek, P.; Stamm, M. *Polymer* **2010**, *52*, 2661–2667.
- (94) Gowd, E. B.; Nandan, B.; Vyas, M. K.; Bigall, N. C.; Eychmüller, A.; Schlörb, H.; Stamm, M. *Nanotechnology* **2009**, *20*, 415302.
- (95) Nandan, B.; Gowd, E. B.; Bigall, N. C.; Eychmüller, A.; Formanek, P.; Simon, P.; Stamm, M. *Adv. Funct. Mater.* **2009**, *19*, 2805–2811.
- (96) Miyake, M.; Matsumoto, H.; Nishizawa, M.; Sakata, T.; Mori, H.; Kuwabata, S.; Yoneyama, H. *Langmuir* **1997**, *13*, 742–746.
- (97) Granot, E.; Patolsky, F.; Willner, I. *J. Phys. Chem. B* **2004**, *108*, 5875–5881.
- (98) Etgar, L.; Moehl, T.; Gabriel, S.; Hickey, S. G.; Eychmüller, A.; Gratzel, M. *ACS Nano* **2012**, *6*, 3092–3099.
- (99) Sheeney-Haj-Ichia, L.; Basnar, B.; Willner, I. *Angew. Chem., Int. Ed.* **2005**, *44*, 78–83.
- (100) Sheeney-Haj-Ichia, L.; Pogorelova, S.; Gofer, Y.; Willner, I. *Adv. Funct. Mater.* **2004**, *14*, 416–424.
- (101) Torimoto, T.; Nagakubo, S.; Nishizawa, M.; Yoneyama, H. *Langmuir* **1998**, *14*, 7077–7081.
- (102) Göbel, G.; Schubert, K.; Schubart, I. W.; Khalid, W.; Parak, W. J.; Lisdat, F. *Electrochim. Acta* **2011**, *56*, 6397–6400.
- (103) Zhao, W.-W.; Wang, J.; Xu, J.-J.; Chen, H.-Y. *Chem. Commun.* **2011**, *47*, 10990–10992.
- (104) Zhao, W.-W.; Yu, P.-P.; Shan, Y.; Wang, J.; Xu, J.-J.; Chen, H.-Y. *Anal. Chem.* **2012**, *84*, 5892–5897.
- (105) Robel, I.; Bunker, B. A.; Kamat, P. V. *Adv. Mater.* **2005**, *17*, 2458–2463.
- (106) Tu, W.; Wang, W.; Lei, J.; Deng, S.; Ju, H. *Chem. Commun.* **2012**, *48*, 6535–6537.
- (107) Brown, P.; Kamat, P. V. *J. Am. Chem. Soc.* **2008**, *130*, 8890–8891.
- (108) Nasr, C.; Kamat, P. V.; Hotchandani, S. *J. Electroanal. Chem.* **1997**, *420*, 201–207.
- (109) Robel, I.; Subramanian, V.; Kuno, M.; Kamat, P. V. *J. Am. Chem. Soc.* **2006**, *128*, 2385–2393.
- (110) Wang, G.-L.; Xu, J.-J.; Chen, H.-Y.; Fu, S.-Z. *Biosens. Bioelectron.* **2009**, *25*, 791–796.
- (111) Yildiz, H. B.; Tel-Vered, R.; Willner, I. *Adv. Funct. Mater.* **2008**, *18*, 3497–3505.
- (112) Shen, Q.; Zhao, X.; Zhou, S.; Hou, W.; Zhu, J.-J. *J. Phys. Chem. C* **2011**, *115*, 17958–17964.
- (113) Yildiz, H. B.; Tel-Vered, R.; Willner, I. *Angew. Chem., Int. Ed.* **2008**, *47*, 6629–6633.
- (114) Tel-Vered, R.; Yildiz, H. B.; Willner, I. *Adv. Mater.* **2009**, *21*, 716–720.
- (115) Ovits, O.; Tel-Vered, R.; Baravik, I.; Wilner, O. I.; Willner, I. *J. Mater. Chem.* **2009**, *19*, 7650–7655.
- (116) Guo, C. X.; Yang, H. B.; Sheng, Z. M.; Lu, Z. S.; Song, Q. L.; Li, C. M. *Angew. Chem., Int. Ed.* **2010**, *49*, 3014–3017.
- (117) Zhang, X.; Li, S.; Jin, X.; Zhang, S. *Chem. Commun.* **2011**, *47*, 4929–4931.
- (118) Wang, G.-L.; Yu, P.-P.; Xu, J.-J.; Chen, H.-Y. *J. Phys. Chem. C* **2009**, *113*, 11142–11148.
- (119) Baron, R.; Huang, C.-H.; Bassani, D. M.; Onopriyenko, A.; Zayats, M.; Willner, I. *Angew. Chem., Int. Ed.* **2005**, *44*, 4010–4015.
- (120) Xu, J.-P.; Weizmann, Y.; Krikhely, N.; Baron, R.; Willner, I. *Small* **2006**, *2*, 1178–1182.
- (121) Tel-Vered, R.; Yehezkeili, O.; Yildiz, H. B.; Wilner, O. I.; Willner, I. *Angew. Chem., Int. Ed.* **2008**, *47*, 8272–8276.
- (122) Freeman, R.; Gill, R.; Beissenhirtz, M.; Willner, I. *Photochem. Photobiol. Sci.* **2007**, *6*, 416–422.
- (123) Gill, R.; Patolsky, F.; Katz, E.; Willner, I. *Angew. Chem., Int. Ed.* **2005**, *44*, 4554–4557.
- (124) Pardo-Yissar, V.; Katz, E.; Wasserman, J.; Willner, I. *J. Am. Chem. Soc.* **2003**, *125*, 622–623.
- (125) Tanne, J.; Schäfer, D.; Khalid, W.; Parak, W. J.; Lisdat, F. *Anal. Chem.* **2011**, *83*, 7778–7785.
- (126) Tang, L.; Zhu, Y.; Yang, X.; Sun, J.; Li, C. *Biosens. Bioelectron.* **2008**, *24*, 319–323.
- (127) Wang, G.-L.; Xu, J.-J.; Chen, H.-Y. *Nanoscale* **2010**, *2*, 1112–1114.
- (128) Zheng, M.; Cui, Y.; Li, X.; Liu, S.; Tang, Z. *J. Electroanal. Chem.* **2011**, *656*, 167–173.
- (129) Riedel, M.; Göbel, G.; Abdelmonem, A. M.; Parak, W. J.; Lisdat, F. *Chemphyschem* **2013**, DOI: 10.1002/cphc.201201036.
- (130) Zhao, W.-W.; Yu, P.-P.; Xu, J.-J.; Chen, H.-Y. *Electrochim. Commun.* **2011**, *13*, 495–497.
- (131) Zhao, W.-W.; Ma, Z.-Y.; Yu, P.-P.; Dong, X.-Y.; Xu, J.-J.; Chen, H.-Y. *Anal. Chem.* **2012**, *84*, 917–923.
- (132) Chen, D.; Zhang, H.; Li, X.; Li, J. H. *Anal. Chem.* **2010**, *82*, 2253–2261.

- (133) Yang, X.; Wang, P.; Zhu, Y.; Li, C. *J. Solid State Electrochem.* **2011**, *15*, 731–736.
- (134) Curri, M. L.; Agostiano, A.; Leo, G.; Mallardi, A.; Cosma, P.; Della Monica, M. *Mater. Sci. Eng., C* **2002**, *22*, 449–452.
- (135) Vastarella, W.; Nicastri, R. *Talanta* **2005**, *66*, 627–633.
- (136) Zhang, X.; Li, S.; Jin, X.; Li, X. *Biosens. Bioelectron.* **2011**, *26*, 3674–3678.